THE UNIVERSITY OF MANITOBA

OPTICAL BEHAVIOR, CHARGE CARRIER INJECTION AND SWITCHING PHENOMENA IN ORGANIC THIN FILMS

by

ABDELRAHMAN R. ELSHARKAWI

A Thesis

Submitted to the Faculty of Graduate Studies

in Partial Fulfillment of the Requirements for the Degree

of Doctor of Philosophy

Department of Electrical Engineering

Winnipeg, Manitoba

February, 1976

"OPTICAL BEHAVIOR, CHARGE CARRIER INJECTION AND SWITCHING PHENOMENA IN ORGANIC THIN FILMS"

by

ABDELRAHMAN R. ELSHARKAWI

A dissertation submitted to the Faculty of Graduate Studies of the University of Manitoba in partial fulfillment of the requirements of the degree of

DOCTOR OF PHILOSOPHY

Dedicated to the memory of my Father.

ACKNOWLEDGEMENTS

The author wishes to express his grateful appreciation to Professor K. C. Kao for suggesting this thesis subject and for his constant encouragement, advice and supervision throughout the entire work.

Sincere thanks are given to the graduate students of the Material Research Laboratory and the staff and students of the Department of Electrical Engineering of the University of Manitoba for their assistance and co-operation, and to Mrs. Lynn Wilson for typing this thesis.

Finally, this research was supported by the National Research Council of Canada through the research grant (Grant Number A3339) awarded to Professor Kao.

ABSTRACT

By employing the least-square technique to fit the experimental ellipsometric data and an algorithm to yield values of refractive indicies and film thickness, the optical constants of biaxially anisotropic anthracene thin films have been measured as functions of film thickness in the visible-frequency region. The results show that the refractive indicies in all directions decrease with increasing ratio of film thickness to wavelength and reaches a practically constant value for the ratio higher than 10. This phenomenon is attributed to the effect of surface states on the contribution of excitons to the optical constants.

Switching and memory phenomena have been observed in thin anthracene films sandwiched between matallic electrodes. In general, thin films exhibiting switching and memory phenomena do not exhibit electroluminescence and vice versa. The threshold voltage for the onset of switching decreases with increasing temperature. The "ON" state conductance decreases with increasing temperature, reaches a minimum at about 37^{0}C and then increases with increasing temperature. All the observed phenomena are attributed to double injection coupled with the effects of traps on excitons and charge carriers, carrier-exciton interactions and the formation of charge transfer complexes.

A unified theoretical approach is presented for the

calculation of electric field and charge carrier concentration in an insulator in the absense of applied voltages, and for the calculation of the space-charge limited-current in an insulator-electrolyte system as a function of applied voltage due to single injection into an insulator containing traps of various distributions in energy and space. The computed results are in good agreement with the presently available experimental results for organic thin film-electrolyte systems. It is concluded that the effect of non-uniformity of trap distribution in space is very significant for thin films and should not be ignored when dealing with transport problems in thin films.

A unified theoretical approach to the theory of planar and filamentary double injection in solids with traps non-uniformly distributed in space and in energy is also presented, and expressions for the current-voltage (I-V) relations are derived. The computed results based on those expressions show that the effect of non-uniformity of spatial trap distribution is also very significant for thin films.

TABLE OF CONTENTS

LIST OF FIGURES

LIST OF TABLES

LIST OF MOST USED SYMBOLS

B	Beta function
D_n, D_p	electron and hole diffusion coefficients, respectively
d	specimen thickness
E	energy level
E_c, E_v	energy level at the conduction band and the valence band edges, respectively
E_{Fn}, E_{Fp}	quasi-Fermi levels for electrons and holes, respectively
Eg	energy band gap
E_ℓ, E_u	lower and upper limits of trapping energy levels, respectively
E_{tn}, E_{tp}	electron and hole trapping energy level, respectively
f_e	error function
f_n, f_p	Fermi-Dirac distribution functions for trapped electrons and holes, respectively
F	electric field
g_n, g_p	degeneracy factors of trap states for electrons and holes, respectively
h_n, h_p	trap density distribution functions for electrons and holes, respectively
H_{an}, H_{ap}	trap densities for electrons and holes, respectively, for the traps confined in a single discrete energy level
H_{bn}, H_{bp}	trap densities for electrons and holes, respectively, for the traps distributed exponentially within the forbidden energy gap.
I	total current

J, J_n, J_p	total, electron and hole current densities, respectively
J_o	exchange current density
k	Boltzmann's constant
n, n_f, n_t	total, free and trapped electron densities, respectively
n_{at}	trapped electron density for the traps confined in a single discrete energy level
n_{bt}	trapped electron density for the traps distributed exponentially within the forbidden energy band gap
n_x^*, n_y^*, n_z^*	complex refractive indicies components in the cartesian coordinates
N_c, N_v	effective densities of states in the conduction and valence bands, respectively
P, P_f, P_t	total, free and trapped hole densities, respectively
P_{at}	trapped hole density for the traps confined in a discrete energy level
P_{bt}	trapped hole density for the traps distributed exponentially within the forbidden energy band gap
q	electronic charge
r, z, θ	cylindrical coordinates
R_s, R_p	amplitude reflectances for light polarized parallel and perpendicular to the plane of incidence
S_n, S_p	electron and hole distribution functions in space, respectively
T	absolute temperature
T_o	characteristic temperature of the trap distribution
v	thermal velocity of carriers
V_a	applied voltage across the specimen
V	voltage across the specimen at zero applied field

x,y,z	cartesian coordinates
Δ	relative phase difference of the parallel and normal components of the polarized light
ε	dielectric constant
λ	wavelength
μ_n,μ_p	electron and hole mobilities, respectively
σ_R	electron-hole recombination cross section
ϕ_1	angle of incidence of the light beam
ψ	relative amplitude change of the parallel and normal components of the polarized light

CHAPTER I

INTRODUCTION

Organic semiconductors are generally referred to as organic solids containing a considerable amount of carbon to carbon bonding and exhibiting electronic conductivities between those of metals and insulators. Organic semiconductors are generally grouped into three categories, namely, molecular crystals, charge transfer complexes and polymers. Research in the field of organic semiconductors has been rapidly growing since the publication of Szent-Görgy in 1941 in which he suggested that the motion of electrons in living biological systems may be associated with that in organic semiconductors. In fact, in biological systems, charge and energy transport occurs across or along the cell membranes. For example, the action potential which initiates the nerve impulse is due to charge transfer across the cell membrane which has an average thickness of approximately 100 $\mathring{A}$ [61]. This should draw the attention to the necessity of investigating the electronic properties of the organic semiconductors in thin film form, based on the assumption that they may exhibit properties quite different from those of the same material in the bulk form. Unfortunately, only little has been published in organic thin films. This might

be, on one hand, due to the technical difficulties encountered in the preparation of organic thin films; and on the other hand, due to the fact that interest in the field of the properties and applications of thin films had not been well realized until the late 1950's.

The object of the present investigation is to achieve a better understanding of the charge and energy transport processes in molecular solids in thin film form in the hope that they would throw some light on the physiochemical structure of the biological systems.

To study the properties of organic thin films, it is essential to develop techniques for fabricating thin films, for measuring their thickness and for examining their quality. Ellipsometry in conjunction with x-ray diffraction and other optical techniques have been used in the present investigation. We have, therefore, studied first the optical constants of anthracene thin films with the aim of investigating the size effect and the anisotropic behaviour of this material. The techniques and the results will be presented in detail in Chapter III.

During the experimental studies of the current-voltage characteristics, we observed the switching and memory phenomena in anthracene films of thicknesses smaller than about 5 μ. In Chapter IV, we shall present our new results and discussion about these phenomena.

From the size effect observed in both optical and electrical properties given in Chapters III and IV, we realized that the size effect may be associated with non-uniform distribution of traps in both energy and space. We have, therefore, carried out a systematic theoretical study of the effects of traps of various distributions in energy and space on the space charge created by single injection into a thin insulating film, and on the current-voltage characteristics of an electrolyte-insulating film system. Chapter V will give the details about this investigation together with the presently available experimental results on organic thin films.

At high fields it is most likely that the electric conduction involves a double injection and is filamentary. For this reason we have also carried out a theoretical study of the current-voltage characteristics resulting from planar and filamentary double injection into an insulating film with traps uniformly and non-uniformly distributed in energy and space. A unified approach to this problem will be presented in Chapter VI.

As a considerable amount of work in this field is now available in the literature, it is desirable to review briefly the presently available knowledge about the optical and electrical properties of organic thin films, and this will be given in Chapter II. Conclusion arising from the present investigation will be given in Chapter VII.

CHAPTER II

BRIEF REVIEW OF PREVIOUS WORK

In this chapter some previous work relevant to the present investigation is briefly reviewed.

2.1 FABRICATION TECHNIQUES AND THICKNESS MEASUREMENTS OF ORGANIC THIN FILMS

2.1.1 Fabrication techniques

Thin films of organic semiconductors may be prepared by several methods. Among them some important ones are described as follows:

(i) Vacuum Sublimation

Many organic compounds can be sublimed in vacuum at moderate temperatures without decomposition. The nature of the compound to be sublimed determines the temperature necessary for evaporation in order to obtain homogeneous film. For aromatic hydrocarbons, the compounds with a greater number of carbon atoms require somewhat higher evaporation temperatures. In general, the temperature gradient between the evaporator and the substrate should be kept as low as practicable in order to produce a thin, homogeneous and uniform deposited film. A suitably purified sample of the test compound is placed onto a crucible with indirect heating. Evaporation is carried out under a pressure of 10^{-5} torr onto a substrate

(e.g., glass, or quartz plate) which is placed opposite to the vapour source. Films of aromatic compounds may be produced by evaporation at temperatures of the order of 100^{0}C to 350^{0}C. The heat of sublimation rises by about 1.5 K cal/mole per carbon atom starting with 9.2 K cal/mole for benzene. The atomic and molecular arrangement in the film depends mainly on the temperature at which it is laid down and on the type of the lattice bonds existing in the solid. Thin films of polycyclic molecules prepared by this method tend to align themselves with their ab plane parallel to the substrate [84]. However, this method is seldom employed for the fabrication of polymer films because degradation due to high temperatures often occurs.

(ii) Glow discharge polymerization

A glow discharge in an organic vapor causes a solid film to be deposited on surfaces exposed to the limineous plasma. This deposit consists of a complex intermolecular rearrangement of the chemical bonds at certain positions in the monomer molecules yielding a three dimensional network of atoms built up of the original compound in an irregular but homogeneous pattern. Most organic vapors in which a glow discharge can be maintained yield films; unsaturated and aromatic compounds thus polymerize. The glow discharge usually involves a vapor pressure of about 1 torr, a field of a few hundred volts per cm, preferably at frequencies in the 10 - 50 KH_z range, and a current of the order of several mA/cm^2. Polymeric films of

approximately 1 micron in thickness have been prepared by glow discharge polymerization of the monomers by Bradly and Hammes [17], and these films have been reported to have good chemical and thermal stability.

(iii) Decomposition or suspension from solution

The most simple method of film preparation is the deposition of the material onto the substance from a solution. The control of deposition rate is usually achieved by controlling the gas pressure to regulate the evaporation rate of the solvant. Weigh [188] has used this method to produce thin films of cationic dye; and Ince and Oatly [82] have also used this method by suspending a known quantity of phosphor powder in a solution of polystrene in benzene and allowing it to settle on a metal electrode. Generally, the films prepared by this method are relatively thick, in the range of 0.0005 cm - 0.01 cm; and are rarely uniform. The deposit is microcrystalline in structure and therefore the film usually contains a great deal of grain boundaries and similar discontinuties. However, careful decomposition from solution can yield satisfactory films equivalent to those obtained by sublimation.

(iv) Blodgett - Langmuir method [16]

This is a well known technique for depositing monolayer films of fatty acids. For example, by raising a glass plate through barium stearate spread on water, a well defined 48Å thick monolayer with the hydrocarbon surface oriented outwards

is formed [32]. This plate can be dipped again into the film covered surface to deposit a second monolayer (same thickness) back to back or with like orientation depending on the direction of dipping the plate. Using this method, many monolayers can be built up to form a thick film. The films produced by this method are generally fragile.

A comprehensive review of various deposition techniques is available in several excellent articles [32].

2.2.2 Thickness measurements

Thickness is the single most significant film parameter. It may be measured either in situ by monitoring the rate of deposition or after the film is taken out of the deposition chamber. There are a number of techniques available for the measurement of film thickness, the method to be used in a particular case will be dictated by the type of deposit, deposition technique and particular use of the film. In the following, only those methods suitable for the case of organic (dielectric) thin films are briefly described.

(i) Capacitance monitors

The thickness of dielectric films may be determined by directly monitoring the electrical capacitance of a capacitor configuration. The method is not very sensitive and special care must be taken to avoid spurious effects due to stray

electrical charges in the surroundings of the specimen.

(ii) Microbalance

This method is sometimes referred to as the gravimetric or momentum method depending on whether it measures the weight or the momentum of impinging vapor. The gravimetric method is among the earliest and most convenient to use for film thickness measurements. Various types of balances, such as pivotal, torsion, fiber, quartz or tungestun helical spiral and magnetic suspension have found applications as monitors [77]. The detection sensitivities of various balances range from 1 - 10^{-2} μgm. The electrical signal from the microbalance detection system may be used to monitor and control the deposition rate. However, this method is not accurate, since it assumes that the film density is always uniform.

(iii) Photometric method

If a transparent or slightly absorbing film is deposited on a transparent substrate of a different refractive index, the optical reflectance and transmittance of an incident monochromatic light due to the film-substrate combination show an oscillatory behaviour related to film thickness because of interference effects. Reflectance is reduced or enhanced depending on the relative values of the indicies of the film and substrate material. Film thickness can thus be obtained from the maxima and minima of the reflectance. High intensity laser sources may be used as the source of monochromatic light [145].

(iv) Interference fringes

When two reflecting surfaces are brought into close proximity, interference fringes are produced, the measurement of which makes possible a direct determination of the film thickness and surface topography with high accuracy. Interference fringe methods have been developed to a remarkable degree of accuracy and are now accepted as the absolute standard method [180]. Thickness as low as 100 Å with an accuracy of ~ 20 Å can be measured by this technique.

(v) Polarimetric methods (Ellipsometry)

A plane polarized light reflected from a film covered substrate at non-normal incidences assumes elliptical polarization. The ellipticity (the ratio of minor to major axis) of the reflected beam is determined by the relative phase difference Δ and azemith ψ [7]. The film thickness as well as the optical constants of the film and substrate can be determined from the values of Δ and ψ. The exact ellipsometric equations relating Δ and ψ to the film thickness are extremely complicated and their solution and use for interpreting ellipsometric data requires numerical computation. The technique and the use of ellipsometry in the measurement of organic film thickness are discussed in Chapter III.

2.2 OPTICAL PROPERTIES OF ORGANIC THIN FILMS

Visible and ultraviolet light absorption in organic solids is usually anisotropic. Consequently, plane-polarized light is used together with single crystals of known orientation

for studies of optical properties. There are a few precautions that should be observed when investigating the optical properties of organic semiconductors, and they are:

(a) Complete polarization of the light by the use of two polarizers.

(b) Exact alignment of the crystal.

(c) Use of suitable temperature.

(d) Purification of the crystal.

(e) Avoidance of strain in mounting the crystals.

So far, theoretical and experimental investigations of the optical behaviour of organic thin films deal primarily with optical reflection, transmission and absorption properties and their relation to the optical constants of the films. These studies have led to a variety of interesting thin film optical phenomena which have thrown light on the electronic structure of the organic semiconductors. In general, the optical properties of thin films show profound sensitivity on the film microstructure. Since the deposition parameters affect the film microstructure, strong dependence of the optical properties of thin films on the deposition parameters have been constantly observed. The results are further complicated by aging effects and consequently, violent disagreements between results of different investigators employing different deposition parameters have been reported. With increasing film thickness, the effect of the initial granular structure on the optical properties

is decreased but not eliminated completely. Therefore, thickness dependence is still observed although the general behaviour of the optical parameters follows that of the bulk. A summary of the commonly used methods for the measurement of optical constants of transparent and absorbing thin films is given in table 2.1.

2.2.1 Optical constants

Among the earliest investigations of the optical properties of organic thin films, Gheorghita-Oancea [55] has investigated the absorption, fluorescence and electron diffraction spectra of anthracene thin films which were fabricated by thermal evaporation in vacuum. The film thicknesses ranged between 1000 $\overset{0}{A}$ and 20,000 $\overset{0}{A}$, were measured by microweighing. He found that the anthracene films deposited on various substrates have structures ranging from a perfect crystalline state to an amorphous one, indicating the effect of the properties of substrates. The results obtained from the ultraviolet absorption studies have shown that as the film thickness decreases, the absorption decreases; and that this phenomenon depends on the wavelength of the incident light. The absorption has an exponential dependence on thickness for thicknesses from 2000 $\overset{0}{A}$ upwards. The fluorescence spectra does not show any thickness dependence, and this is ascribed to the existence of superficial layers of the deposit.

TABLE 2.1

SUMMARY OF COMMONLY USED METHODS FOR MEASURING OPTICAL CONSTANTS OF TRANSPARENT (T) AND ABSORBING (A) FILMS [32]

Method	Quantities measured	Film	Substrate	Optical constant	Remarks
Abelés	Brewster angle	T	T,A	n	Simple
Schultz	Reflectance and Transmittance	A	T	n,k	Convenient
Malé	Reflectance and Transmittance	T,A	T	n,k,t	Simultaneous n,k,t
Hadley	Reflectance and Transmittance at several Wavelengths	T,A	T	n,k	Convenient, Charts Available
Spectrophotometric	Wavelength of interference maxima and minima	T,A	T,A	n,t	Simple, dispersion problems
VAMFO	Fringe displacement of two angles of incidence	T	T	n,t	Simple
Ellipsometer	Δ,ψ	T,A	T,A	n,k,t	Valuable for ultrathin films. Indirect, tables and charts required

The optical properties of thin single crystals of anthracene obtained by vacuum sublimation have been reported by Nakada [137]. They were measured for polarized radiation along various crystal axes. The absorption coefficient measured in the fundamental absorption tail for polarized radiation along the b-axis is five times larger than that along the a-axis. The absorption spectrum along the c-axis is a little different from that along the a-axis or b-axis, but it is not as different as is expected from the arrangement of the molecules in the crystal. All absorption coefficients decrease exponentially with increasing wavelength.

Bree and Lyons [21,22] have studied the absorption of ultraviolet light in thin monocrystals of anthracene. They introduced two different optical methods for thickness measurement, namely the multibeam method and the two beam method. Their results have shown a strong thickness dependence of the optical density at the respective peaks in the spectrum. Measurements of the extinction coefficient in the region between 3500 $\mathring{A}$ and 3900 $\mathring{A}$ have shown a pronounced thickness dependence leading to a deviation from Lamber's Law of light absorption. The value of the extinction coefficient measured with unpolarized light decreases monotonically up to the thickness of about 0.8 μm and then reaches a steady value.

Optical properties of thin organic films have also proven to be an effective tool in investigating exciton properties. The migration of excitons in thin anthracene films

has been studied by Simpson [167] in an effort to determine the diffusion length and life time of exciton states in anthracene. The anthracene films were fabricated by vacuum deposition onto cooled glass substrates and the range of film thicknesses used is between 0.01 μm and 0.6 μm. The optical transmission data yielded a value of 0.122 μm for the extinction depth and 0.045 μm for diffusion length of excitons in anthracene. Moreover, thickness dependence studies have shown that for thicknesses greater than about 0.2 μm the total transmittance varies exponentially with thickness and that for thicknesses below 0.2 μm the behaviour is quite different. This is attributed to the fact that when the diffusion length is less than the extinction depth, only the exponential behaviour is observed.

Kepler et al [92] have also investigated the diffusion of triplet excitons in anthracene thin films produced by vacuum sublimation. They studied the effect of the film thickness on the time dependence of the fluorescent light emitted in anthracene after excitation by a Q-spoiled ruby laser, and found that there is a marked decrease in the apparent life time of the triplet excitons with decreasing film thickness. They attributed this to the effects of surface quenching.

A theoretical approach to the theory of excitons in thin organic films has been reported by Davydov [38]. It has been shown that, at low temperatures, the intensity of interaction of light with exciton states in thin films is a monotonic function of the film thickness. This monotonic behaviour is

due to the discrete values of energy and wave vector of the exciton.

In a series of publications Pekar et al [23,24,142-144] have investigated the theory of electromagnetic waves in thin films in which excitons are produced. The effects of the film surface on the exciton states have been considered. The film surfaces turn out to be nodal surfaces for exciton waves, thus surface exciton states can exist in which the excitation waves move only in the layer near the surface of the crystal. The intensity of transmitted light was found to oscillate with the thickness in approximately the same manner predicted by the theory [25].

Using the method of ellipsometry, Allen [5,6] has studied the kinetics of thin organic films of DC-704 and DC-705 diffusion fluids. These materials are high-molecular-weight methylsiloxanes and the thin films were fabricated by the method of molecular effusion. This ellipsometric method enables accurate determination of the thickness and the optical constants of the thin films.

Den Engelson [40] had also used the method of ellipsometry to measure the thickness and optical constants of some cyanine dye thin films prepared by Blodgett-Langmuir method deposited on silicon oxide substrates, and from these data, the strong anisotropic behaviour, structural defects and thickness dependence of the optical parameters have been determined.

Using the anisotropic ellipsometric theory, Tomar et al [182] have also investigated the optical properties of built up films of barium stearate, palimate, megarate and behanate, which were prepared by the Blodgett-Langmuir method on slide glass substrates. Their experimental results of the refractive indicies of the films are in good agreement with the theoretical values based on Schopper's theory for transparent substrates.

We adapt the method of ellipsometry for the measurements of the optical constants of biaxially anisotropic organic thin films, and this will be presented in Chapter III.

2.2.2 Electroluminescence and excitons

Electroluminescence has been observed in undoped anthracene [70,71,190], tetracene doped anthracene [44,90,195], naphthalene [113] and in a large number of inorganic semiconductor thin films [72,73]. It is well understood that electroluminescence is produced in the bulk of the solid by recombination of electrons and holes simultaneously injected into the specimen from injecting electrodes. Two recombining carriers (an electron and a hole) once they are trapped by their Coulomb field, come closer together until they are finally on neighboring molecules, where they form what is known as a charge transfer exciton which can have either singlet or triplet spin character [39]. This charge transfer exciton may then decay into an

electronically excited singlet or triplet exciton. The singlet excitons will radiatively decay to the ground state producing electroluminescence. The triplet excitons either make a transition to the singlet ground state or undergo triplet-triplet annihilation to form either singlet or triplet excitons via a charge transfer intermediate. The process can be summarized by the following equation:

$$4\ (e + h) \rightarrow 1[S]_{dir} + 3[T] \tag{2.1}$$

and

$$4\ ([T] + [T]) \rightarrow 1[S]_{ind} + 3[T]^{*} \tag{2.2}$$

or

$$\begin{aligned} 20\ (e + h) &\rightarrow 5[S]_{dir} + 15[T] \\ &\rightarrow 5[S]_{dir} + 3[S]_{ind} \end{aligned} \tag{2.3}$$

where e and h represent, respectively, the electron and hole, $[S]_{dir}$ and $[S]_{ind}$, respectively, the singlet excitons produced by the direct and indirect processes, and [T] represents the triplet excitons. Thus, there are two channels for any continuing decay, namely either the singlet or the triplet exciton manifold. The singlet channel gives rise to prompt electroluminescence while the triplet channel gives rise to delay electroluminescence. The difference in the temporal behaviour of these two components is due to the difference in lifetimes between triplet excitons

(10^{-2} sec) and singlet excitons (10^{-8} sec). The electroluminescent intensity is governed by the generation efficiency, and hence, the population of singlet excitons produced both directly and indirectly. The location and width of the luminous zone inside the specimen depends upon the local concentration of electron-hole pairs distribution, which in turn depends upon the mobility and recombination coefficient of the carriers. In anthracene, for example, the charge carrier mobility is small and the recombination coefficient is large, thus the luminous zone is comparably narrow.

The excitons may be depopulated by the interaction of the excitons with other excitons, charge carriers or surface states; and hence, the electroluminescent phenomena depend greatly on these processes. In the following we shall briefly review these interaction processes.

(i) Exciton-exciton interaction

The exciton-exciton interaction can be devided into free-free exciton interaction and free-trapped exciton interaction.

The free-free exciton interaction includes triplet-triplet (T-T), singlet-singlet (S-S) and triplet-singlet (T-S) exciton interaction. As has been pointed out earlier in this section, T-T annihilation may take place resulting in the formation of singlet excitons, as indicated by Eqn. (2.2). On the other hand, two singlet excitons could interact to form a pair of charge carriers (an ionized molecule and a free electron) and an unexcited (neutral) molecule [60]. Free charge carrier

generation has also been reported to occur via collisions of triplet and triplet excitons; and singlet and triplet excitons [91]; however, the probability of forming carriers from an exciton pair is 10^4 times as great for either two singlet excitons or a singlet and triplet exciton than it is for two triplet excitons.

In real crystals, the unavoidable presence of lattice defects and impurities can yield what is known as trapped excitons [39]. For example, assymetrically situated molecules having energies slightly different from those in the purely crystalline regions can occur near a defect (or impurity molecule). This energy difference can result either in trapping the excitation energy at the defect or in the diversion of excitation energy from the region. Also, the wave functions of the exciton states are perturbed by the defects and, consequently, the selection rules for allowed transitions are modified. Hence, the presence of traps changes the spectral energy distribution, especially the fluorescence and electroluminescence, and also changes the time dependence of the exciton population and depopulation processes in the specimen. For example, one part in a million of naphthalene in anthracene, appreciably quenches the luminescence of anthracene [69].

Trapping of excitation energy reduces the generation of carriers and can cause an exponential increase of the quantum yield of photogenerated carriers such as that observed with a rise in temperature [165]. This may be due to the temperature dependence of the trapping probability. This conclusion applies also to any generation process which requires the transport of

electronic excitation throughout the crystal [171].

(ii) Exciton-carrier interaction

The destruction of excitons, both singlet and triplet, by charge carriers in organic crystals has been investigated by several investigators [152,186,187]. The interaction of triplet excitons with charge carriers is usually determined by monitoring (1) the steady state delayed fluorescence intensity, (2) the delayed fluorescence decay rate, (3) the steady state phosphorence intensity, or (4) the phosphorescence decay rate as a function of the free charge carrier density. The quenching of delayed fluorescence, in anthracene, by the injected charge carriers has been observed when either monomolecular or bimolecular exciton decay processes are dominant [187]. At low triplet exciton densities, the injected carriers destruct the triplet excitons, thus reducing their effective lifetime. A reduction in the delayed fluorescence intensity due to this mechanism has been observed [8]. At high exciton densities, however, the bimolecular exciton decay mechanism becomes important and the triplet-triplet annihilation rate constant has been found to increase, while the singlet component of the annihilation rate constants to decrease, in the presence of charge carriers. The quenching of delayed fluorescence by charge carriers is a complex process in which many different exciton states may participate. The thermal velocity of the charge carriers has also been found to affect the interaction rates. The trapped charge carriers also affect the exciton lifetime, but less efficiently than the free charge

carriers [187]. Triplet excitons-trapped holes interaction has been proposed as the most probable mechanism accounting for the magnetic field dependence of photoconductivity in anthracene crystals [60]. Carrier-exciton interaction may also influence the quantum efficiency of the electroluminescence, since it results in exciton quenching [81].

(iii) Exciton-surface interaction

The termination of the lattice periodicity at the surface alters the energies of the electronic states in that region. Also, a metal on the surface of an organic semiconductor would have the same effect due to the discontinuity of the dielectric constant across the interface. An exciton produced or diffusing near such region, might find it energetically impossible to depart. Thus, it would be either constrained to travel along the surface or become trapped [38,89] . Surface quenching of mobile excitons can occur either by charge transfer, in which an exciton transfers an electron to an adjacent surface trapping center, or by energy transfer in which an exciton transfers its energy to the acceptor molecules present at the surface [60] . The exciton quenching zone depends on the depth of penetration of the perturbation introduced by the surface. The exciton quenching rate, by a surface, decreases as the temperature increases [81]. However, the effect of surface states on excitons is generally small compared with the interaction processes (i) and (ii) [152].

2.3 ELECTRICAL PROPERTIES OF ORGANIC THIN FILMS

Studies of the electrical properties of many organic substances have revealed that most organic compounds have semiconductor character. Among the earliest studies in this field was the work of Eley and coworkers [46,47]. They studied the effects of temperature and pressure on the electric conductivity of crystallised organic compounds in powdered form. Their results showed that the activiation energy for conduction decreases with increasing pressure and that the linear polymers are less active semiconductors than polynuclear systems with an equal number of π-electrons. Inokuchi and Akamutu [1-4,83] have studied the electric-and-photoconductivity of a number of crystalline organic powders, and on the basis of their results, they concluded that the resistance as a function of temperature follows an exponential law in a manner similar to that in most inorganic intrinsic semiconductors and that the conductivity of the polynuclear hydrocarbons increases with the number of π-electrons in the molecule. The current-voltage characteristics consist of an Ohmic region, at low applied fields, followed by another region of non-Ohmic behaviour at higher fields; the critical field for the onset of non-Ohmic behaviour increases with decreasing temperature.

Mett, Pick and Wissmann [129,148] have investigated the effects of temperature on the electrical conductivity, at different crystallographic direction, for a number of aromatic hydrocarbons. Their results show that the electrical conductivity exhibits strong anisotropy.

Several Canadian researchers [34-36,96-99,111,161] have studied the photoconductivity of anthracene single crystals grown by various methods, using surface and sandwich-type cells. Their experiments have revealed the existance of surface currents and of currents originating in the deeper layers of the substance.

Besides the studies being carried out on aromatic hydrocarbons, new research trends in the field of organic semiconductors are directed towards the domain of molecular complexes [33,76,100,101], Polymers [115,181] and Proteins [28,48,120].

The above are only a few of the available results on the electrical properties of organic semiconductors. Recently, several excellent review articles [49,60,66,140] give quite a comprehensive review on these properties.

On the basis of experimental results, the electrical conductivity in most organic semiconductors is believed to be due to the overlap of π-electron molecular orbitals on adjacent molecules. However, when the interaction between molecules is relatively small, the electrons become highly localized so that they do not easily move through the solid. Therefore, the electrons must move either by tunneling through the barrier between the molecules, or by acquiring sufficient energy to go over the barrier. This latter process is called the hopping process. Therefore, the relative weakness of the intermolecular bonding in organic compounds results in rather narrow energy bands, wide band gaps, low carrier mobility and low melting points, as shown in table 2.2.

The effect of exciton population on the formation of free carriers in media of low mobility has been investigated by Pohl

TABLE 2.2

CHEMICAL STRUCTURE, MELTING POINT AND DRIFT MOBILITIES OF NAPHTHALENE, ANTHRACENE AND TETRACENE.

Organic Semiconductor	Chemical Structure	Melting Point	Types of Charge Carriers	Crystal Axis	Mobilities (cm^2/v.se)	Temperature Dependence	Reference
Naphthalene $C_{10}H_8$	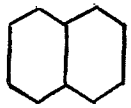	80.2°C	electrons	a b c'	0.51 0.63 0.68	$T^{-0.1}$ $T^{-0.0}$ $T^{-0.9}$	[130]
			holes	a b c'	0.88 1.41 0.99	$T^{-1.0}$ $T^{-0.8}$ $T^{-2.1}$	
Anthracene $C_{10}H_{14}$	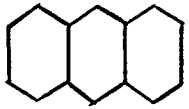	216° C	electrons	a b c'	1.7 1.0 0.4	$T^{-1.0}$ $T^{-1.5}$	[91,135]
			holes	a b c'	1.0 2.0 0.8	$T^{-0.0}$ $T^{-2.0}$ $T^{-1.7}$	
Tetracene $C_{18}H_{12}$	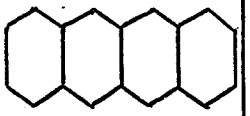	357° C	electrons	a b c'	0.5		[10,53,172]
			holes	a b c'	0.01		

[149,150]. He introduced a different hopping model in which ion-exciton complexes are formed. Because of their lower energy of formation, the number of excitons present may be comparable to the number of free carriers in an intrinsic material [8,39]. Moreover, there is an appreciable energy of association of the ions with the excitons because of the large polarizability of the latter. Therefore, the formation of ion-exciton complexes might be appreciable in an organic semiconductor. Their formation might not only increase the likelihood of free carrier formation but might also aid in the hopping process. A transfer of charge can be envisaged as taking place by the reaction.

$$M_1^+ + M_2^- M_3^+ \rightarrow M_1^+ M_2^- + M_3^+$$

where the charge has been transferred from site 1 to site 3, or by

$$M_1^+ + M_2^- M_3^+ \ldots . M_n^- M_{n+1}^+ \rightarrow M_1^+ M_2^- \ldots . M_n^- + M_{n+1}^-$$

where the transfer is from site 1 to site n+1. Hopping thus occurs between the ion and the exciton. It is required, however, that specific orientations of the molecules be available. Furthermore, ion-pair dissociation could be aided by sufficiently strong fields, thermally or at suitable lattice discontinuity. Based on this model, the effect of external electric field will be to accentuate dissociation of the properly oriented ion-exciton islands. The presence of such island complexes is expected to form regions of high polarizability towards which the external field will be highly concentrated resulting in the formation of loci of ready dissociation. As a consequence, the ohmic behaviour is exhibited only at very low field strengths and an appreciable deviation is usually observed at higher fields well before actual breakdown of the material.

We shall now discuss briefly some of the electrical properties of the organic semiconductors in thin film form as follows.

2.3.1 Electrical conduction mechanisms

Physical phenomena peculiar to thin films and the basis for their study, are generally the consequences of their planar geometry, size and unique structure. The mobility in most organic semiconductors is so low that it is the thickness of the space charge rather than the mean free path which imposes the limit on the film thickness. A space charge immediately below the surface arises from the presence of the surface states. For low carrier concentrations, as it is the case for organic semiconductors, the surface field can penetrate into the interior of the solid for many lattice spacings, causing the formation of depletion, accumulation or inversion layer. Thus, the thickness of the space charge may be quite large. The space charge thickness has been estimated to be of the order of a few thousand Angestroms for organic solids [86]. Another factor which may affect the film characteristics is its texture. Many films are microcrystalline and the contact resistance between the grains may affect the electrical properties [32].

Various experimental results have been reported on the electrical conductivity of organic thin films. The electrical conductivities of α,α'-Diphenyl-β-picrylhydrazl (DPPH) of two forms, single crystals and polycrystalline thin films have been measured by Inokuchi et al [84]. The resistivity

at room temperature along the c-axis is 10^5 times smaller than that perpendicular to the axis. For surface type cells the value of the resistivity and activiation energy along the c-axis are 10^{10} ohm-cm and 1.7 ev respectively whereas they have the values 10^{13} ohm-cm and 2.7 ev for sandwich-type cells. A great difference in the photoconduction and the dark current-voltage characteristics for these two types of cells has been observed. The variation of the current with the applied potential obeys Ohm's law at low fields, but at higher fields (over 10^3 v/cm), however, the current-voltage relation become strongly non-linear for sandwich-type cells, but became more linear for surface cells.

In a further investigation of the electrical properties of the electric conductivity of organic thin films, Inokuchi et al [85] have measured the electrical resistivity and activiation energy for thin films of perylene, coronene and violanthrene. For the cyclic aromatic hydrocarbons a large anisotropy was observed in electrical resistivities, whereas no measurable anisotropy was noticed for the energy gap. Thus, such anisotropic behaviour was attributed to the large difference in mobility of charge carriers, which depends on the direction of drift.

The electrical conductivity of thin anthracene films prepared by vacuum evaporation has been investigated by Gherghita-Oancea [54,56], and the experimental results show that the anthracene thin films display a wide domain in which Ohm's law is valid. The critical field for the onset of non-

linear behaviour is around 200 KV/cm, in comparison with monocrystals whose critical field is about 1.5 KV/cm. Thin films have also shown the phenomena of remenant polarization which is higher in air than in a vacuum. Under the influence of air at atmospheric pressure, the dark current is 5-6 times greater than that at a pressure of 10^{-5} torr. The observed variation of the electrical resistivity of the thin anthracene films as a function of pressure shows that it is not due to the change of the contact surfaces among crystallites under a growing pressure, but rather to a phenomena of gas adsorption on the substance, which modifies the electronic state of the film surface.

The electrical conduction in amorphous organic films of naphthalene and violantherene-A, prepared by low temperature evaporation method, have been studied by Marayama et al [122]. The analysis of the temperature dependence results suggests that the transport mechanism is a thermally activated one with an activiation energy of 0.2 eV. Moreover, it has been observed that the activiation energy for conduction becomes larger when the films become more amorphous.

A field effect has been observed in thin films of several organic semiconductors. Petrova et al [146,147] have investigated the field effect phenomena in thin films of some chloranils which were prepared by vacuum sublimation. The sign of charge carriers in those materials is determined on the basis of their field effect measurement results.

On the basis of the available experimental results, several review articles have discussed the possible electric conduction mechanisms in thin organic films [32,102]. These mechanisms are:

(i) Ionic conduction

This conduction mechanism is more profound in amorphous films. The conduction is mainly due to the drift of lattice defects or moisture content under the action of applied electric fields. Actually, it involves the jump of ions (or vacancies) over the potential barrier. The activiation energy is relatively large (2.9 - 4.3 ev) compared with that for electronic conduction (< lev). Ionic conduction results in the polarization effects in films. The film resistivity increases with the time, since the transient time of ions is relatively large (several hundreds of seconds). The ionic conduction results in material transport from one electrode to the other.

(ii) Space-charge-limited flow

Space-charge-limited currents are usually observed in organic thin films at room temperature or lower. The electrical conductivity is enhanced by Ohmic contacts for charge carrier injection. The character and magnitude of the current are determined by the presence of localized states which trap and store the charge carriers.

A perfect Ohmic contact is an impractical situation and there always exists a barrier and the interface between the film and the electrode. However, at high applied electric

fields, electron emission into the conduction band of the solid from the metal contact electrode may take place. Emission is achieved by thermal activiation of the electrons sufficiently to surmount the interface barrier or by tunneling through it.

(iii) Tunneling

This is usually observed in thin films of very small thicknesses ($< 300\text{Å}$). Electrons may tunnel from one metal electrode (cathode) to the other (anode); the carriers can be injected into the conduction (or valence) band of the film by thermionic or Schottky emission over the metal-film interface barrier; or the carriers may tunnel through the insulator barrier gap at high applied fields (field or cold emission). In the presence of traps, conduction can also take place by tunneling via traps, and if the number of traps is small and the contacts are ohmic, the current flow may be regulated by the prevailing space-charge conditions.

(iv) Pool-Frenkel effect

The Pool-Frenkel effect is much similar to the Schottky effect. However, in this case emission of electrons takes place from charge carrier traps into the conduction band. At low temperatures conduction is by tunneling emission out of the traps into the quasi-conduction band of the host material, whereas at high temperatures thermal emission becomes dominant. The Pool-Frenkel effect is commonly used to explain part of the direct current-voltage characteristics amorphous films. The experimental evidence for the process is a region of linearity in a plot of the logarithm of the current against the square

root of the applied voltage or field. Generally, it is found that the range of voltage or field over which linearity is observed is limited to about 1 order [102].

(v) Impurity conduction

Electrons (or holes) may move between the donor (or acceptor) levels without activiation to the conduction (or valence) band. For low impurity concentration, the overlap between the wave functions of adjacent donor sites is small and the charge carriers are localized. However, if one neighboring donor site becomes vacant, an electron transfers to it. At no applied field, the motion is random and, hence, the net current is zero. However, the applied electric field produces a gradient of donor state energy, thus increasing the electron transfer to sites of lower energy, and conduction currents are observed. The electron transfer between donor sites is accompanied by emission or absorption of phonons (energy conservation).

The type, structure and thickness of the film determine which of the above mechanisms is dominant under a given experimental condition.

2.3.2 Charge carrier injection

The relatively wide energy gap associated with organic semiconductors makes it almost impossible to generate a large number of charge carriers by thermal excitation processes, and

therefore, external sources are usually needed for carrier induction into the bulk of the organic semiconductors. The main sources for carrier generation are carrier induction from chemically active ohmic contacts, carrier generation in the bulk by the photo-excitation and carrier emission from electrodes through photoemission process. Recently, Lampert et al [104] have given a quite comprehensive review on this subject. Charge carrier injection in solids is generally classified into single and double injection. In single injection, the current flow is mainly due to one type of carriers (electrons or holes) injected from an injecting contact into the solid. These injected carriers gradually establish a space charge leading to the well known space-charge-limited-current (SCLC). On the other hand, the double injection involves current flow consisting of two types of charge carriers, electrons being injected from the cathode and holes from the anode. In double injection, recombination kinetics play an important role in the electrical properties. The recombination process may either be bimolecular (i.e. band to band electron hole recombination) or may occur through one or more sets of localized recombination centers.

The critical property of a contact, for most purposes, is the number and type of carriers the contact is capable of injecting into the solid under the experimental conditions. The most important factor in determining this is the relation between the chemical potential of the contact and the

conducting state in the solid. The conditions under which photoemission of electrons and holes can take place from different metal contacts into anthracene, have been discussed in detail by Caywood [31]. From the photoemission measurements the potential barrier to the injection of carriers from various contact materials into anthracene have been determined. Materials most widely used as injecting contacts to anthracene are given in table 2.3.

Space-charge-limited-currents have been widely observed in organic thin films. In fact, space-charge-limited-currents have proven to be an unusual tool for measuring defect structure usually associated with organic thin films. Sussman [170] has measured space-charge-limited-currents in thin films of the compound copper phthalocyanine using metallic ohmic contacts. A complete study of the current as a function of voltage, temperature, thickness and illumination has indicated the presence of charge carrier traps in which they are exponentially distributed within the forbidden energy gap. The analysis of the results enables the determination of the parameters related to the trap density and distribution.

Hwang et al [78] have investigated, both theoretically and experimentally, the current injection into anthracene thin films with traps uniformly and non-uniformly distributed in energy and space. Their results have shown that for thin films, the spatial trap distribution can never be homogeneous because there always exist dicontinuities between the material and the electrodes. The thinner the film specimen used for experimental

TABLE 2.3

MATERIALS USED AS CARRIER INJECTION ELECTRODES TO ANTHRACENE

Electrodes from	Electron injecting materials	Hole injecting materials	Reference
Liquid contacts	A solution of negative anthracen ion sodium + anthracene + tetrahydrofuran	A solution of positive anthracene ion (1) $KI+I_2$ in water (2) $AlCl_3$ + anthracene + nitromethane	[70,71]
	Lithium + anthracene + nitromethane	$AlCl_3$ + anthracene + ethylenediamine	[195]
Solid contacts	Sodium-potassium alloy	Evaporated gold	[127]
	Na + tetrahydrofuran + anthracene	(1) $AlCl_3$ + anthracene + nitromethane (2) Silver paste (3) Gold paste (4) Evaporated silver (5) Evaporated Al (6) Conducting glass	[189]
	(1) N^+-Si wafers covered with 20-40 Å SiO_2 (2) A fine grid structure of evaporated Al on glass substrate oxidized to approximately 50 Å of Al_2O_3.	(1) Evaporated transparent film of Cu_2O-CuI (2) Evaporated S_e-T_e Alloy (3) Calloidal black p+ paste (4) Iodized Cu paste	[44]
	Carbon-fibers	Evaporated indium	[191]

studies, the more is the influence of the form of spatial distribution of traps on the current-voltage characteristics.

Space-charge-limited-currents in polycrystalline films of cadmium sulphide with metalic contacts have also been reported by several authors [26,45,169].

Experiments on the transient space-charge-limited-currents in thin anthracene films have been carried out by several authors [75,91,106] in an effort to determine the trap density and distribution in this material. They used sandwich type cells with two conducting glass electrodes illuminated through one of the electrodes by pulsed light, and applied a constant electric field across the film. The rate of the decay of the photocurrent is used for the determination of the concentration and depth of charge carrier traps.

In the course of investigating space-charge-limited-currents in organic thin films, electrolytic electrodes have been often employed [121,125,151]. The essential difference between electrolytic and metal contacts is that in the former, the currents across the junction are limited by both the charge transport through the solid as well as the rate at which the charge carriers are supplied from the charged species in the electrolytes. Kallmann and Pope and their collaborators [87,88,153], have used iodine in sodium iodide solution and aqueous solution of $Ce(HSO_4)_4$ as electrodes in different experiments on charge

carrier injection into anthracene thin films. Other materials, such as p-terpheynl, p-quaterphenyl and phthalocyanines, have been investigated using electrolytic electrodes [68,121].

2.3.3 Effects of traps

In organic semiconductors two types of carrier trap distributions have been reported [49,60], and they are traps confined in discrete energy levels in the forbidden energy gap; and traps with quasi-continuous distribution of energy levels (normally having an exponential form), having a maximum trap density near the band edges [49,121]. Both types of traps have been extensively investigated in anthracene crystals [14,152,154,155,158,160,163,171,173,179]. Simultaneous presence of both types of carrier trap distribution have also been observed [158,179]. The energy levels and the distribution of carrier traps can be experimentally determined either by space-charge-limited-current method [49], by the thermo-stimulated current method [179] or by the photoemission method [31]. Although these methods may provide some information about the energetic and kinetic parameters of traps, they do not give any hint as to the possible physical nature of traps. Some general considerations have been suggested to relate discrete traps with chemical impurities introduced into the lattice (chemical traps) and to relate the quasi-continuous trap distribution

with the imperfections of the crystal structure (structural traps). For example, it has been shown [75] that tetracene molecules doped into anthracene crystals form shallow discrete traps both for electrons and for holes. Furthermore, measurements of the steady state space-charge-limited-current in single crystals (possibly containing a large quantity of structural defects) and polycrystalline specimens of naphthalene [113], anthracene [121,154,158,174,179], tetracene [10], perylene [130], p-terphenyl [176], p-quaterphenyle [176] and phthalocyanines [63,170] as well as inorganic semiconductors [156] have shown that the currents are controlled by the traps distributed in the forbidden energy band gap following the relation

$$h(E) = \frac{H_b}{kT_c} \exp\left(-\frac{E}{kT_c}\right) \qquad (2.4)$$

where H_b is the total density and T_c is the characteristic temperature for the energy distribution. This indicates that the traps in those specimens may be due to the structural defects. Based on the experimental results, some data of carrier traps in anthracene are listed in table 2.4.

In order to elucidate the effects of traps on space-charge-limited-currents, several investigators have derived the expression for the current-voltage relationship for a trap free case [109,133,141,156] and in the presence of traps [10,79,104,121,134,158,183] for both single and double injection. The results are summarized in tables 2.5, 2.6 and 2.7.

TABLE 2.4

SUMMARY OF PREVIOUS EXPERIMENTAL RESULTS OF HOLE TRAPS IN ANTHRACENE.

Specimen Preparation	Trap Density H_b (cm^{-3})	ℓ (from $J\alpha v^{\ell+1}$)	KT_c (ev)	Trapping Level E_t (ev)	Trap Density N_t (cm^{-3})	Reference
Melt-grown	1.5×10^{19}	1.4	0.035			[155,179]
	2.73×10^{18}	1.5	0.0375			
	1.5×10^{18}	1.64	0.041			
	3.5×10^{13}	4.8	0.12			
	1.1×10^{17}	1.0	0.25			
Vapor-grown	1.2×10^{17}	2.28	0.057			[155,179]
	1.1×10^{13}	2.5	0.0625			
	3.6×10^{15}	2.6	0.065			
Solution-grown	5.75×10^{16}	1.9	0.0475			[155,179]
	1.75×10^{15}	4.2	0.13			
	4.2×10^{14}	5.6	0.14			
Melt-grown (Zone refined)				0.53 ± 0.03 ev	1.5×10^{19}	[158,174,179]
Doped with Tetracene				0.43 ev		[75]
Doped with Perylene				0.25 ev		[75,173]

TABLE 2.5

I-V RELATIONSHIP FOR SINGLE INJECTION (METALLIC ELECTRODES)

h(E)	UNIFORM SPATIAL TRAP DISTRIBUTION	REF.	NON-UNIFORM SPATIAL TRAP DISTRIBUTION	REF.
o	$J = \frac{9}{8} \varepsilon \mu_p \frac{V^2}{d^3}$			[133]
$H_a \delta(E-E_t)$	$J = \frac{9}{8} \frac{\varepsilon\mu_p}{K_a} \frac{V^2}{d^3}$	[104]	$J = \frac{9}{8} \frac{\varepsilon\mu_p}{K_a} \frac{V^2}{d^3_{eff}}$	
	$K_a = 1 + \frac{H_a}{gN_v} \exp(\frac{E_t}{kT_c})$	[121]	$d_{eff} = \{\frac{3}{2} \int_o^d (\int_o^x [1+\eta(S-1)]dt)^{\frac{1}{2}} dx\}^{2/3}$	[78]
$\frac{H_b}{kT_c} \exp(-\frac{E}{kT_c})$	$J = q^{1-\ell} \mu_p N_v (\frac{2\ell+1}{\ell+1})^{\ell+1} (\frac{\ell}{\ell+1} \frac{\varepsilon}{H_b})^{\ell} \frac{V^{\ell+1}}{d^{2\ell+1}}$	[121]	$J = q^{1-\ell} \mu_p N_v (\frac{2\ell+1}{\ell+1})^{\ell+1} (\frac{\ell}{\ell+1} \frac{\varepsilon}{H_b})^{\ell} \frac{V^{\ell+1}}{d^{2\ell+1}_{eff}}$	[78]
	$\ell = T_c/T$	[156]	$d_{eff} = \{\frac{2\ell+1}{\ell+1} \int_o^d [\int_o^x S\, dt]^{\ell/\ell+1} dx\}^{\ell+1/2\ell+1}$	

TABLE 2.6

I-V RELATIONSHIP FOR SINGLE INJECTION (ELECTROLYTIC ELECTRODES)

h(E)	UNIFORM SPATIAL TRAP DISTRIBUTION	REF.	NON-UNIFORM SPATIAL TRAP DISTRIBUTION	REF.
0	$V_a + V = \frac{2}{3} F(0)\, x_{of} \left[1 - \left(1 + \frac{d}{x_{of}}\right)^{3/2}\right]$ $F(0) = \left[q\mu_p p_f(0) \left(\frac{1}{J} - \frac{1}{J_o}\right)\right]^{-1}$ $x_{of} = \frac{\varepsilon}{2q^2 \mu_p p_f^2(0)} \frac{J}{\left(1 - \frac{J}{J_o}\right)^2}$			[128]
$H_a \delta(E-E_t)$	SEE CHAPTER V		SEE CHAPTER V	
$\frac{H_b}{kT_c} \exp\left(-\frac{E}{kT_c}\right)$	SEE CHAPTER V		SEE CHAPTER V	

TABLE 2.7

I-V RELATIONSHIP FOR DOUBLE INJECTION

h(E)	UNIFORM SPATIAL TRAP DISTRIBUTION	REF.	NON-UNIFORM SPATIAL TRAP DISTRIBUTION	REF.
o	$J = \frac{9}{8} \varepsilon \mu_{eff} \frac{V^2}{d^3}$ $\mu_{eff} = \frac{8}{9} \frac{\mu_n \mu_p}{2\mu_o} \frac{[B(\frac{\mu_n}{\mu_o}, \frac{\mu_p}{\mu_o})]^3}{[B(\frac{3\mu_n}{2\mu_o}, \frac{3\mu_p}{2\mu_o})]^2}$			[141]
$H_a \delta(E-E_t)$	$J = \frac{9}{8} \varepsilon \mu_{eff} \frac{V^2}{d^3}$ $\mu_{eff} = \frac{8}{9} \frac{\mu_n \mu_p}{2\mu_o} \frac{1}{K_{an} K_{ap}} \frac{[B(\frac{\nu_{an}}{\mu_o}, \frac{\nu_{ap}}{\mu_o})]^3}{[B(\frac{3\nu_{an}}{2\mu_o}, \frac{3\nu_{ap}}{2\mu_o})]^2}$	[79]	SEE CHAPTER VI	
$\frac{H_b}{kT_c} \exp(-\frac{E}{kT_c})$	SEE CHAPTER VI		SEE CHAPTER VI	

2.3.4 Switching and memory phenomena

Anamalous electrical conductivity phenomena have been observed in thin films of polymers [11,27,52,58], thin films of organic dyes [184] and thin films of aromatic hydrocarbons [50,51,93,176,178]. Field induced switching and memory between two electric conductivity states have been observed. Typically, the initial state is a low conductivity or "OFF" state; when the applied voltage reaches the threshold value the specimen is rapidly switched to a high conductivity "ON" state. These phenomena have been observed by Carchano et al [27] in polymer films of thickness d, between 500-5000$\mathring{A}$, with gold electrodes of an active area of 0.5 x 0.5 mm^2. The "OFF" state has a resistance of 100 Mohm, whereas the "ON" state resistance is in the range of 1-20 ohms. The threshold voltage, V_{TH} is in the range of 50-150 V for the specimen thickness of the range of 670-4000$\mathring{A}$. A current pulse applied to a specimen in the memory state will switch it back to the original "OFF" state. However, after a few switching cycles, the specimen may not function again; generally, the smaller the thickness, the more switching cycles the specimen can sustain. Small sparks on the gold electrodes at each switching cycle and circular holes have been observed on the failed specimens.

Szymanski et al [178] have observed the switching effect in amorphous tetracene films of thickness between

1000-6000 Å. The resistance of the device is 10^{10} ohms in the "OFF" state and 10^5 ohms in the "ON" state. The threshold voltage is typically 4-8 V for d = 6000 Å. In the "OFF" state, the current is superlinear with the applied voltage, and it is very sensitive to temperature and illumination. Such behaviours have been attributed to space-charge-limited-currents with a continuous distribution of traps. The "ON" state ohmic current is both temperature- and photo-insensitive, and this has been attributed to trap-free space-charge conduction. The trap-free case is reached when the injection levels become sufficiently high that the traps are outnumbered by the free charge carriers.

Kevorkian et al [93] have reported their observation of switching and memory phenomena in tetracene and perylene (pure and doped) films with different metal electrodes. They concluded that the switching phenomena in doped organic films is associated with donor-acceptor complexes potentially leading to reproducible switching behaviour, and that pure organic films may undergo switching via electrode material diffusion to form a filament of metalic nature.

In Chapter IV, some new switching and memory phenomena in anthracene thin films are reported.

2.3.5 Biological thin films

Several investigators [101,138] have studied the electric conductivity of some biological thin films. Liang et al [107]

have investigated the electric conductivity of thin films of proteins and reported that the relative humidity strongly affects the electric conductivity. This has been explained in terms of water molecules adsorption on the film surfaces. The primary effect of water is to lower the activiation energy for electron injection into the conduction band of a protein. It should be mentioned that the investigation of the effects of water on the electric conductivity of biologically important materials is so important, since the biological systems are normally embeded in a quite hydrous medium.

The photoconductivity of films of hemoglobin, gelatin and gelatin sensitized with anramine has been studied by Nelson [138]. The photoconductivity rises on illumination with light having a wavelength shorter than 3000 $\mathring{A}$, i.e. in the region of the intrinsic absorption of the proteins.

Switching and memory phenomena have also been observed in several thin films of biologically important materials such as proteins [64,65] and cholesterol [168].

CHAPTER III

MEASUREMENTS OF THE OPTICAL CONSTANTS OF ANTHRACENE THIN FILMS BY ELLIPSOMETRY

In the past decade, ellipsometry has been extensively used to investigate the optical properties of thin films and to measure the thickness of extremely thin films. Although, this method has been successfully applied to uniaxially anisotropic substrates and films [9,40,41,131], there is, so far, no report in the literature about its application to biaxially anisotropic films. In this chapter we describe the technique of extending ellipsometry to biaxially anisotropic films for measuring the thickness and the optical constants of anthracene thin films.

3.1 ELLIPSOMETRY

Reflection and refraction of light at an interface separating two homogeneous isotropic and anisotropic media have been treated by several investigators [65,162]. In the following, we shall describe briefly the principle of ellipsometry based on the theory of reflection and refraction.

We shall use the following conventions to denote our system. The plane of incidence is the xz plane, and the media interfaces are parallel to the xy plane, the z axis

being normal to the interfaces. A monochromatic beam of wavelength λ in an ambient isotropic medium of refractive index n_1 (medium 1) is incident on an anisotropic film of thickness d (medium 2) deposited on an isotropic transparent substrate of refractive index n_3 (medium 3). For an anisotropic and optically absorbing film, the refractive index is complex, expressed by

$$\begin{aligned} n_x^* &= n_x - ik_x \\ n_y^* &= n_y - ik_y \\ n_z^* &= n_z - ik_z. \end{aligned} \tag{3.1}$$

By denoting the angle of incidence between the incident light wave and the normal to the reflecting surface (the z direction) as ϕ_1 in medium 1, we obtain the phase constants, $\alpha_s, \beta_s, \alpha_p$ and β_p, according to Schopper's theory [152],

$$\left.\begin{aligned} \beta_s^2 - \alpha_s^2 &= n_x^2 - k_x^2 - n_1^2 - \sin^2\phi_1 \\ \beta_s \alpha_s &= n_x k_x \end{aligned}\right\} \tag{3.2}$$

$$\left.\begin{aligned} \text{and } \beta_p^2 - \alpha_p^2 &= n_y^2 - k_y^2 - n_1^2 \sin^2\phi_1 \frac{(n_y^2 - k_y^2)(n_z^2 - k_z^2) + 4n_y k_y n_z k_z}{(n_z^2 + k_z^2)^2} \\ \beta_p \alpha_p &= n_y k_y + n_1^2 \sin^2\phi_1 \frac{n_z k_z (n_y^2 - k_y^2) - 2n_y k_y (n_z^2 - k_z^2)}{(n_z^2 + k_z^2)^2}; \end{aligned}\right\} \tag{3.3}$$

where the subscripts p and s denote light polarized parallel

and perpendicular to the plane of incidence. In terms of $\alpha_s, \beta_s, \alpha_p$ and β_p, Fresnel's coefficients for the interfaces 12 between media 1 and 2 and 23 between media 2 and 3 are given by

$$r_{12}^s = \frac{n_1\cos\phi_1 - \beta_s + i\alpha_s}{n_1\cos\phi_1 + \beta_s - i\alpha_s}$$

$$r_{12}^p = \frac{-(n_y - ik_y)^2 \cos\phi_1 - n_1 (\beta_p - i\alpha_p)}{(n_y - ik_y)^2 \cos\phi_1 + n_1 (\beta_p - i\alpha_p)} \qquad (3.4)$$

and

$$r_{23}^s = \frac{\beta_s - i\alpha_s - n_3 \cos\phi_3}{\beta_s - i\alpha_s + n_3 \cos\phi_3}$$

$$r_{23}^p = \frac{n_3 (\beta_p - i\alpha_p) - (n_y - ik_y)^2 \cos\phi_3}{n_3 (\beta_p - i\alpha_p) + (n_y - ik_y)^2 \cos\phi_3}, \qquad (3.5)$$

where ϕ_3 is the angle between the transmitted wave and the normal to the surface in medium 3. The amplitude reflectances R_s and R_p of a film-covered substrate, due to multiple reflections of polarized light between two interfaces, are given by

$$R_s = \frac{r_{12}^s + r_{23}^s \exp[4\pi (\alpha_s - i\beta_s) d/\lambda]}{1 + r_{12}^s r_{23}^s \exp[4\pi (\alpha_s - i\beta_s) d/\lambda]} \qquad (3.6)$$

$$R_p = \frac{r_{12}^p + r_{23}^p \exp[4\pi (\alpha_p - i\beta_p) d/\lambda]}{1 + r_{12}^p r_{23}^p \exp[4\pi (\alpha_p - i\beta_p) d/\lambda]}. \qquad (3.7)$$

According to the general definition in ellipsometry, the ratio R_p/R_s is related to the ellipsometric parameters [7], the angle Δ defined as the relative phase difference, and the angle ψ defined as the arctangent of the relative amplitude change of the parallel and the normal components of the polarized light,

$$\frac{R_p}{R_s} = \tan \psi \exp (i \Delta). \qquad (3.8)$$

It should be noted, however, that the values of Δ and ψ at extinction of the light beam depend on the orientation of the optic axis. Dignam and Moskovitz [42] have pointed out that extinction can be obtained for anisotropic reflectors only when the plane of incidence contains one of the optic axis lying in the surface of the reflector.

If all of the optical constants of a thin film and its substrate are known, the film thickness can easily be determined by a direct measurement of Δ and ψ at a fixed angle of incidence.

In anthracene films, optical absorption is negligibly small in most of the visible wavelength region [124] though it becomes appreciable for wavelengths shorter than 4000 $\mathring{A}$. The value of k is thus negligibly small as compared with n; therefore, for mathematical simplicity, we assume that both the anthracene films and glass substrates are transparent in the visible region. By use of the following parameters

$n_1 = 1.0$
$k_1 = 0$ } (medium 1: Air)

$n_x = 1.570$
$n_y = 1.817$
$n_z = 2.220$
$k_x = k_y = k_z = 0$ } (medium 2: Anthracene)

$n_3 = 1.526$
$k_3 = 0$ } (medium 3: Borosilicate glass)

$\phi_1 = 50^0$
$\lambda = 5461\ \mathring{A}$

(the parameters for anthracene films being assumed to be the same as those of bulk anthracene crystals [192]), we have computed Δ and ψ as functions of film thickness; the results are shown in Fig. 3.1. The anisotropic behaviour of the anthracene films results in a spiral-shaped Δ - ψ curve rather than a closed one, as in the case of isotropic films. Figure 1 can be used to determine the film thickness by measuring Δ and ψ at $\phi_1 = 50^0$ without previous knowledge of the order of magnitude of the film thickness. Figure 3.1 assumes constancy of all optical parameters over the range of film thicknesses measured. This is true only for thick films. For very

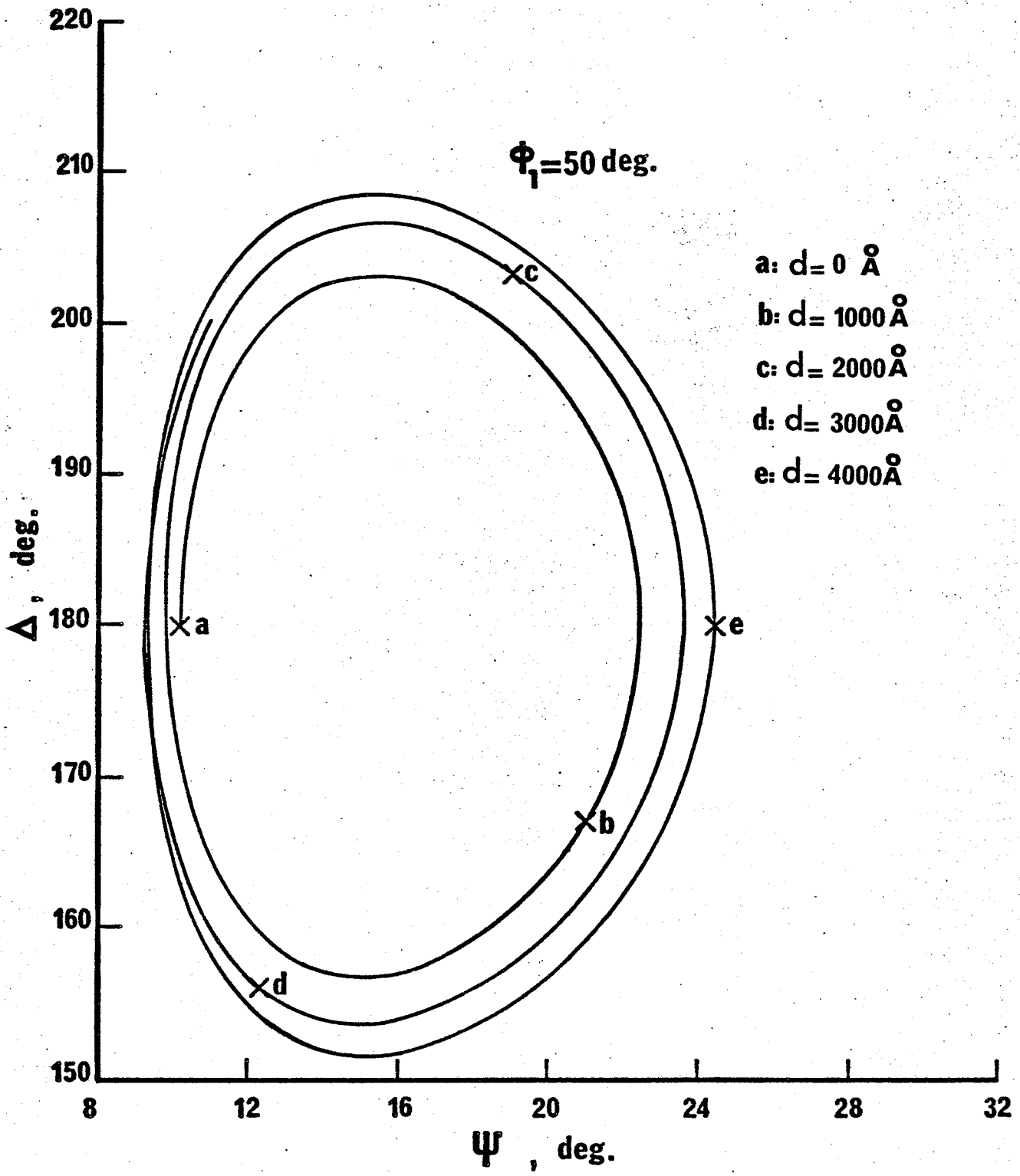

Fig. 3.1 Dependence of Δ and Ψ on the thickness of anthracene thin films on borosilicate glass substrates

thin films, those parameters are generally thickness-dependent. In order to determine both the optical constants and the thickness of a film, a set of ellipsometric measurements of Δ and ψ at various angles of incidence ϕ is required.

From Eqn. (3.8), we obtain

$$\Delta = \tan^{-1}\left\{\frac{\mathrm{Im}(R_p)}{\mathrm{Re}(R_p)}\right\} - \tan^{-1}\left\{\frac{\mathrm{Im}(R_s)}{\mathrm{Re}(R_s)}\right\} \tag{3.9}$$

and

$$\psi = \tan^{-1}\left\{\frac{[\mathrm{Re}(R_p)]^2 + [\mathrm{Im}(R_p)]^2}{[R_e(R_s)]^2 + [\mathrm{Im}(R_s)]^2}\right\}^{\frac{1}{2}} . \tag{3.10}$$

An error function can now be defined as

$$f_e(n_x, n_y, n_z, d) = \sum_{i=1}^{N} W_i \left[(q_\Delta^i)^2 + (q_\psi^i)^2\right] , \tag{3.11}$$

where

$$q_\Delta^i = \Delta_{obs}^i - \Delta_{cal}^i \tag{3.12}$$

$$q_\psi^i = \psi_{obs}^i - \psi_{cal}^i \tag{3.13}$$

Δ_{obs}^i, ψ_{obs}^i, Δ_{cal}^i and ψ_{cal}^i are, respectively, the observed (or measured) and calculated values of Δ and ψ at the i^{th} observation point, W_i is a weighting factor, and N is the number of the observation points. The least-square technique can then be applied to find the values of the unknown parameters, namely n_x, n_y, n_z and d, by curve-fitting the experimental points.

The algorithm, [112] starting with an initial set of values for the unknown parameters estimated to be within 20 - 25% of the exact values, will yield accurate values of the unknown parameters by minimizing iteratively the error function. In the present investigation, we used the least-square technique on a gradient-search basis.

To aid in determining the experimental range of the angles of incidence ϕ_1 and the corresponding weighting factors, we plot $|R_p|/|R_s|$ as a function of ϕ_1 in Fig. 3.2 using $d/\lambda = 0.18$, $n_x = 1.57$, $n_y = 1.82$ and $n_z = 2.22$. The appropriate range of ϕ_1 should be within the region that contains the largest deviation between the observed and predicted values of tan ψ. In Fig. 3.2, ϕ_1 took 30 values within the range from 45^0 to 75^0 at 1^0 intervals. The value 5 was used for W_i for the points between 50^0 and 65^0 and the value 1 was used for W_i for other values of ϕ_1. In order to guess an initial set of values for the unknown parameters, the values of n_x, n_y and n_z were first constrained to constant values (for instance, the values for bulk crystals); then a reasonable estimate for d was obtained after a few iterations. Such an estimated value was then used together with the other three parameters in a four-parameter search. This usually required fewer iterations, and the convergence was always achieved if the initial values were within 20 - 25% of the final-solution set. The accuracy of the final result was within $\pm$ 0.1%. This standard least-square approach had been previously applied

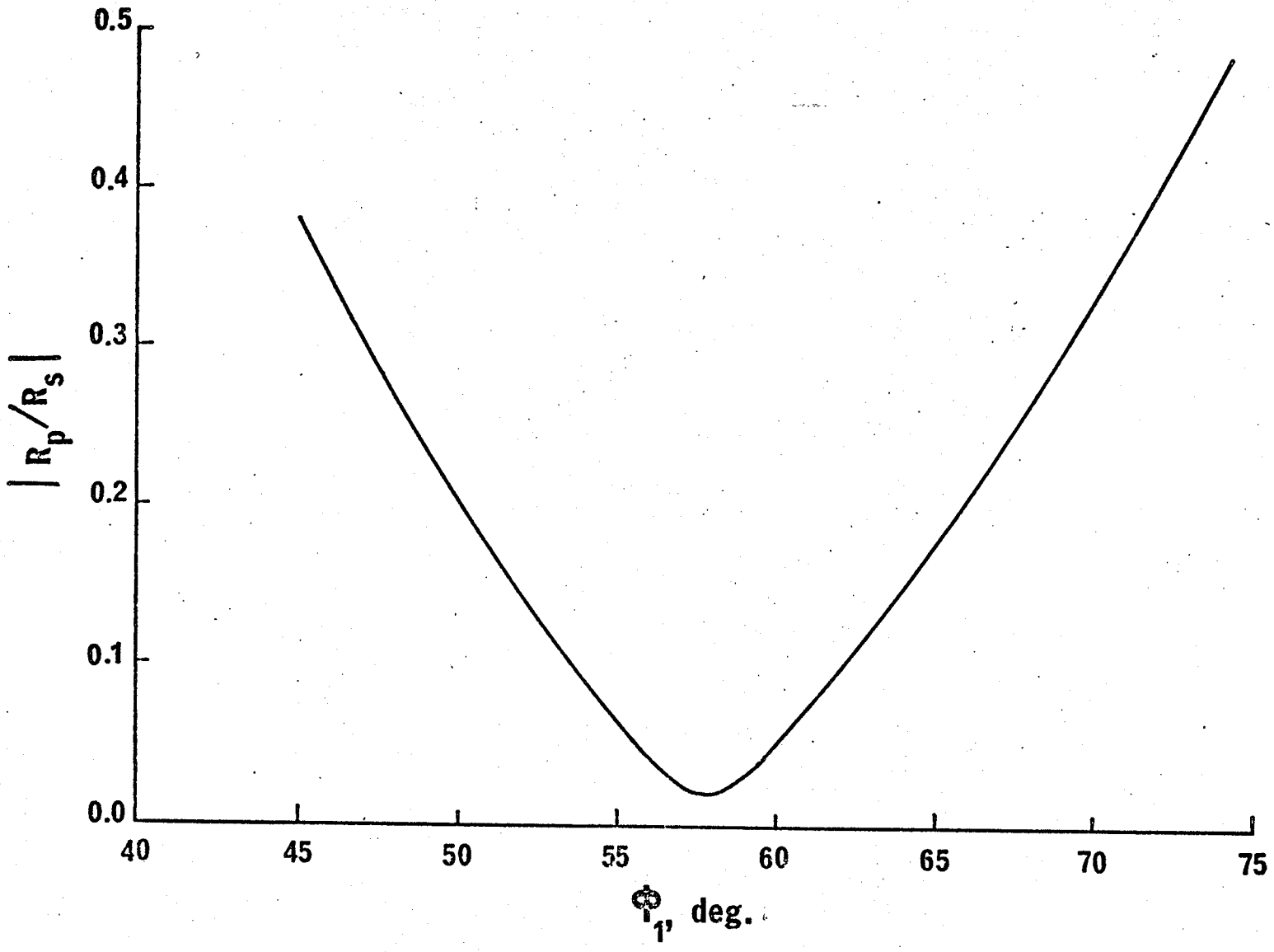

Fig. 3.2 $|R_p/R_s|$ as a function of angle of incidence

to similar problems in ellipsometry, with satisfactory results [15, 57,112,131].

3.2 EXPERIMENTAL TECHNIQUES

The crystal structure of anthracene is based on a monoclinic unit cell with cell dimensions [123] a = 8.542 $\mathring{A}$, b = 6.038 $\mathring{A}$, c = 11.184 $\mathring{A}$ and $\beta = 124^0\ 42'$. There are two molecules per unit cell and the structure is closely packed, and each molecule has twelve nearest neighbors. The heat of sublimation is 22 Kcal $mole^{-1}$, the melting point is 216.5°C and the density is 1.24 gm cm^{-3}. The bonds have the double-bond characters and the molecules are held together mainly by van der Waals-London forces. With such a structure, the crystal is biaxially anisotropic and the refraction is, therefore, governed by three principle refractive indicies. The optic plane is [010].

The anthracene-film specimens were fabricated by vacuum sublimation of anthracene crystals under a vacuum of 10^{-6} torr onto glass substrates of size 22 x 22 mm (corning microscope cover glass) at a source temperature of 70°C. The substrates were kept at -130°C during deposition by means of a cooling tank to increase the effective sticking coefficient of the film [59]. The thickness of the substrate in 0.018 $\pm$ 0.002 cm. Deposition was started and terminated by means of a controlling mechanical shutter, and a thin copper mask produced by photoetching was inserted between the source

and the substrate to obtain the desired shape of the film, the shape of the thin films used being circular with a diameter of 0.6 cm. Substrate and source temperatures were measured by means of copper-constantan thermo couples. The experimental set is shown in Fig. 3.3. Because anthracene is highly volatile, the vacuum chamber was filled with dry nitrogen gas and kept at a pressure of 5×10^{-3} torr after deposition and during the slow changing of the specimen temperature from -130^{0}C to room temperature.

Before ellipsometric measurements, the specimens were carefully examined.

(i) They were first examined under a Zeiss polarizing microscope with a magnification of 400. Specimens that were not uniform in thickness were discarded.

(ii) The surface textures of the uniform specimens were then studied by use of a Cambridge mark II scanning electron microscope. Before this study, the specimen surfaces were vacuum-coated with a thin gold layer, in order to avoid charge accumulation on the specimen surfaces due to the low conductivity of anthracene. The scanning electron micrographs for a typical anthracene film surface shown in Fig. 3.4 inciate a fairly smooth surface.

(iii) The crystallographic structure of the films was studied by means of x-ray diffraction. A Philips horizontal goniometer x-ray unit was used with Cu Kα radiation of wavelength 1.542 $\mathring{A}$. The reflection was measured from scattering angle

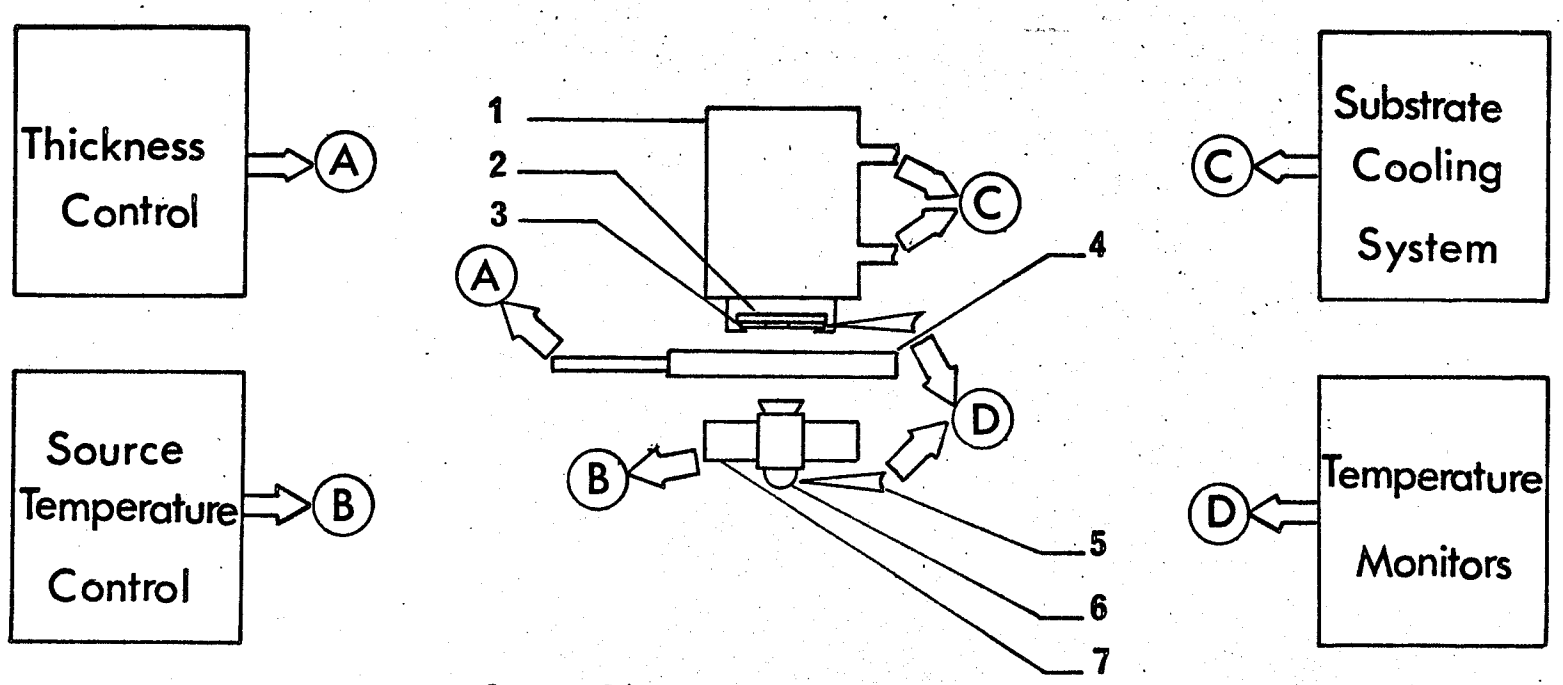

1 cooling tank
2 substrate
3 mask
4 shutter
5 thermocouple
6 crucible
7 heater

Fig. 3.3 The assembly inside the vacuum chamber for fabrication of thin films

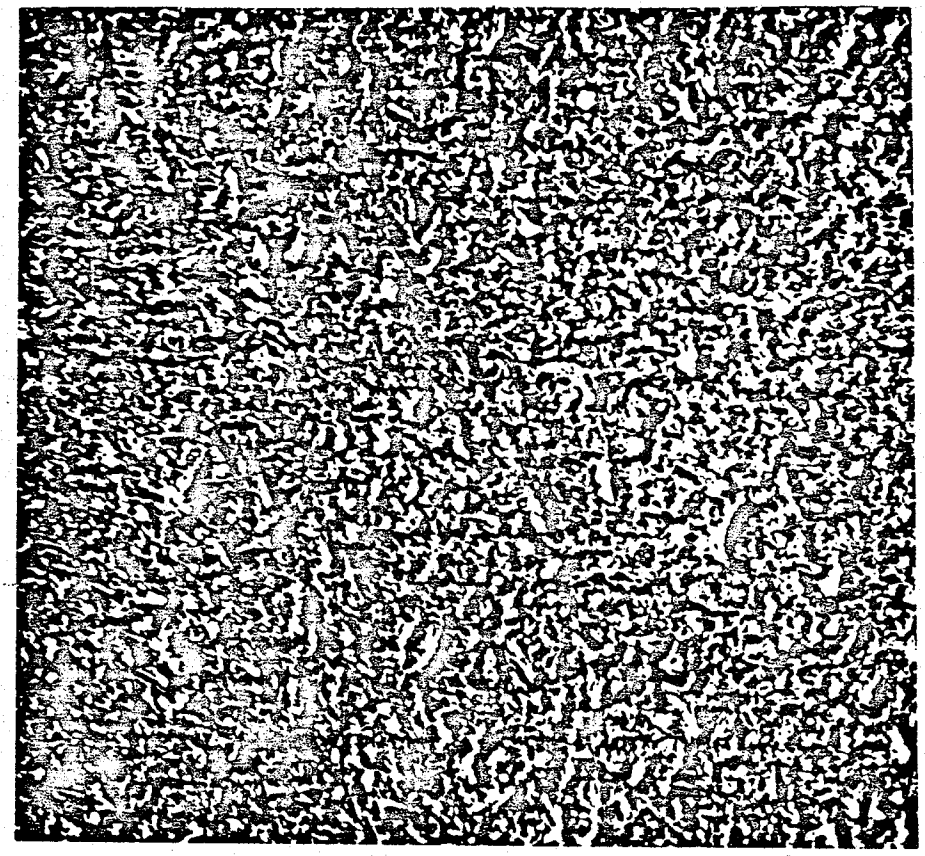

Fig. 3.4 Scanning electron micrograph of typical anthracene film surface. Film thickness = 4000 Å, magnification = x 2,500

$2\theta = 3^0$ to $2\theta = 50^0$ at a scanning speed of 2^0/min with a slit divergence of 0.25^0 and 3db attenuation. Figure 3.5 shows the x-ray diffraction amplitude as a function of scattering angle. To determine the Miller indicies $hk\ell$ of the reflecting planes, the ASTM powder-diffraction file and the expression for $\sin^2\theta_{hk\ell}$ for monoclinic crystals [95]

$$\sin^2\theta_{hk\ell} = \frac{\lambda^2}{4}\left[\frac{h^2/a^2 + k^2/b^2 + \ell^2/c^2 - 2h\ell\cos\beta/ac}{\sin^2\beta}\right] \qquad (3.14)$$

were used. Table 3.1 summarizes the results obtained from the x-ray diffraction experiment in comparison with those given in the ASTM powder-diffraction file. The close agreement between the two results indicates that the film has a preferred orientation with ab plane parallel to the substrate surface.

(iv) The optical absorption spectrum was measured with a Cary 14 spectrophotometer; the results are shown in Fig. 3.6. The absorption spectrum resembles that of bulk crystalline or dilute anthracene [22] in the corresponding band, though in certain respects, it is different. For example, the peaks are shifted towards shorter wavelengths; the highest peak for the crystal is located at 3950 $\mathring{A}$, whereas it is at 3670 $\mathring{A}$ for the film. Also, the first peak for the film is more distinguishable.

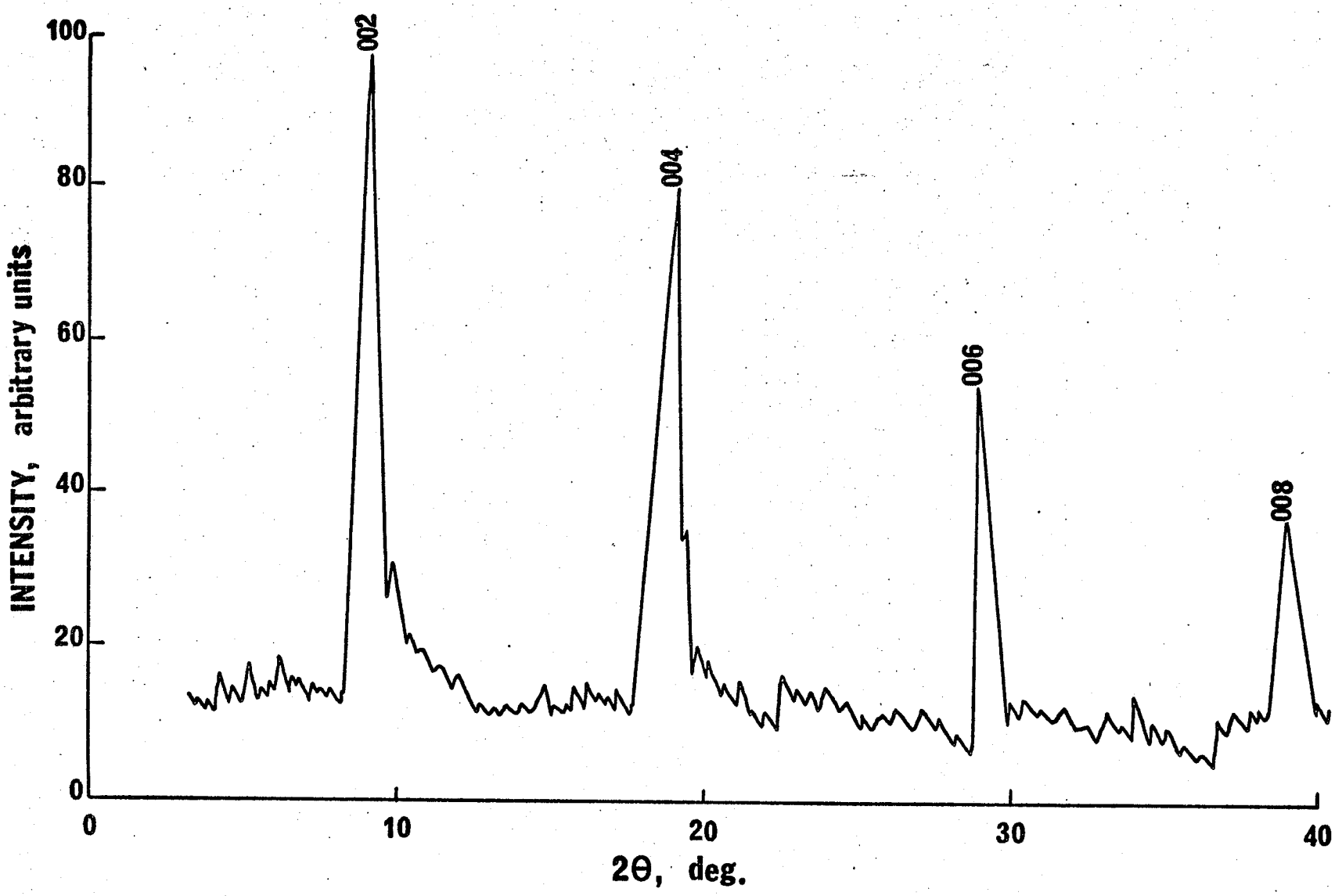

Fig. 3.5 Diffraction amplitude as a function of scattering angle for anthracene thin film

TABLE 3.1 COMPARISON OF THE X-RAY DIFFRACTION DATA OBTAINED FROM THE DIFFRACTION PATTERN WITH THOSE FROM THE ASTM POWDER-DIFFRACTION FILE

Peak	2θ	Interplanar spacing, Å		$\sin^2\theta_{hk\ell}$		h k ℓ
		measured	calculated	measured	calculated	
1	9.7	9.11845	9.00	0.00715	0.00704	002
2	19.4	4.57600	4.53	0.02762	0.02817	004
3	29.2	3.05808	3.03	0.06354	0.06339	006
4	39.3	2.29267	—	0.11308	0.11269	008

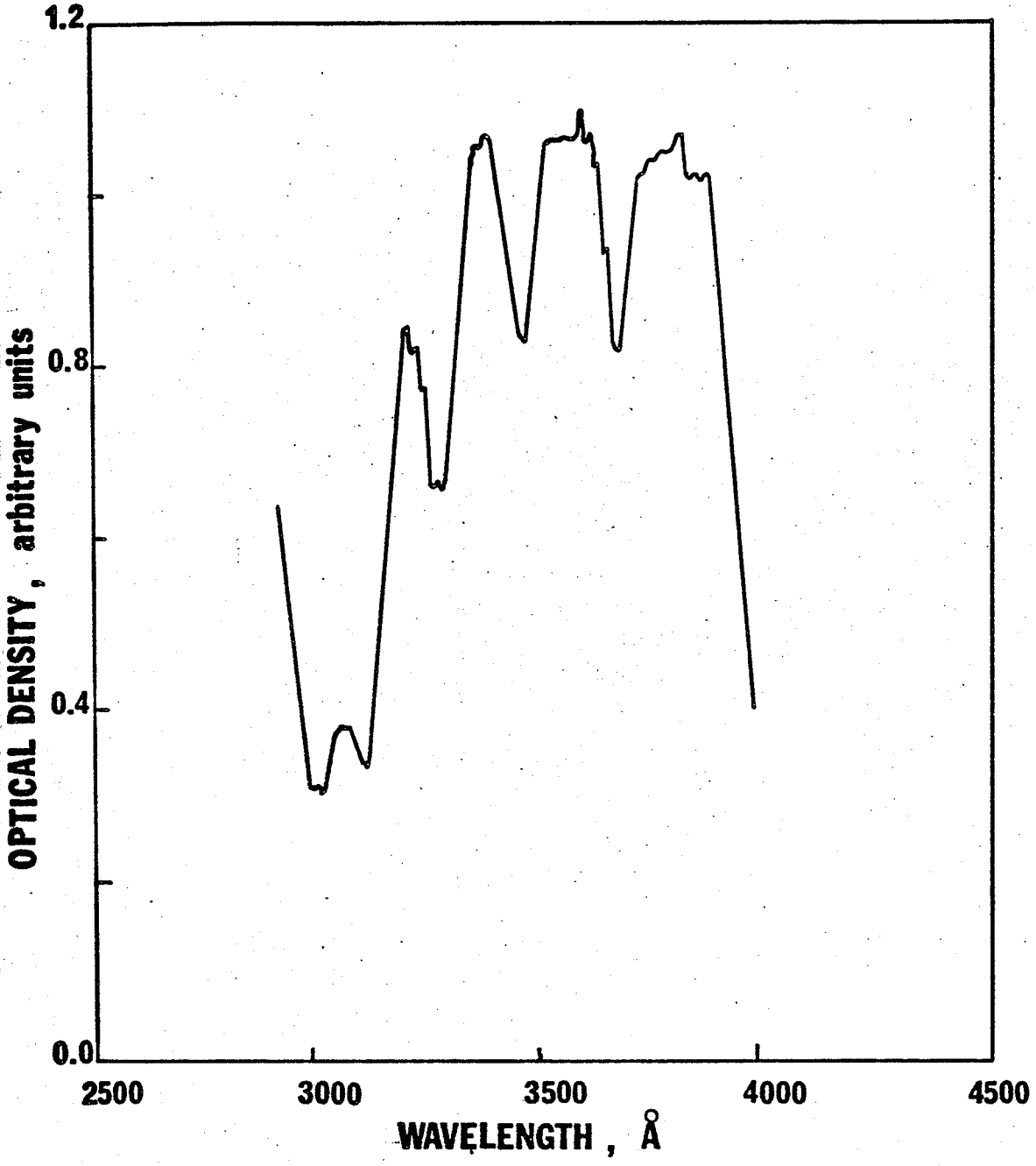

Fig. 3.6 The optical absorption spectrum of the combination of anthracene film and a glass substrate

We produced several specimens of about the same thickness in one batch, some of which were used for these tests; the rest were used for ellipsometric measurements. A Gaertner type L119 ellipsometer in the PQSA arrangement was used in conjunction with a Bauch and Lomb grating monochromator throughout the present investigation. As shown in Fig. 3.7, the ellipsometric measurements were made by null setting the polarizer and analyzer, the errors in Δ and ψ being within $\pm$ 0.005°. The shortest wavelength that could be used, 3600 Å, was limited by the quality of the optical elements of the ellipsometer, whereas the longest, 6000 Å, was limited by the photomultiplier sensitivity. Measurements were performed at 250 Å wavelength intervals, at room temperature (20°C). For film specimens, a polarization microscope was used to determine the direction of the optical axes with an accuracy [110] of 1-2°; for bulk-anthracene specimens it could be determined by direct observation [137].

3.3 RESULTS AND DISCUSSION

With the ellipsometric data Δ and ψ measured at 30 angles of incidence ϕ_1 at 1° intervals, the calculation of n_x, n_y, n_z and d was first carried out for the thickest film, whose thickness was estimated by microbalance. These preliminary results were then used to initialize the iterative scheme for the next-thinner film and so on. For the determination of the dispersion of n_x, n_y and n_z, we started with the calculation for λ = 5461 Å;

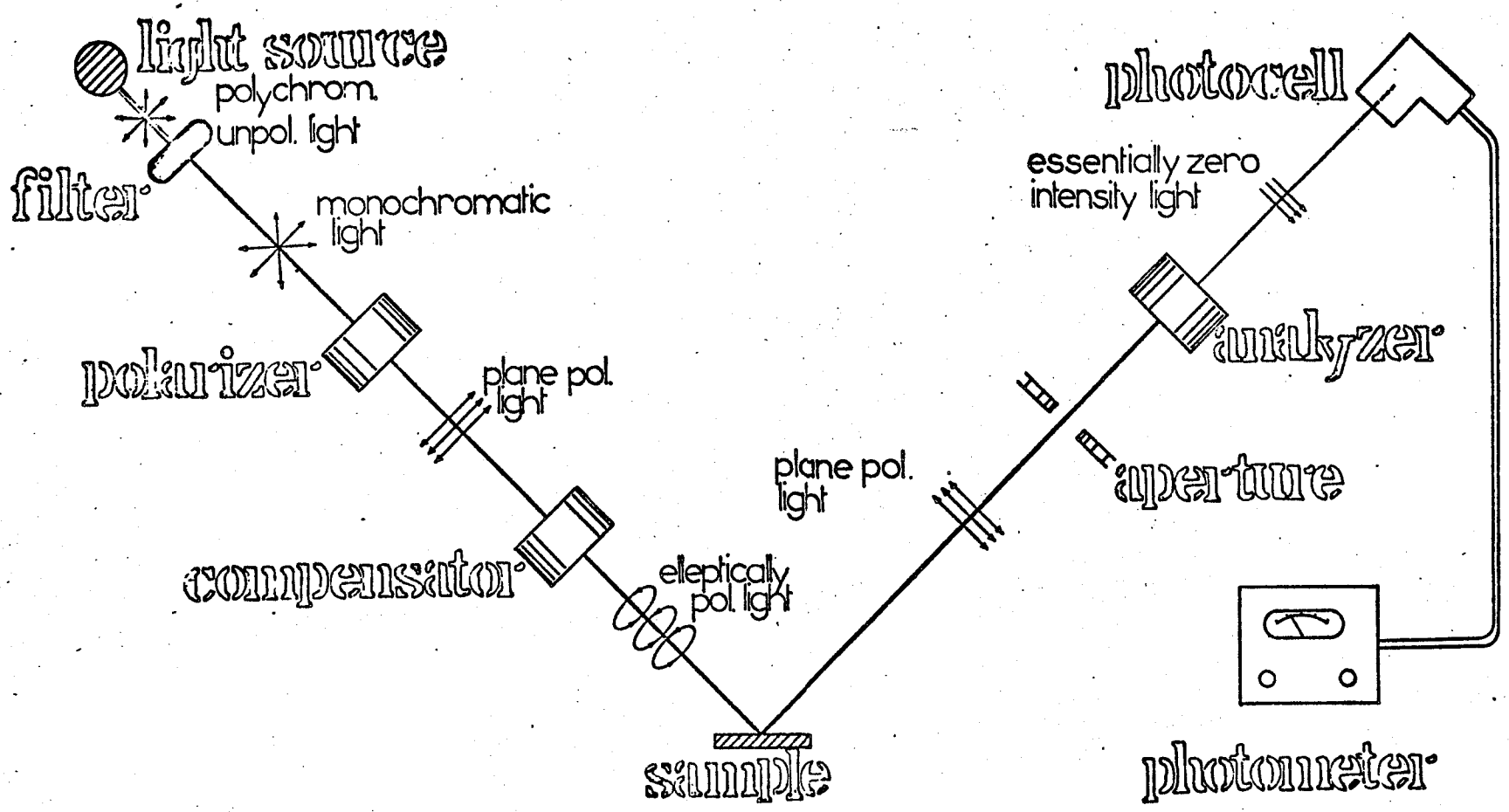

Fig. 3.7 The component parts of the ellipsometer

the results were used to initialize the iterative scheme for next-shorter and longer wavelengths. It should be noted that the ratio of substrate thickness to wavelength is larger than 500 for the shortest wavelength and larger than 320 for the longest wavelength. Moreover, the back surface of the substrate was coated with a black material to eliminate the reflection from it [157]. This suggests that the substrate can be considered an infinite medium as compared with the film thicknesses in the present investigation. The dependence of n_x, n_y and n_z on the wavelength (λ) and film thickness (d) is shown in Figs. 3.8 and 3.9. Figure 3.8 shows that the anthracene is optically anisotropic and that the z polarization exhibits a behaviour different from the others, as expected from the arrangement of the molecules in the crystal. Figure 3.9 shows that the refractive indicies in all three directions decrease monotonically with increasing film thickness, and approach a constant value at film thicknesses greater than about 10 times the wavelength. Because such a great thickness is required before the refractive indicies become independent of thickness, it is unlikely that the mechanism responsible for the thickness dependence is similar to that for semiconductor films [67]. However, our results can be explained as due to the interaction between surface states and excitons near the anthracene film surfaces.

The effect of the crystal surface on the behaviour of excitons has been studied by several investigators [38,165].

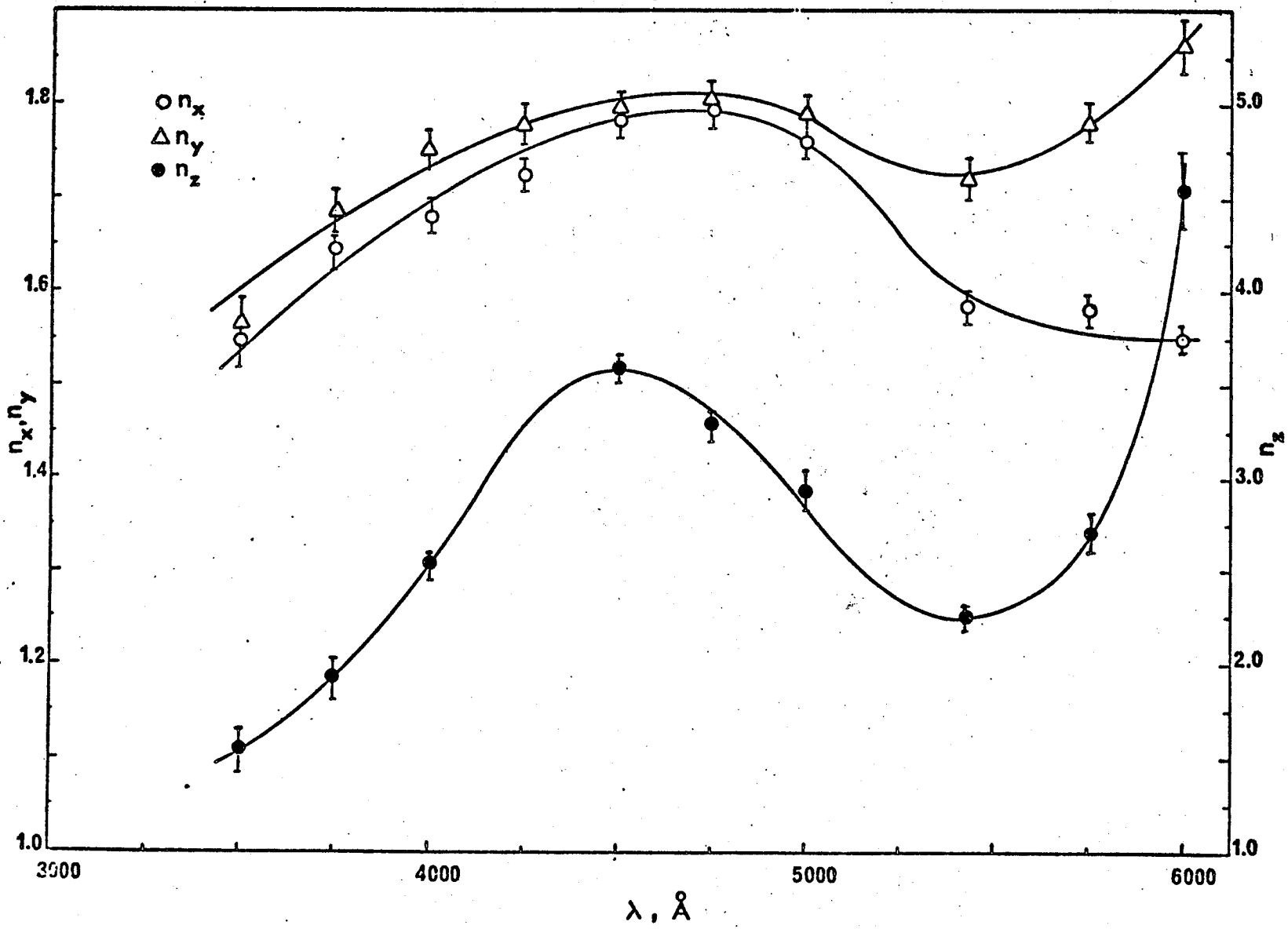

Fig. 3.8 n_x, n_y and n_z of anthracene films as functions of wavelength (d = 4000 Å)

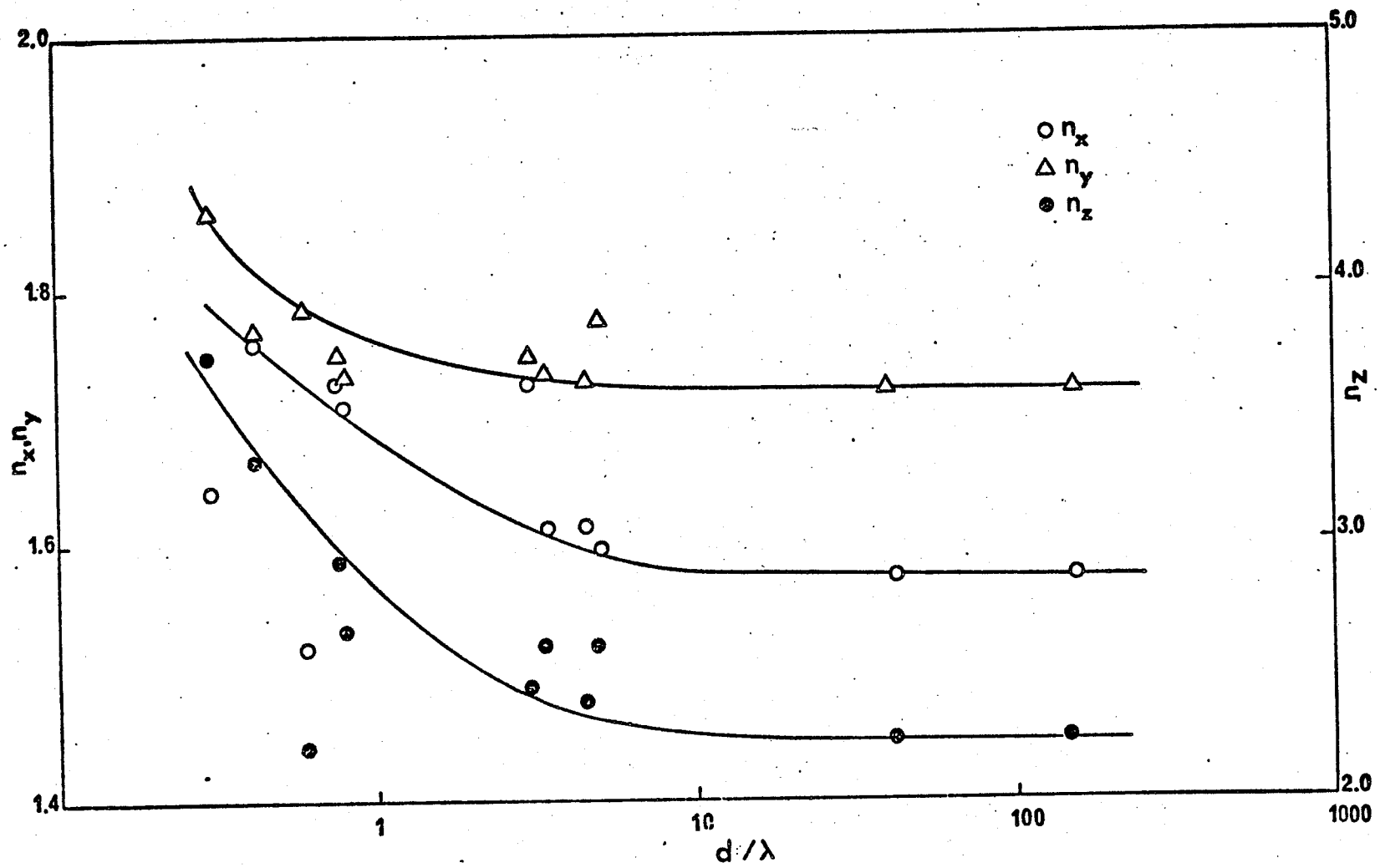

Fig. 3.9 n_x, n_y and n_z of anthracene films as functions of d/λ (λ = 5461 Å)

Defects in the crystal structure, such as the termination of lattice periodicity, would scatter mobile electrons and result in the localization of excitons on the surface. The energy levels occupied by surface excitons are different from those occupied by volume excitons. The number of lattice planes into which the surface excitons can penetrate is dependent on the depth of penetration of the surface perturbations. Thus, surfaces with mosaic structures may cause surface excitons to appear at interval surfaces. Furthermore, rapid sublimation would produce a high surface to volume ratio [89], and, hence, increase the density of surface states. Surface imperfections act to decrease the degree of surface order, thus raising the energy levels. This may account for the observed shift in the peaks in the absorption spectrum towards shorter wavelengths for their films, as shown in Fig. 3.6, as compared with the peaks for bulk crystals.

Surface states play an important role in retarding the energy migration, and hence altering the contribution of excitons to the optical constants. As the film thickness decreases, the surface-to-volume ratio increases, thus causing an increase in the effect of the localization of surface excitons on the retardation of energy migration. This may explain why a thinner film has a higher value of refractive indices as shown in Fig. 3.9. For thick films the number of surface excitons becomes small as compared with the number of cells in the bulk [8], thus the refractive indices become practically independent of film thickness

because the effect of surface states becomes insignificant. That both the exciton lifetime and light transmissivity in anthracene films are dependent on film thickness [23,92] may be associated with the effect of surface states on excitons.

Because the binding energy of molecules within a single plane is much larger than that between planes for the anisotropic crystals with a layer structure, the optical behaviour in the z-polarization is, therefore, different from that in the x or y polarization, as shown in Figs. 3.8 and 3.9.

3.4 CONCLUDING REMARKS

The technique of ellipsometry has been used to measure the refractive indicies and thickness of biaxially anisotropic anthracene thin films. The refractive indicies in all directions decrease with increasing ratio of film thickness to wavelength and reaches a practically constant value for the ratio higher than 10. This thickness dependence phenomena is attributed to the effect of surface states on the contribution of excitons to the optical constants.

CHAPTER IV

SWITCHING AND MEMORY PHENOMENA IN ANTHRACENE THIN FILMS

Switching phenomena have been observed in several organic thin films [27,93,168,178] and biological materials [64,65,74]. In this chapter, some new switching and memory phenomena in anthracene thin films are given.

4.1 EXPERIMENTAL TECHNIQUES

The metal-anthracene-metal structure was fabricated by vacuum deposition techniques. A set of base metalic electrodes were vacuum deposited onto a Corning microscope cover glass substrate (size 22 mm x 22 mm x 0.18 mm). The copper masks produced by photoetching were used to obtain the desired electrodes shapes. To avoid possible contamination of anthracene by metal vapor, the anthracene thin film was fabricated in another vacuum chamber using vacuum sublimation technique as described in Chapter III. Slow annealing was necessary in order to prevent rupture of the film and base electrodes due to the large difference in their thermal expansion coefficient. After the anthracene thin film is fabricated, the counter metalic electrode was then vacuum deposited onto it in the first vacuum chamber. During this

last deposition, the specimen was cooled at -70°C in order to obtain a fairly good contact between the counter electrodes and the thin film. Metalic electrodes of aluminum and silver were used and, in some cases, silver paste was used for counter electrodes but all these electrodes give practically the same results. The effective area of the electrodes is about 1 x 1 mm^2 and the electrode thickness is about 20 μm. A typical structure of the specimens is shown in Fig. 4.1. Thin silver wire leads were then attached to the electrodes by means of silver paste. The film thickness was measured by an ellipsometer and the film uniformity and texture were examined under a scanning electron microscope , before they were used for experiments, as described in Chapter III. The current-voltage characteristics of the different specimens were displayed on a storage oscilloscope (Tektronix 545) with a series current limiting resistor, together with a 100 Ohm resistor to monitor the specimen current. The current-voltage characteristics were also measured with a Keithly 601 electrometer. The specimen temperature was measured by a Hewlett Packard thermometer type 2802A.

4.2 EXPERIMENTAL RESULTS

4.2.1 Switching phenomena

Fig. 4.2 shows a typical dc current-voltage (I-V) characteristic for a silver-anthracene-silver specimen,

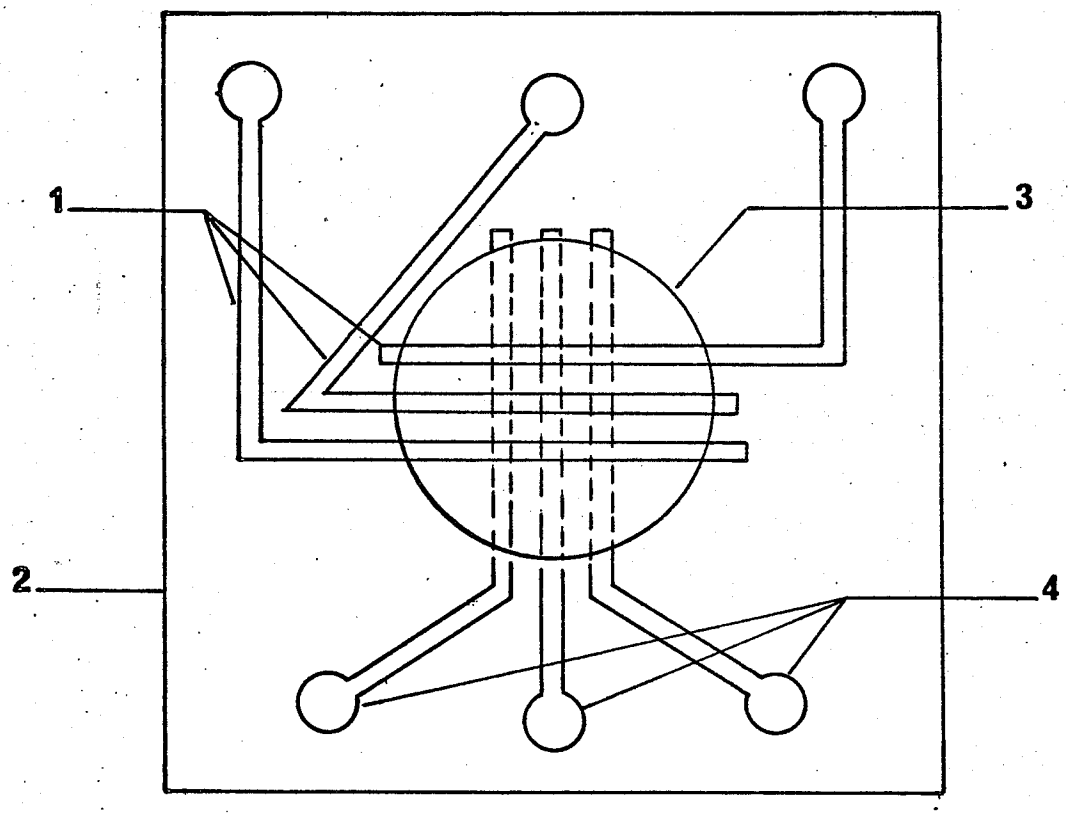

1 top electrodes 3 thin film
2 substrate 4 bottom electrodes

Fig. 4.1 Typical electrodes arrangement

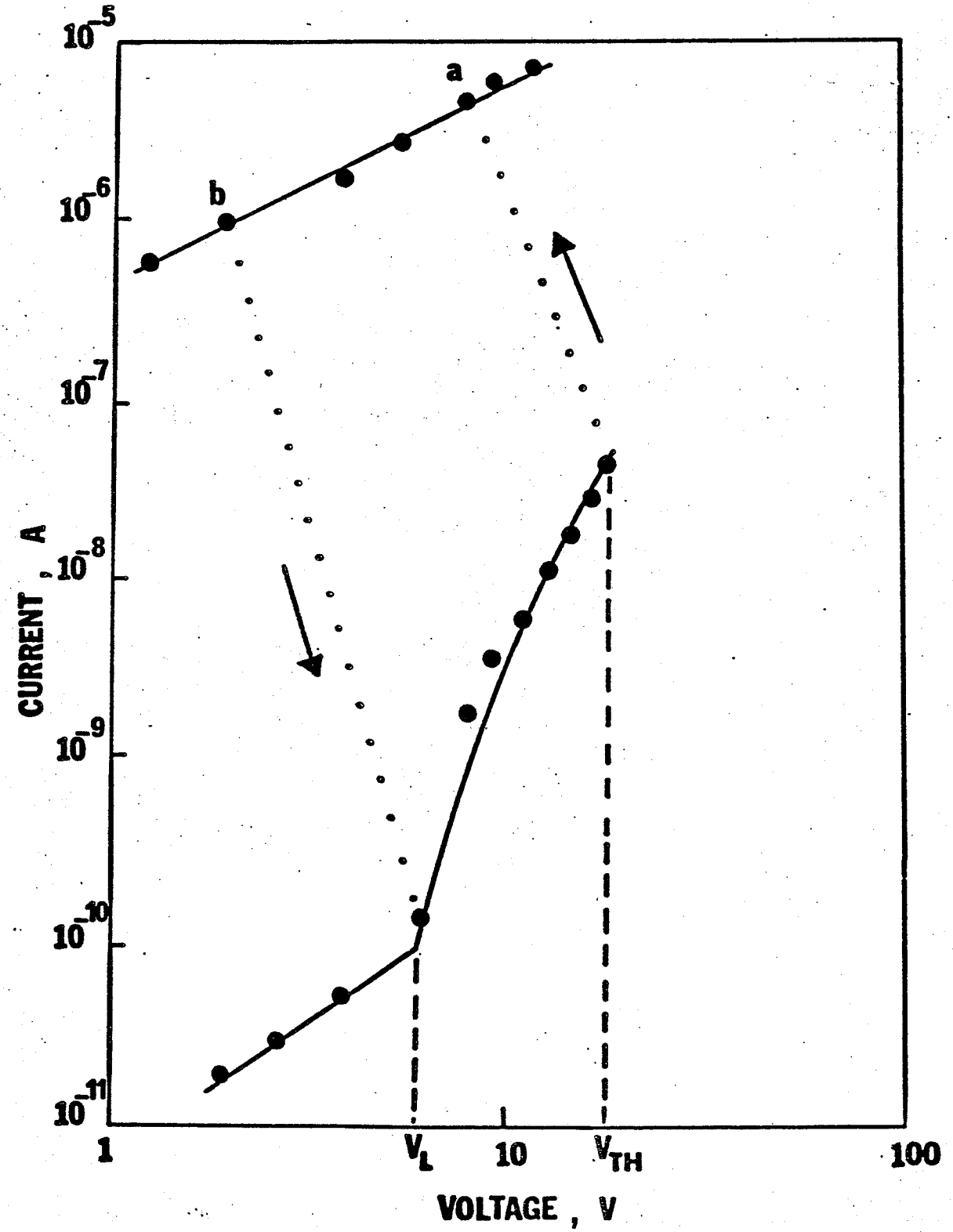

Fig. 4.2 Current-voltage characteristics

with thin film thickness of about 6000 Å. At voltages below V_L (average field of about 0.1 MV/cm) the I-V relationship is Ohmic (Region 1); and at voltages higher than V_L but below V_{TH} (the threshold voltage for the onset of switching corresponding to an average field of about 1 MV/cm) it becomes non-linear (Region II). At V_{TH} the specimen is rapidly switched from its "low conductivity" or "OFF" state to a "high conductivity" or "ON" state. The conductivity in the "ON" state is about 10^5 times that in the "OFF" state. The "ON" state will be retained as long as the current is not reduced below I_H (the holding current). But when the current is reduced below I_H the specimen returns back to its "OFF" state. This phenomena was observed in all specimens using either silver or aluminum electrodes. It should be noted that prior to the threshold switching, the current was unstable; and that an excessive current in the "ON" state sometimes caused breakdown, but in this case a dark spot appeared on the electrode surfaces and the specimen lost its switching behaviour.

In Region 1, the current is directly proportional to the voltage obeying Ohm's law. In Region II, however, the current increases with voltage, following steep power law whose exponent is approximately 3.3. The investigation of the effect of temperature on the behaviour of the "OFF" state indicates that the current increases exponentially as the temperature increases within the range of temperature of 20^0C - 50^0C. From the results given in Fig. 4.3 we have

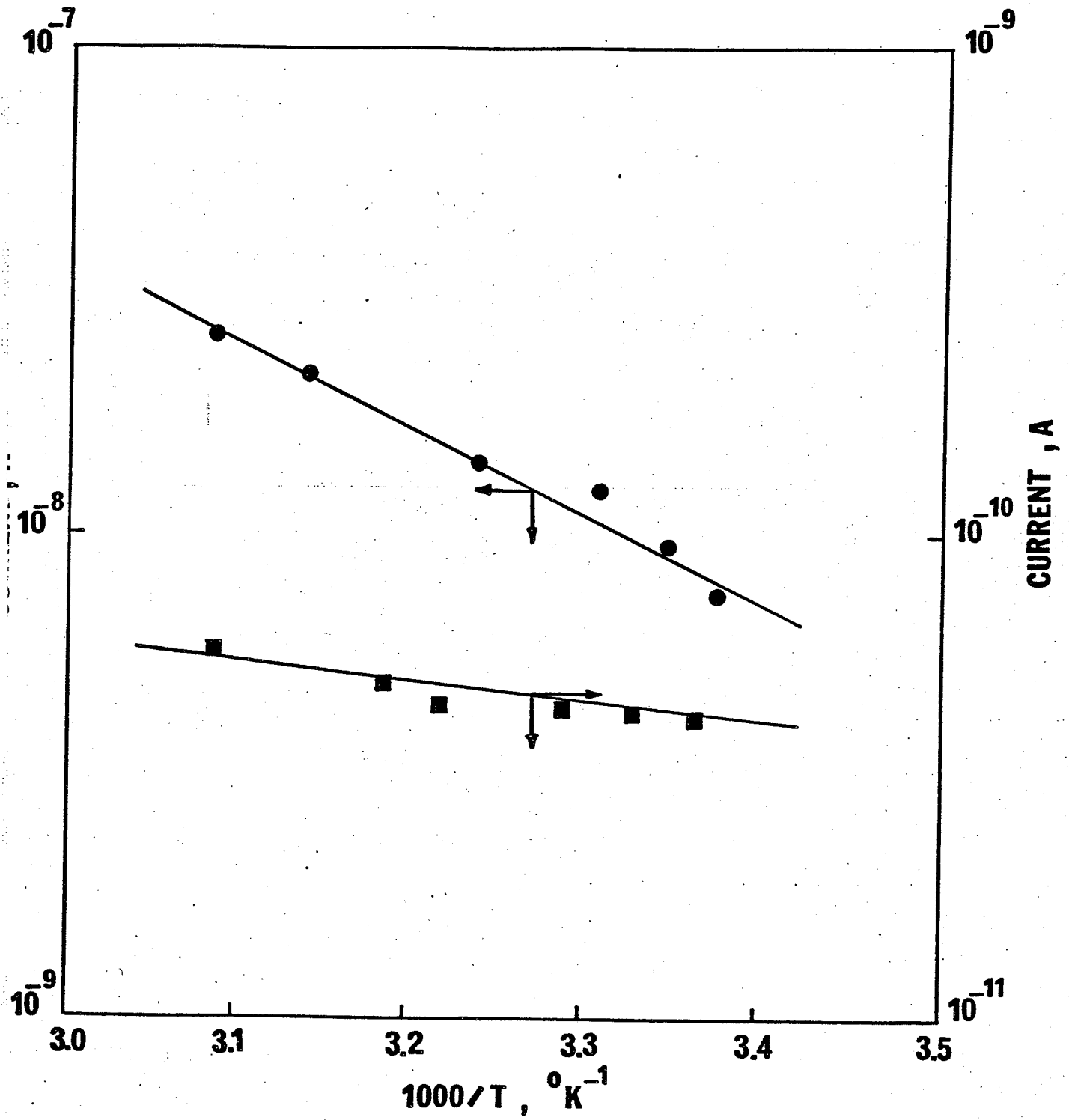

Fig. 4.3 Temperature dependence of dc current in the "OFF" state. ■ Region I, ● - Region II

calculated the activation energy of the two different regions in the "OFF" state

and
$$E_a = 0.1 \text{ eV} \qquad 0 < V < V_L$$
$$E_a = 0.37 \text{ eV} \qquad V_L < V < V_{TH}$$

The current-voltage relation in the "ON" state also obeys Ohm's Law but at a much higher current. However, a different behaviour in the current-temperature relationship was observed in the "ON" state. As the temperature increases, the current decreases reaching a minimum at about 37^0C, and then increases with increasing temperature as shown in Fig. 4.4.

Difficulties were encountered in the measurements of the threshold voltage as a function of temperature due to the instabilities near the threshold. However, the general trend is that the threshold voltage decreases as the temperature increases.

4.2.2. Memory Phenomena

After one or several switching cycles some specimens were changed from their "Switching-On" state to a "Memory" state. This "Memory" state could persist for quite a long time, and could be erased by passing a current pulse of either polarity through the specimen, but generally, a pulse with polarity opposite to that of the applied voltage initiating the "Memory"

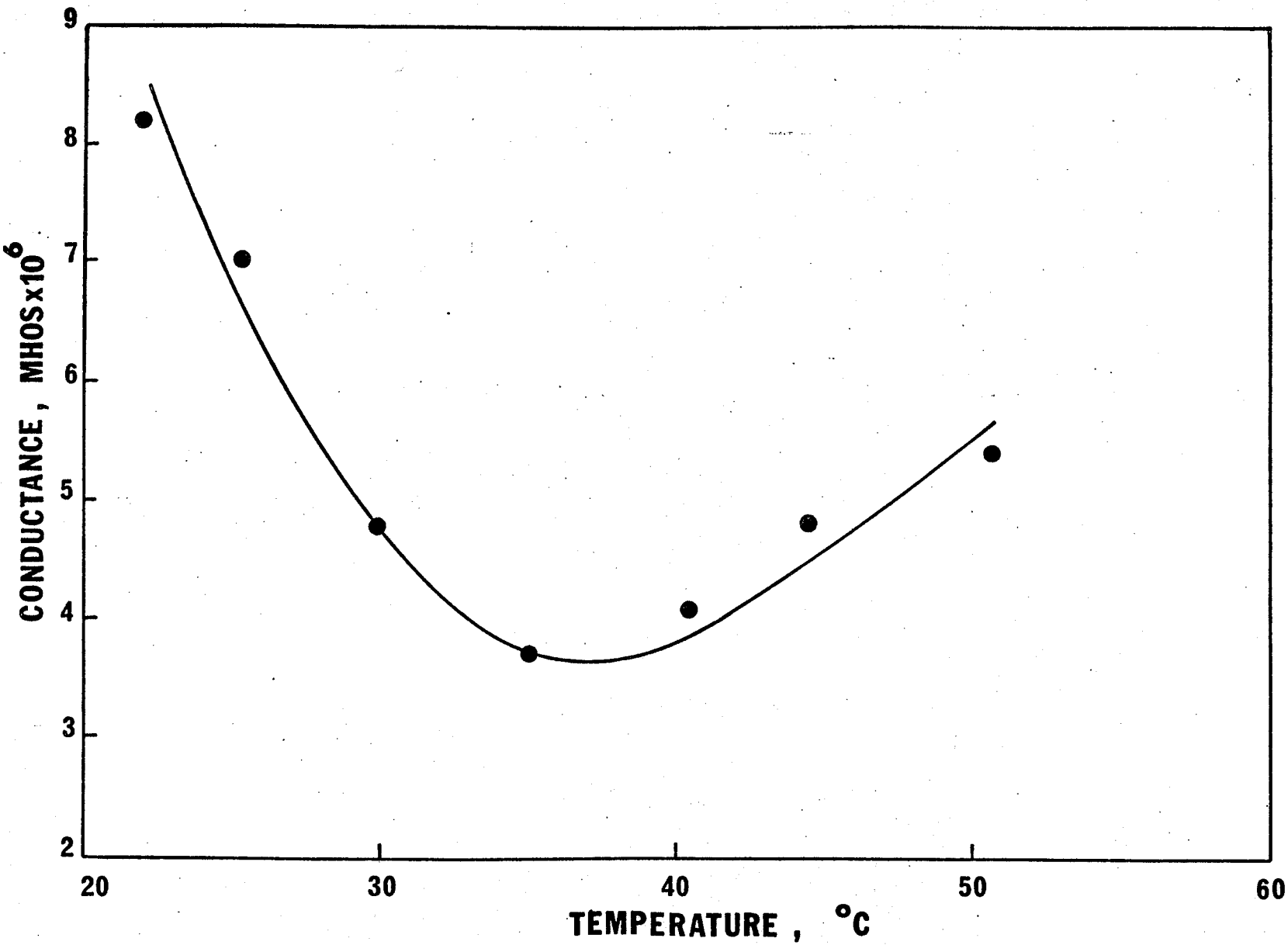

Fig. 4.4 Temperature dependence of dc electric conductance in the "ON" state

state is more effective.

The switching and memory phenomena occur only in specimens of thickness less than 5 μm. In thick films electroluminescence was observed, accompanied with a sharp increase in the current, which is similar to that observed in anthracene crystals [80]. The general trend is that the specimens exhibiting switching and memory phenomena do not exhibit electroluminescence and vice-versa. No thickness dependence has been studied in sufficient detail; however, the threshold voltage appeared to decrease as the film thickness decreases.

4.3 DISCUSSION

In the "OFF" state the electric conduction is most likely due to single-injection space charge limited current in the samples with traps because the Ag-anthracene-Ag or Ag-anthracene-Al systems used for the present investigation are most likely to provide only hole injection at low fields [31]. However, at sufficiently high fields the Ag electrode will become also an electron-injecting contact leading to double injection [80]. Under such a condition most traps will become filled and the conduction become filamentary [81]. These actions coupled with the Joule heating in the filament cause the current to increase rapidly to switch the sample to the "ON" state as shown in Fig. 4.2. Similar current-controlled switching phenomena have been observed in inorganic semiconductors [12,103].

In general, double injection in anthracene should yield excitons and thus produce electroluminescence. But it should be noted that before switching the traps and surface states in the thin film, specimens play a very important role in quenching excitons, while after switching, the carrier-exciton interactions become a dominant factor in quenching excitons due to the increase in temperature and free carrier concentration in the filament [81]. This may explain why no electroluminescence was observed in the specimens which exhibited switching phenomena.

Since the temperature in the filament is equal to the temperature produced by Joule heating plus the ambient temperature, the true temperature in the filament may be much higher than the ambient temperature. It should be noted that the result shown in Fig. 4.4 refers to only the ambient temperature. However, the temperature dependence of conductance in the "ON" state may be explained in terms of the following processes: (i) carrier-exciton interactions, (ii) detrapping, and (iii) carrier scatterings by phonons and other defects [60]. Processes (i) and (ii) tend to increase the concentration of free carriers, while process (iii) tends to decrease the carrier mobility.

The combination of strong field and high temperature due to Joule heating coupled with impurities and defects in the filament may cause the formation of stacks of charge transfer complexes across the sample between electrodes leading

to an easy charge transfer through donor-acceptor interactions [60]. Such stacks, once formed, may remain unchanged even after the removal of the applied field, thus producing the memory state. A sharp pulse, of course, would break the stacks and destroy the charge transfer complexes, and hence, cause the sample to switch back to its "OFF" state. Our present experimental results are not sufficient to identify the donors and acceptors which form the complexes.

The explanation of the above phenomena is still open, but it seems that the reproducibility of the switching and memory phenomena and the property shown in Fig. 2 rule out the possibility of the formation of a metallic filament in the "ON" state [51,93].

4.4 CONCLUDING REMARKS

The switching and memory phenomena observed in anthracene thin films occur only in films of thickness less than 5 μm. The general trend is that specimens exhibiting switching and memory phenomena do not exhibit electroluminescence and vice-versa. The threshold voltage for the onset of switching, decreases with increasing temperature. The "ON" state conductance decreases with increasing temperature, reaches a minimum at 37^{0}C and then increases with increasing temperature. All the observed phenomena are attributed to double injection coupled with the effects of traps on excitons and charge carriers,

carrier-exciton interactions and the formation of charge transfer complexes.

Although our results are new, they are not sufficient to disclose the true mechanism responsible for switching and memory beyond doubt. However, our explanation is still open and it is obvious that more work along this line is necessary.

CHAPTER V

SINGLE INJECTION OF CHARGE CARRIERS INTO THIN FILMS

A. SPACE CHARGE CREATED BY SINGLE INJECTION

Space charge, electric field and free carriers created by an injecting ohmic contact at the surface of an insulator or a semiconductor have been previously studied for some special cases, such as for the solid free of traps, or with traps uniformly distributed in both energy and space [94,164]. However, the assumptionsmade for their analysis are unlikely to be applicable to the case of insulating thin films, since the spatial distribution of traps can never be homogeneous because of the discontinuities between the material and the electrodes [139,172], and the uniform distribution of trap energy levels is unlikely to occur from the physical structure point of view [81]. Obviously, the thinner the material specimen, the more is the influence of the form of spatial distribution of traps on the space charge distribution. The purpose of this part is to present a unified approach to the calculation of space charge, electric field and carrier concentration due to single injection at the surface of an insulating film having an arbitrary dis-

tribution of traps in energy and in space and to present some computed results to show the effect of different types of trap distribution.

5.1 THEORY

In single crystals the trap energy levels, if there are any, are generally discrete due mainly to chemical impurities, while in amorphous and polycrystalline materials they are distributed in accordance with certain distribution functions due mainly to structural defects [170]. Material specimens in thin film form are generally polycrystalline. Furthermore, in these cases, the trap distribution in space near any boundaries, for example, between specimen surface and metallic electrode, or near grain boundaries, would be different from that in other regions in the bulk. In the present analysis we make the following assumptions but the treatment is general and, therefore, can be applied to thick or thin specimens.

(i) The energy band model can be used to treat the behaviour of injected carriers.

(ii) Only injected hole carriers are considered and the ohmic contact to inject them is perfect (A similar treatment can be easily extended to the case for only injected electron carriers).

(iii) For simplicity, the treatment is one dimensional with the plane at $x = o$ as the injecting contact and that

at x = d as the blocking contact.

(iv) The effect of image forces is ignored.

(v) The free hole density follows the Maxwell-Boltzmann statistics, while the trapped hole density follows the Fermi-Direc statistics.

(vi) The mobility and the diffusion coefficient of the holes are not affected by the presence of traps.

(vii) The edge of the valence band, E_v, is chosen as the reference level, and is made equal to zero.

The steady state behaviour of single injection in a solid is governed by the current flow equation

$$J = q\mu\, p_f F - qD \frac{dp_f}{dx} \tag{5.1}$$

and the Poisson equation

$$\frac{dF}{dx} = \frac{q}{\varepsilon} (p_f + p_t) \tag{5.2}$$

in which

$$p_f = N_v \exp (- E_F/kT) \tag{5.3}$$

and

$$p_t = \int_{E\ell}^{E\mu} \frac{h\ (E,x)\ dE}{1 + g \exp [E_F - E)/kT]} \tag{5.4}$$

where h (E,x) is the distribution function for the trap density as a function of energy level E above the edge of the valence

band and the distance x from the hole injecting contact. In the absence of applied fields and at thermal equilibrium, J = 0. Thus, equation (1) becomes

$$\frac{dp_f}{dx} = \frac{\mu}{D} p_f F \tag{5.5}$$

and using the boundary conditions

$$F = 0 \quad \text{at} \quad x = d \tag{5.6}$$

and

$$V = -\int_0^d F dx \tag{5.7}$$

we can solve Eqns. (5.1) and (5.2). In the following we shall consider three general cases:

5.1.1 In the absence of traps

For this case equation (4) becomes

$$p_t = h(E,x) = 0 \tag{5.8}$$

Therefore, solving Eqns. (5.2) and (5.5) with the aid of Eqns. (5.6) and (5.7) we obtain

$$F(x) = -\frac{2V_T}{d} \cos^{-1}\exp(-V/2V_T) \tan\left[(1-x/d)\cos^{-1}\exp(-V/2V_T)\right] \tag{5.9}$$

and

$$p_f(x) = \frac{2\varepsilon V_T}{qd^2}\left[\cos^{-1}\exp(-V/2V_T)\right]^2 \sec^2\left[(1-x/d)\cos^{-1}\exp(-V/2V_T)\right] \tag{5.10}$$

where

$$V_T = D/\mu = kT/q \tag{5.11}$$

based on the Einstien's relation.

At the surface, x = 0. Thus, we have

$$F(0) = -\frac{2V_T}{d}\cos^{-1}\exp(-V/2V_T)\,[\exp(V/V_T) - 1]^{\frac{1}{2}} \tag{5.12}$$

and

$$p_f(0) = \frac{2\varepsilon V_T}{qd^2}\,[\cos^{-1}\exp(-V/2V_T)]^2\exp(V/V_T) \tag{5.13}$$

Equations (5.12) and (5.13) are similar to those obtained by other investigators [94,164].

5.1.2 The traps distributed non-uniformly in energy but uniformly in space

(i) The traps confined in a single discrete energy level

For this case h(E,x) can be written as

$$h(E,x) = H_a\,\delta(E - E_t) \tag{5.14}$$

where $\delta(E - E_t)$ is the Dirac delta function. For shallow traps, $E_t < E_F$. Then, substitution of Eqn. (5.14) into Eqn. (5.4) and integration give

$$p_t = \frac{H_a}{g}\exp[(E_t - E_F)/kT] \tag{5.15}$$

Thus, the total charge carrier density is

$$p = p_f + p_t$$

$$= \left[1 + \frac{H_a}{gN_v} \exp\left(E_t/kT\right)\right] p_f \qquad (5.16)$$

$$= K_a\, p_f$$

and Eqn. (5.2) becomes

$$\frac{dF}{dx} = \frac{q}{\varepsilon} K_a\, p_f \qquad (5.17)$$

in which

$$K_a = 1 + \frac{H_a}{gN_v} \exp\left(E_t/kT\right) \qquad (5.18)$$

Solving Eqns. (5.5) and (5.17) with the aid of Eqns. (5.6) and (5.7), we obtain

$$F(x) = -\frac{2V_T}{d} \cos^{-1}\exp(-V/2V_T) \tan\left[(1-x/d)\cos^{-1}\exp(-V/2V_T)\right] \qquad (5.19)$$

and

$$p_f(x) = \frac{2\varepsilon V_T}{K_a q d^2}\left[\cos^{-1}\exp(-V/2V_T)\right]^2 \sec^2\left[(1-x/d)\cos^{-1}\exp(-V/2V_T)\right] \qquad (5.20)$$

At the surface, x = 0. Thus, we have

$$F(0) = \frac{-2V_T}{d} \cos^{-1}\exp\left(-V/2V_T\right)\left[\exp\left(V/V_T\right) - 1\right]^{\frac{1}{2}} \qquad (5.21)$$

$$p_f(0) = \frac{2\varepsilon V_T}{K_a q d^2}\left[\cos^{-1}\exp(-V/2V_T)\right]^2 \exp(V/V_T) \qquad (5.22)$$

and

$$p(0) = K_a\, p_f(0) \tag{5.23}$$

(ii) The traps distributed exponentially within the forbidden energy gap

For this case $h(E,x)$ can be written as

$$h(E,x) = \frac{H_b}{kT_c} \exp(-E/kT_c) \tag{5.24}$$

If $T_c > T$, we can assume that [81] $f(E) = 1$ for $E_F < E < \infty$ and $f(E) = 0$ for $E < E_F$ as if we take $T = 0$. This is a good approximation particularly when T_c is much larger than T. With this assumption, integration of Eqn. (5.4) gives

$$p_t = \int_{E_F}^{\infty} \frac{H_b}{kT_c} \exp(-E/kT_c)\, dE$$

$$= H_b \left(\frac{p_f}{N_v}\right)^{1/\ell} \tag{5.25}$$

where $\ell = T_c/T$ (5.26)

For thin films the trap density is generally high and, therefore, we can assume $p_t >> p_f$. Thus, the total charge carrier density can be approximated to [156]

$$p = p_f + p_t \tag{5.27}$$

$$= K_b\, p_f^{1/\ell}$$

in which

$$K_b = H_b/N_v^{1/\ell} \tag{5.28}$$

Thus, Eqn. (5.2) becomes

$$\frac{dF}{dx} = \frac{q}{\varepsilon} K_b p_f^{1/\ell} \tag{5.29}$$

Solving Eqns. (5.5) and (5.29) with the aid of Eqns. (5.6) and (5.7), we obtain

$$F(x) = -\frac{\ell V_T}{d} \cos^{-1} \exp(-V/\ell V_T) \tan\left[(1-x/d) \cos^{-1} \exp(-V/\ell V_T)\right] \tag{5.30}$$

and

$$p_f(x) = \left\{\frac{\ell \varepsilon V_T}{K_b q d^2} \left[\cos^{-1}\exp(-V/\ell V_T)\right]^2 \sec^2\left[(1-x/d)\cos^{-1}\exp(-V/\ell V_T)\right]\right\}^{\ell} \tag{5.31}$$

At the surface, x = 0. Thus, we have

$$F(0) = -\frac{\ell V_T}{d} \cos^{-1}\exp(-V/\ell V_T)\left[\exp(2V/\ell V_T) - 1\right]^{1/2} \tag{5.32}$$

$$p_f(0) = \left(\frac{\ell \varepsilon V_T}{K_b q d^2}\right)^{\ell} \left[\cos^{-1}\exp(-V/\ell V_T)\right]^{2\ell} \exp(2V/V_T) \tag{5.33}$$

$$p(0) = K_b p_f^{1/\ell} \tag{5.34}$$

5.1.3 The traps distributed non-uniformly in energy and in space

The distribution function for the trap density as a function of energy level E above the edge of the valence band and distance x from the hole-injecting contact can be written as

$$h(E,x) = N_t(E)\, S(x) \tag{5.35}$$

To treat this problem, we can divide the region $0 \leq x \leq d$ into M equal intervals as shown in Fig. 5.1. The average value of S(x) over this region can be approximated by

$$\langle S(x) \rangle \rightarrow b_j = \frac{M}{d} \int_{x_{j-1}}^{x_j} S(x)\, dx \tag{5.36}$$

To calculate the voltage across the interval between x_{j-1} and x_j, we solve Eqn. (5.4) first by taking

$$h_j(E,x) = b_j N_t(E) \tag{5.37}$$

and then solve Eqns. (5.2) and (5.5) as if the traps are uniformly distributed. By matching the solutions at the respective boundaries and applying the boundary conditions given in Eqns. (5.6) and (5.7), we can obtain a complete solution for the whole region $0 \leq x \leq d$. After determining the electric field F_j due to the trap distribution h_j [Eqn. (5.37)], the voltage across the interval between x_{j-1} and x_j is

$$V_j = -\int_{x_{j-1}}^{x_j} F_j\, dx \tag{5.38}$$

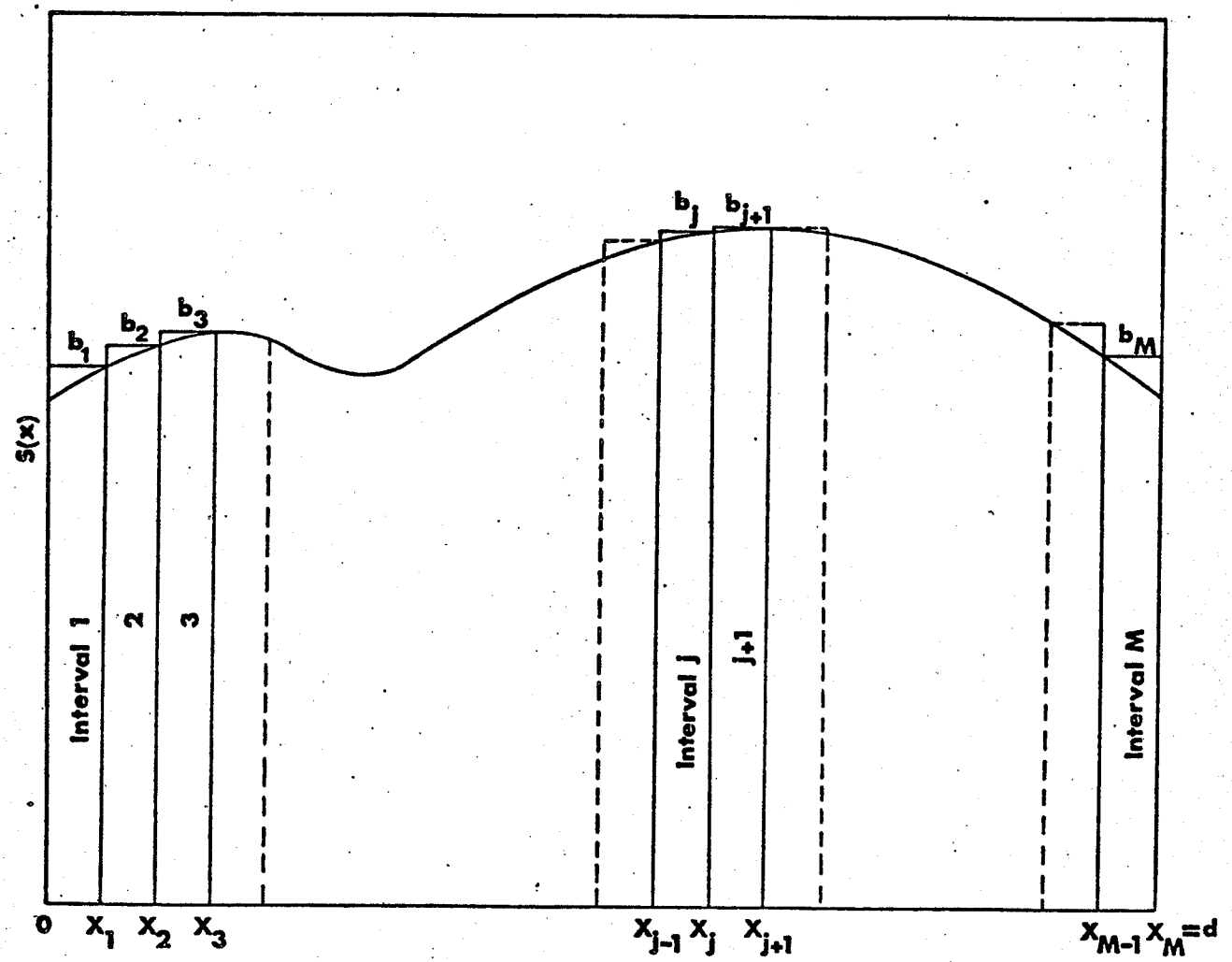

Fig. 5.1 Illustrating the discrete regional approximation for an arbitrary spatial distribution function of traps

Using the same procedure, we can find the voltages across other intervals. The total voltage across the specimen is then

$$V = \sum_{j=1}^{M} V_j \tag{5.39}$$

(i) The traps confined in a single discrete energy level

For this case, h(E,x) can be written as

$$h(E,x) = H_a \, \delta (E - E_t) \, S(x) \tag{5.40}$$

For shallow traps, $E_t < E_F$. Then, substitution of Eqn. (5.40) into Eqn. (5.4) and integration give

$$p_t = \frac{H_a}{g} \exp[(E_t - E_F)/kT] \, S(x) \tag{5.41}$$

Thus, the total charge carrier density is

$$p = p_f + p_t$$

$$= [1 + \frac{H_a}{gN_v} \exp (E_t/kT) \, S(x)] \, p_f$$

$$= K_{ax} \, p_f \tag{5.42}$$

where

$$K_{ax} = 1 + \frac{H_a}{gN_v} \exp (E_t/kT) \, S(x) \tag{5.43}$$

Using the method described in Eqns. (5.36) - (5.39), we can write K_{ax} for the interval between x_{j-1} and x_j as

$$K_{aj} = 1 + \frac{H_a}{gN_v} b_j \exp (E_t/kT) \tag{5.44}$$

Equations (5.2) and (5.5) due to K_{aj} become

$$\frac{dF_j}{dx} = \frac{q}{\varepsilon} K_{aj} p_{fj} \tag{5.45}$$

and

$$\frac{dp_{fj}}{dx} = p_{fj} F_j/V_T \tag{5.46}$$

The solution of Eqns. (5.45) and (5.46) gives

$$F_j = A_j^{\frac{1}{2}} \left(\frac{K_{aj} q V_T}{\varepsilon}\right)^{\frac{1}{2}} \tan\left[A_j^{\frac{1}{2}} \left(\frac{K_{aj} q}{\varepsilon V_T}\right)^{\frac{1}{2}} x + B_j \right] \tag{5.47}$$

where A_j and B_j are the integration constants. Applying the boundary condition given in Eqn. (5.6) in the interval $x_{M-1} \leq x \leq x_M$ with $x_M = d$, then we obtain

$$B_M = - A_M^{\frac{1}{2}} \left(\frac{K_{aM} q}{\varepsilon V_T}\right) d \tag{5.48}$$

Since F and $p_f = \frac{\varepsilon}{K_a q} \frac{dF}{dx}$ are continuous at the boundary between any two intervals, we can write

$$F_j \ (x = x_j) = F_{j+1} \ (x = x_j) \tag{5.49}$$

and

$$\left[\frac{1}{K_{aj}}\frac{dF_j}{dx}\right]_{x=x_j} = \left[\frac{1}{K_{aj+1}}\frac{dF_{j+1}}{dx}\right]_{x=x_j} \tag{5.50}$$

This implies that

$$A_j = A_{j+1}\left\{1+\left(1-\frac{K_{aj+1}}{K_{aj}}\right)\tan^2\left[A_{j+1}^{\frac{1}{2}}\left(\frac{K_{aj+1}q}{\varepsilon V_T}\right)^{\frac{1}{2}}\frac{dj}{M}+B_{j+1}\right]\right\} \tag{5.51}$$

and

$$B_j = \sec^{-1}\left\{\left(\frac{A_{j+1}}{A_j}\right)^{\frac{1}{2}}\sec\left[A_{j+1}\left(\frac{K_{aj+1}q}{\varepsilon V_T}\right)^{\frac{1}{2}}\frac{dj}{M}+B_{j+1}\right]\right\}-A_j\left(\frac{K_{aj}q}{\varepsilon V_T}\right)^{\frac{1}{2}}\frac{dj}{M} \tag{5.52}$$

Equations (5.51) and (5.52) are the recurrence formulae for determining A_j's and B_j's for successive intervals. It can be seen that all these constants are functions of A_M. To determine A_M, we use the boundary condition given in Eqn. (5.7). Integration of Eqn. (5.47) based on Eqn. (5.38) gives the voltage across the interval between x_{j-1} and x_j

$$V_j = -\int_{x_{j-1}}^{x_j} F_j\,dx$$

$$= -V_T \ln\left\{\frac{\cos\left[A_j^{\frac{1}{2}}\left(\frac{K_{aj}q}{\varepsilon V_T}\right)^{\frac{1}{2}}\frac{d(j-1)}{M}+B_j\right]}{\cos\left[A_j^{\frac{1}{2}}\left(\frac{K_{aj}q}{\varepsilon V_T}\right)^{\frac{1}{2}}\frac{dj}{M}+B_j\right]}\right\}$$

Using Eqn. (5.39) to obtain the total voltage across the entire specimen, we obtain

$$\exp(-V/V_T) = \prod_{j=1}^{M} \frac{\cos\left[A_j^{\frac{1}{2}} \left(\frac{K_{aj}q}{\varepsilon V_T}\right)^{\frac{1}{2}} \frac{d(j-1)}{M} + B_j\right]}{\cos\left[A_j^{\frac{1}{2}} \left(\frac{K_{aj}q}{\varepsilon V_T}\right)^{\frac{1}{2}} \frac{dj}{M} + B_j\right]}$$

As has been mentioned, Eqn. (5.54) is a function of A_M only, so the solution of it by means of the error minimization techniques will give the value of A_M. Once A_M is found, all the A_j's and B_j's can be easily determined, and hence, $F(x)$, $p_f(x)$, and $p_t(x)$ can be obtained.

At the surface, $x = 0$. Then, we have

$$F(0) = A_1^{\frac{1}{2}} \left(\frac{K_{a1}qV_T}{\varepsilon}\right)^{\frac{1}{2}} \tan B_1 \qquad (5.55)$$

$$p_f(0) = A_1 \sec^2 B_1 \qquad (5.56)$$

$$p(0) = A_1 K_{a1} \sec^2 B_1 \qquad (5.57)$$

(ii) <u>The traps distributed exponentially within the forbidden energy gap</u>

For this case, $h(E,x)$ can be written as

$$h(E,x) = \frac{H_b}{kT_c} \exp(-E/kT_c)\, S(x) \tag{5.58}$$

Following the same procedure described in Section (i), we have

$$p \tilde{-} p_t = K_b\, p_f^{1/\ell}\, S(x) \tag{5.59}$$

$$= K_{bx}\, p_f^{1/\ell}$$

where

$$K_{bx} = \frac{H_b S(x)}{N_V^{1/\ell}} \tag{5.60}$$

For the interval between x_{j-1} and x_j, Eqn. (5.60) becomes

$$K_{bj} = \frac{H_b b_j}{N_V^{1/\ell}} \tag{5.61}$$

Equations (5.2) and (5.5) due to K_{bj} become

$$\frac{dF_j}{dx} = \frac{q}{\varepsilon} K_{bj}\, p_{fj}^{1/\ell} \tag{5.62}$$

and

$$\frac{dp_f}{dx} = p_{fj}\, F_j/V_T \tag{5.63}$$

The solution of Eqns. (5.62) and (5.63) gives

$$F_j = C_j^{\frac{1}{2}} (\ell V_T)^{\frac{1}{2}} \tan\left[C_j^{\frac{1}{2}} (\ell V_T)^{-\frac{1}{2}} x + D_j \right] \tag{5.64}$$

In the interval $x_{M-1} \leq x \leq x_M$ with $x_M = d$ and based on Eqn. (5.6) we have

$$D_M = -C_M^{\frac{1}{2}} (\ell V_T)^{-\frac{1}{2}} d \tag{5.65}$$

The recurrence formulae for C_j's and D_j's are

$$C_j = C_{j+1} \tan^2 [C_{j+1}^{\frac{1}{2}} (\ell V_T)^{-\frac{1}{2}} \frac{dj}{M} + D_{j+1}]$$

$$x \{ \frac{K_{bj}}{K_{bj+1}} \sec^2 [C_{j+1}^{\frac{1}{2}} (\ell V_T)^{-\frac{1}{2}} \frac{dj}{M} + D_{j+1}] - 1 \} \tag{5.66}$$

and

$$D_j = \sec^{-1} \{ (\frac{K_{bj}}{K_{bj+1}})^{\frac{1}{2}} \sec [C_{j+1}^{\frac{1}{2}} (\ell V_T)^{-\frac{1}{2}} \frac{dj}{M} + D_{j+1}] \}$$

$$- C_j^{\frac{1}{2}} (\ell V_T)^{-\frac{1}{2}} \frac{dj}{M} \tag{5.67}$$

All C_j's and D_j's are functions of C_M. From Eqns. (5.38), (5.39) and (5.47), we obtain

$$\exp(-V/\ell V_T) = \prod_{j=1}^{M} \frac{\cos [C_j^{\frac{1}{2}} (\ell V_T)^{-\frac{1}{2}} \frac{d(j-1)}{M} + D_j]}{\cos [C_j^{\frac{1}{2}} (\ell V_T)^{-\frac{1}{2}} \frac{dj}{M} + D_j]} \tag{5.68}$$

Equation (5.68) is a function of C_M only. So we can determine C_M and hence, C_j's and D_j's, and obtain $F(x)$, $p_f(x)$ and $P_t(x)$.

At the surface, $x = 0$. Then, we have

$$F(0) = C_1^{\frac{1}{2}} (\ell V_T)^{\frac{1}{2}} \tan D_1 \qquad (5.69)$$

$$p_f(0) = \left[\frac{C_1 \varepsilon}{K_{b1} q} \sec^2 D_1 \right]^{\ell} \qquad (5.70)$$

$$p(0) = \frac{C_1 \varepsilon}{q} \sec^2 D_1 \qquad (5.71)$$

5.2 COMPUTED RESULTS AND DISCUSSION

In thin films the traps are generally exponentially distributed in energy [78,105]. We shall compute $F(0)$, $p_f(0)$ and $p(0)$ for the following forms of spatial trap distribution.

(A) Uniform spatial distribution

For this case, the distribution function may be written as

$S(x) = 1$

So we can use Eqns. (5.32) - (5.34) for computing $F(0)$, $p_f(0)$ and $p(0)$.

(B) Linear spatial distribution with the maximum density at the injecting electrode (at $x = 0$).

For this case, the distribution function may be written as

$$S(x) = 1 + A - x/x_o \qquad (5.72)$$

where A and x_o are constants. Substitution of Eqns. (5.72) into Eqn. (5.36) gives

$$b_j = 1 + A - \frac{d(j+\frac{1}{2})}{Mx_o} \qquad (5.73)$$

(C) Exponential spatial distribution with the maximum density at the injecting electrode (at x = 0).

For this case, the distribution function may be written as

$$S(x) = 1 + B \text{ Exp } (-x/x_o) \qquad (5.74)$$

where B is a constant. Similarly, substitution of Eqn. (5.74) into Eqn. (5.36) gives

$$b_j = 1 + \frac{BMx_o}{d} \exp\left(-\frac{dj}{Mx_o}\right) \left[\exp(-d/Mx_o) - 1\right] \qquad (5.75)$$

(D) Exponential spatial distribution with the maximum densities at both electrodes (at x = 0 and x = d).

For this case, the distribution function may be written as

$$S(x) = 1 + C \exp(-x/x_o) + D \exp[-(d-x)/x_o] \qquad (5.76)$$

where C and D are constants. Similarly, substitution of Eqn. (5.76) into Eqn. (5.36) gives

$$b_j = 1 - \frac{Mx_o}{d} \{C \exp(-dj/Mx_o)[\exp(-d/Mx_o)-1]$$

$$- D \exp\left[-\frac{d(M-j)}{Mx_o}\right] \left[\exp(d/Mx_o) - 1\right]\} \qquad (5.77)$$

In order to show the effect of traps on the space charge created by single injection, we choose anthracene films as an example. We have computed F(0), p(0) and $p_f(0)$ using

20 intervals (M = 20) for the discrete regional approximation and the following physical parameters for anthracene films at 300^0K [60]

$$N_v = 2.4 \times 10^{25}\ m^{-3}$$

$$\varepsilon = 3.2 \times 10^{-11}\ Fm^{-1}$$

$$\mu = 8 \times 10^{-5}\ m^2v^{-1}sec^{-1}$$

$$H_b = 10^{25}\ m^{-3}$$

$$T_c = 600^0K$$

$$V = -0.125V$$

We consider only the cases with traps distributed exponentially in energy but following four different forms of spatial distribution function S(x): (a) uniform, (b) linear, (c) exponential with the maximum trap density at the injecting electrode, and (d) exponential with the maximum trap density at both electrodes. We use the subscript A to denote the case in absence of traps, the subscript U to denote the case with traps exponentially distributed in energy and uniformly distributed in space, and the subscript NU to denote the cases with traps exponentially distributed in energy and non-uniformly

distributed in space. Figure 5.2 shows $F(0)_U/F(0)_A$, $p(0)_U/p(0)_A$ and $p_f(0)_U/p_f(0)_A$ as functions of specimen thickness. It can be seen that the presence of traps affects greatly the values of $F(0)$, $p(0)$ and $p_f(0)$. Figures (5.3) - (5.5) show $F(0)_{NU}/F(0)_U$, $p(0)_{NU}/p(0)_U$ and $p_f(0)_{NU}/p_f(0)_U$ as functions of specimen thickness for three different types of non-uniform spatial distribution of traps. These results indicate that the thinner the specimen, the more significant is the effect of the non-uniformity of spatial distribution, and that for very thick specimens this effect may become negligible. The critical value of d for this effect to become negligible depends on the distribution function $S(x)$. However, for thin films this effect should not be ignored.

5.3 CONCLUDING REMARKS

The general expressions for the electric field, free and trapped charge carrier densities created by single injection in a solid with traps uniformly and non-uniformly distributed in energy and in space have been derived using a unified mathematical approach. The computed results using anthracene films as an example show that the effect of the non-uniformity of spatial distribution of traps can be very serious if the specimen is very thin, and suggests that for thin films this effect should not be ignored.

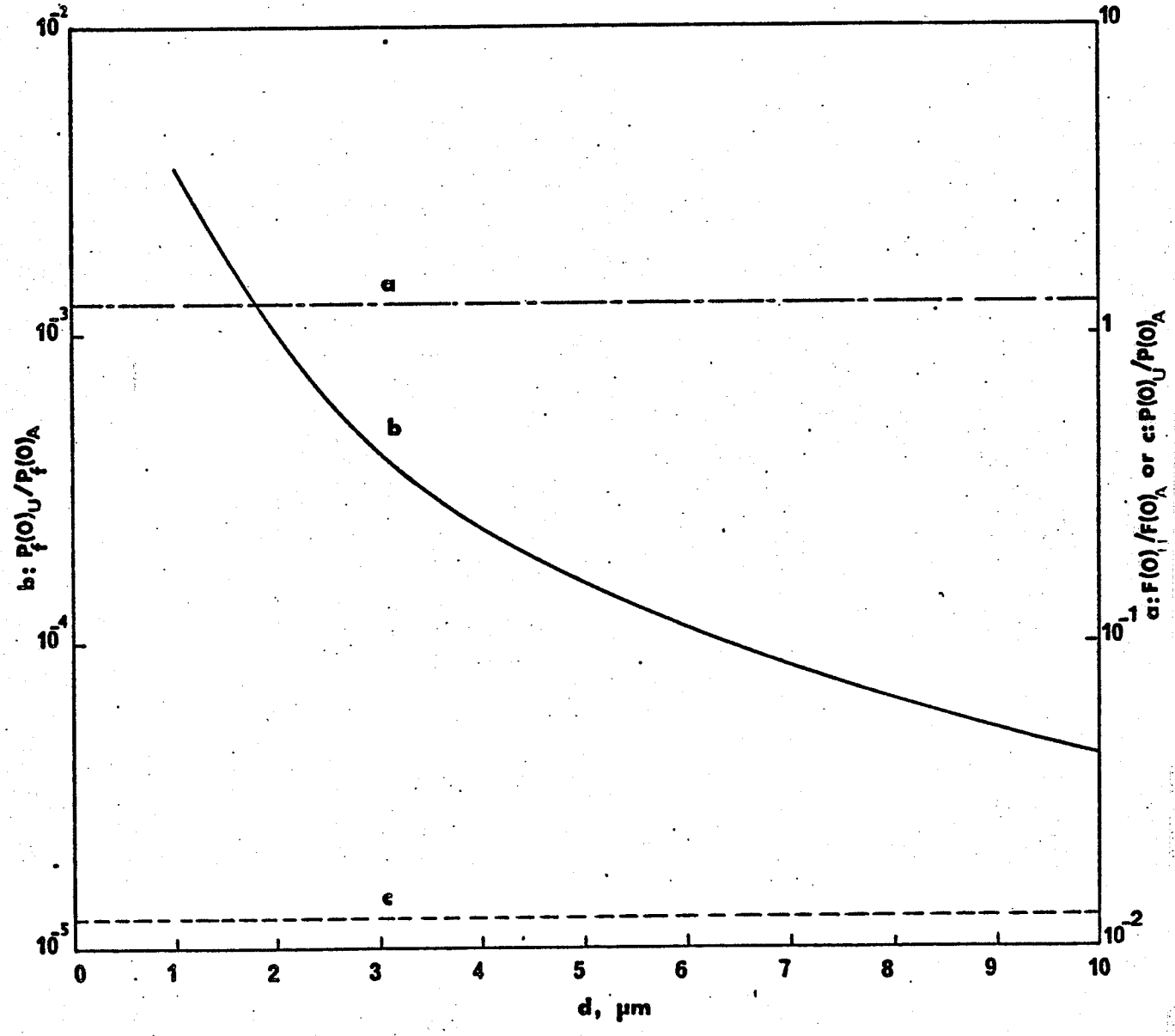

Fig. 5.2 $F(0)_U/F(0)_A$, $P(0)_U/P(0)_A$ and $P_f(0)_U/P_f(0)_A$ as functions of d for the uniform spatial distribution of traps

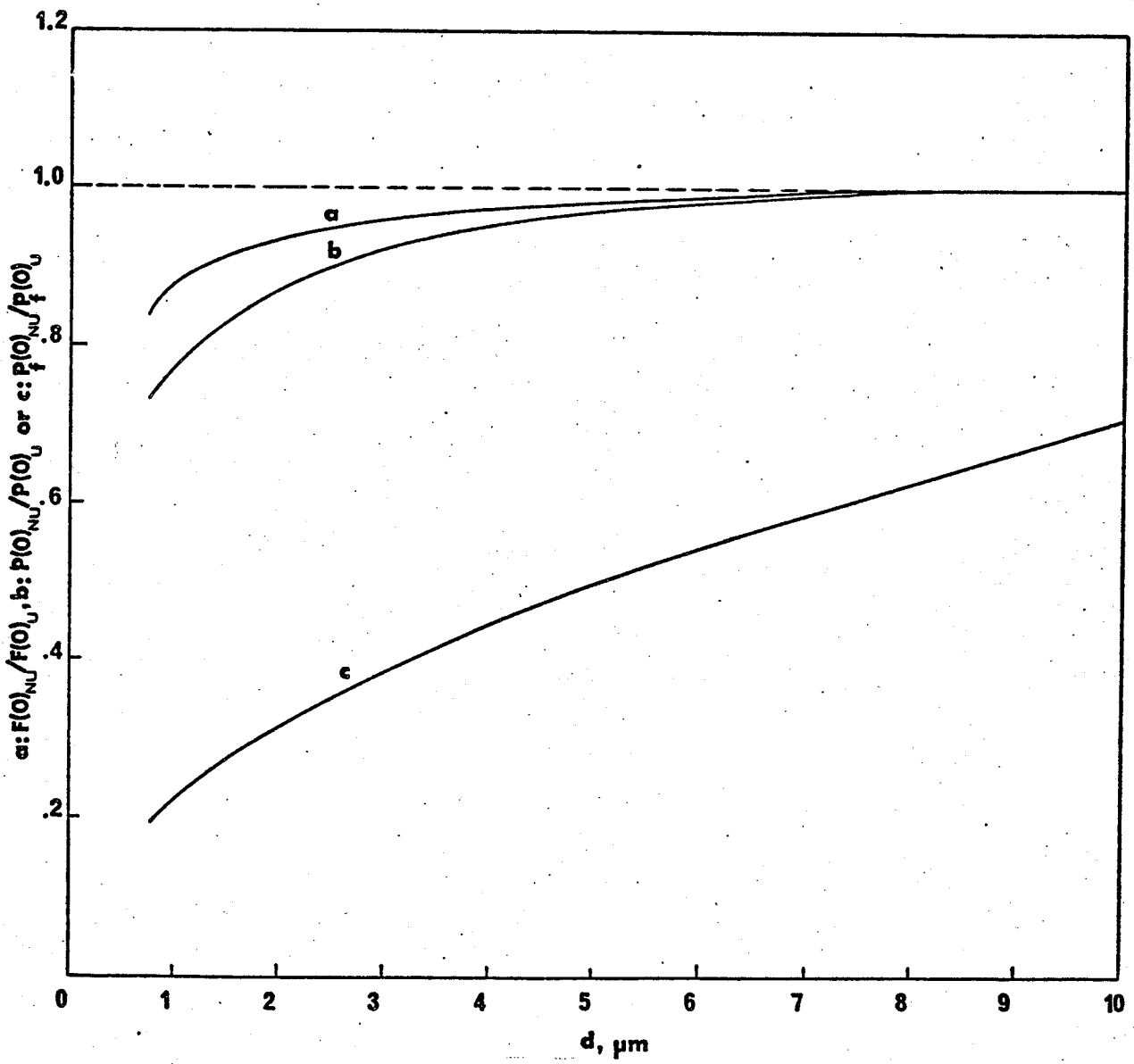

Fig. 5.3 $F(0)_{NU}/F(0)_{U}$, $P(0)_{NU}/P(0)_{U}$ and $P_f(0)_{NU}/P_f(0)_{U}$ as functions of d for the linear spatial distribution of traps based on Eqn. (5.74) with x_o = 15μm and A = 0.6

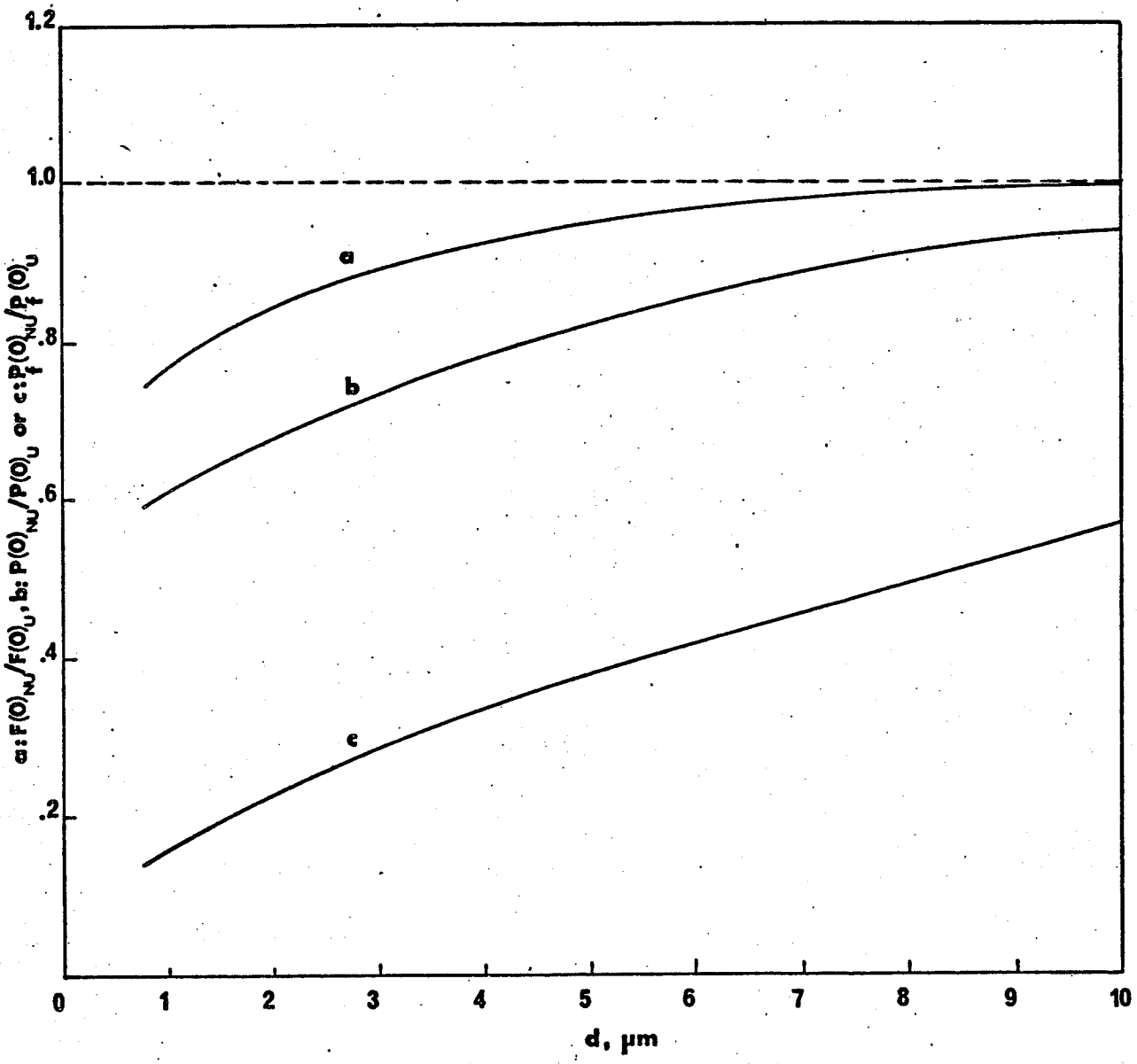

Fig. 5.4 $F(O)_{NU}/F(O)_U$, $P(O)_{NU}/P(O)_U$ and $P_f(O)_{NU}/P_f(O)_U$ as functions of d for the exponential spatial distribution of traps based on Eqn. (5.75) with x_o = 0.5μm and B = 0.9

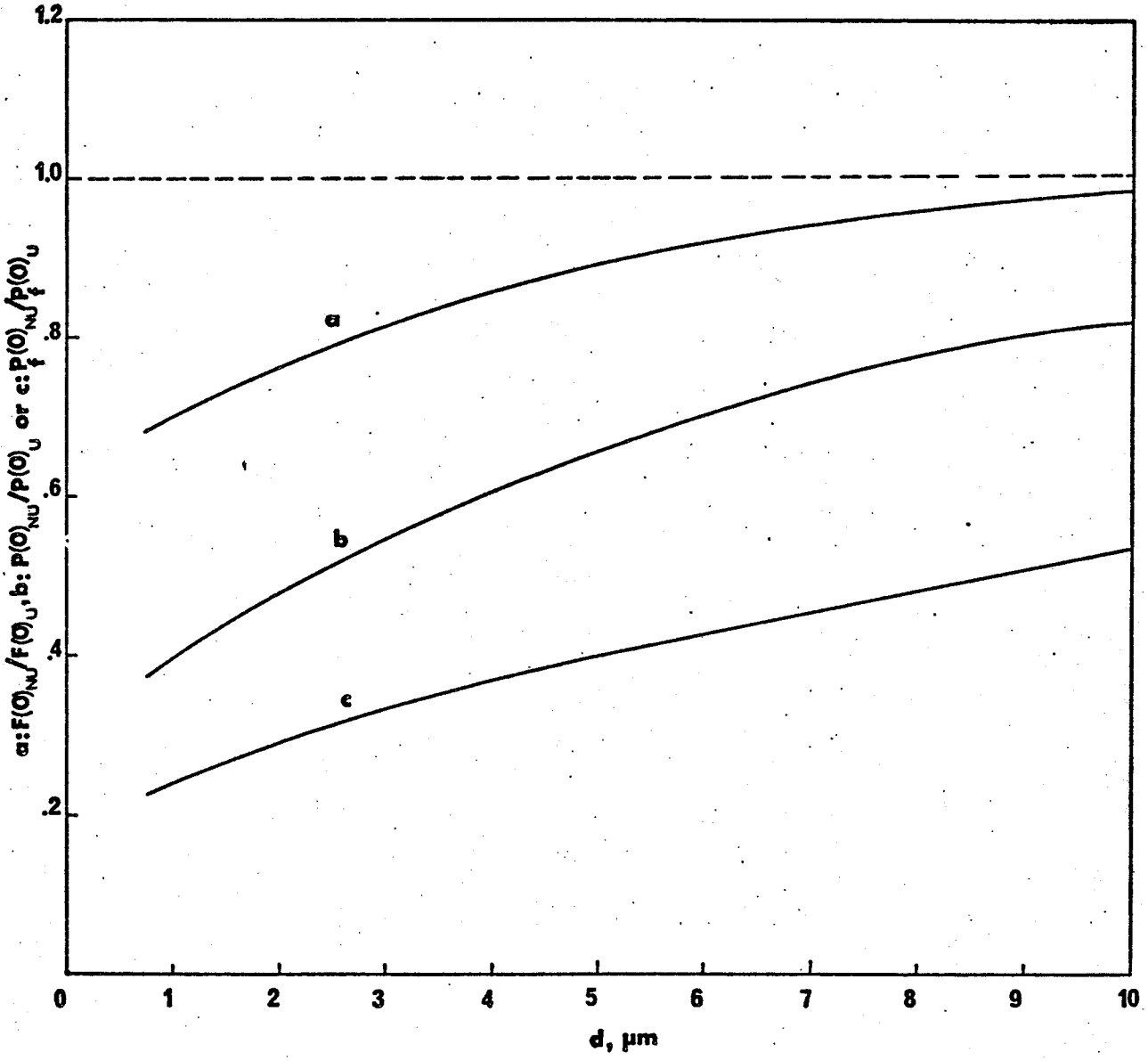

Fig. 5.5 $F(0)_{NU}/F(0)_{U}$, $P(0)_{NU}/P(0)_{U}$ and $P_f(0)_{NU}/P_f(0)_{U}$ as functions of d for the exponential spatial distribution of traps based on Eqn. (5.76) with x_o = 0.5μm, C = 0.9 and D = 0.5

B. STEADY-STATE CURRENT-VOLTAGE CHARACTERISTICS OF INSULATOR-ELECTROLYTE SYSTEMS

To form Ohmic injecting contacts for the measurements of space-change-limited currents, electrolytes have been used as electrodes in both inorganic [13,185] and organic [68,88,121] insulating solids. Using such electrodes, the current flow through an insulator is limited by space charge when carriers in excess of those thermally generated in the bulk can be injected through the insulator-electrolyte interface, as well as by the rate of carrier supply from the charged species in the electrolytic electrode. Furthermore, the current-voltage (I-V) characteristics are strongly affected by the form of trap distribution in energy and in space [78,104,172]. The purpose of this part is to present a unified analysis of the steady state current-voltage characteristics of an insulator-electrolyte system with traps distributed uniformly or non-uniformly in energy and in space, and to show that the computed results based on the expressions derived are in good agreement with the experimental results for some organic insulating film-electrolyte systems.

5.4 THEORY

In the theoretical analysis we make the following assumptions:

(i) The energy band model can be used to treat the behavior of injected carriers.

(ii) Only injected hole carriers are considered and the contact to inject them is perfect but the rate the carriers are injected is controlled by the rate of carrier supply from the charge species in the electrolytic electrode.

(iii) For simplicity, the treatment is one dimensional with the plane at $x = 0$ as the injecting contact and that at $x = d$ as the blocking contact.

(iv) The effect of image forces is ignored.

(v) The free hole density follows the Maxwell-Boltzmann statistics, while the trapped hole density follows the Fermi-Dirac statistics.

(vi) The mobility and the diffusion coefficient of the holes are not affected by the presence of traps.

(vii) The edge of the valence band, E_v, is chosen as the reference level, and is made equal to zero.

(viii) The electric field is so large that the current components due to diffusion and due to carriers thermally generated in the specimen can be neglected.

The steady state behaviour of single injection in a solid is governed by the current flow equation

$$J = q\mu\, p_f^* F \tag{5.78}$$

and the Poisson equation

$$\frac{dF}{dx} = \frac{q}{\varepsilon}\,(p_f^* + p_t) \tag{5.79}$$

in which

$$p_f^* = N_v \exp(-E_F/kT) \tag{5.80}$$

and

$$p_t = \int_{E_\mu}^{E_\ell} \frac{h(E,x)\,dE}{1 + g \exp[(E_F - E)/kT]} \tag{5.81}$$

The boundary conditions used to solve Eqns. (5.78) and (5.79) are:

$$p_f^*(0) = p_f(0)\,[1 - J/J_o] \tag{5.82}$$

and

$$V_a + V = -\int_0^d F\,dx \tag{5.83}$$

where $p_f^*(0)$ and $p_f(0)$ are, respectively, the free hole densities at $x = 0$ with and without applied fields. This implies that at high fields when J approaches J_o, the concentration of carriers at the surface approaches zero, and that the current saturates at J_o due mainly to the exchange of carriers between the surface of the insulator and the ions of the electrolyte[62]. Equation(5.83) implies that the total potential across the insulator specimen is the sum of the applied voltage V_a and the equilibrium potential difference created inside the specimen by carrier injection from the electrolyte V, and that a potential equal to V is assumed to be across the electrolyte to balance V.

5.4.1 Without traps

For this case, Eqn. (5.81) becomes

$$p_t = 0 \tag{5.84}$$

Then, solving Eqns. (5.78) and (5.79) and applying the boundary condition given in Eqn. (5.82), we obtain

$$F = F(0)\,[1 + x/x_{of}]^{\frac{1}{2}} \tag{5.85}$$

where

$$F(0) = [q\mu\, p_f(0)\ (\frac{1}{J} - \frac{1}{J_o})]^{-1} \tag{5.86}$$

and

$$x_{of} = \frac{\varepsilon}{2q^2\mu p_f^2(0)} \quad \frac{J}{(1 - J/J_o)^2} \tag{5.87}$$

Using the boundary condition given in Eqn. (5.83) we obtain

$$V_a + V = \frac{2}{3} F(0) x_{of}[1 - (1 + d/x_{of})^{3/2}] \tag{5.88}$$

(i) Low injection (or low current) case

In this case, we can assume that $x_{of} << d$ and $1 - J/J_o \simeq 1$. After simplification, the result is

$$J = \frac{9}{8} \varepsilon\mu \frac{(V_a + V)^2}{d^3} \tag{5.89}$$

This equation has been derived by other investigators [128] and is similar to that for a trap-free solid with two parallel metallic Ohmic contacts for single injection [133] except that V_a has been replaced with $V_a + V$.

(ii) High injection (or high current) case

In this case, we can assume that $x_{of} >> d$. From Eqns. (5.86)-(5.88), we obtain

$$1/J = 1/J_o - d/q\mu\, p_f(0)\, [V_a + V] \tag{5.90}$$

where $p_f(0)$ is calculated in section 5.1.1 and is given by

$$p_f(0) = \frac{2\varepsilon V_T}{qd^2} [\cos^{-1} \exp(-V/2V_T)]^2 \exp(V/V_T) \tag{5.91}$$

in which

$$V_T = kT/q \tag{5.92}$$

Equation (5.90) has been derived by other investigators [128] It indicates that J approaches J_o as a saturation current when V_a increases to such a value that the second term on the right hand side of Eqn. (5.90) becomes negligibly small. This implies that under such a condition the concentration of donor species in the electrolyte becomes independent of the overpotential, or in other words, the charge carrier supply is exhausted.

5.4.2 With traps distributed uniformly in space

(i) The traps confined in a single discrete energy level

For this case h(E,x) can be written as

$$h(E,x) = H_a \delta (E - E_t) \tag{5.93}$$

For simplicity, we assume that E_t is a shallow trap level located below E_F. Then, we can write

$$P_f^* + p_t = K_a p_f^* \tag{5.94}$$

in which

$$K_a = 1 + \frac{H_a}{gN_v} \exp(E_t/kT) \tag{5.95}$$

Substituting Eqn. (5.94) into Eqn. (5.79) and then solving Eqns. (5.78) and (5.79) with the aid of Eqns. (5.82) and (5.83) we obtain

$$F = F_a(0)\,[1 + x/x_{oa}^{\frac{1}{2}}] \tag{5.96}$$

and

$$V_a + V = \frac{2}{3} F_a(0)\, x_{oa}\,[1 - (1 + d/x_{oa})^{3/2}] \tag{5.97}$$

in which

$$F_a(0) = [q\mu\, p_f(0)\, (\frac{1}{J} - \frac{1}{J_o})]^{-1} \tag{5.98}$$

and

$$x_{oa} = \frac{\varepsilon}{2K_a q^2 \mu p_f^2(0)} \frac{J}{(1 - J/J_o)^2} \tag{5.99}$$

For the case of low injection, we can assume that $x_{oa} << d$ and $1 - J/J_o \simeq 1$. After simplification, Eqn. (5.97) becomes

$$J = \frac{9}{8} \frac{\varepsilon\mu}{K_a} \frac{(V_a + V)^2}{d^3} \tag{5.100}$$

For the case of high injection, we can assume that $x_{oa} >> d$, and then simplification of Eqn. (5.97) yields

$$1/J = 1/J_o - d/q\mu\, p_f(0)\,[Va + V] \qquad (5.101)$$

where $p_f(0)$ is calculated in Section 5.1.2 and is given by

$$p_f(0) = \frac{2\varepsilon V_T}{K_a q d^2}\,[\cos^{-1} \exp(-V/2V_T)]^2 \exp(V/V_T) \qquad (5.102)$$

Equations (5.100) and (5.101) are, respectively, similar in form to Eqns. (5.89) and (5.90), except that the former involve K_a which is equal to 1 for the insulator without traps, and larger than 1 for the insulator with traps.

(ii) The traps distributed exponentially within the forbidden energy gap

For this case, $h(E,x)$ can be written as

$$h(E,x) = \frac{H_b}{kT_c} \exp(-E/kT_c) \qquad (5.103)$$

If $T_c > T$, we can assume that $f(E) = 1$ for $E > E_F$ and $f(E) = o$ for $E < E_F$, as if we take $T = 0$. This is good approximation particularly when T_c is much larger than T. With this assumption we obtain

$$p_t = H_b \left(\frac{p_f^*}{N_v}\right)^{1/\ell} \qquad (5.104)$$

where $\ell = T_c/T$. For thin films we can assume $p_t >> p_f^*$ [156]. Then, Eqn. (5.79) becomes

$$\frac{dF}{dx} = \frac{q}{\varepsilon} K_b {p_f^*}^{1/\ell} \qquad (5.105)$$

where

$$K_b = \frac{H_b}{N_v^{1/\ell}} \tag{5.106}$$

Solution of Eqns. (5.78) and (5.105) with the aid of Eqns. (5.82) and (5.83) yields

$$F = F_b(0)\ [1 + x/x_{ob}]^{\ell/(\ell+1)} \tag{5.107}$$

and

$$V_a + V = \frac{\ell+1}{2\ell+1}\ F_b(0)\ x_{ob}\ [1 - (1 + d/x_{ob})^{\frac{2\ell+1}{\ell+1}}] \tag{5.108}$$

in which

$$F_b(0) = [q\mu\ p_f(0)\ (\frac{1}{J} - \frac{1}{J_o})]^{-1} \tag{5.109}$$

and

$$x_{ob} = (\frac{\ell}{\ell+1})\ \frac{\varepsilon\mu^{1/\ell}J}{K_b q^{(\ell-1)/\ell}}\ [q\mu\ p_f(0)\ (1 - J/J_o)]^{\frac{-(\ell+1)}{\ell}} \tag{5.110}$$

For the case of low injection, we can assume that $x_{ob} << d$ and $1 - J/J_o \simeq 1$, and then simplification of Eqn. (5.108) yields

$$J = q^{1-\ell}\mu N_v (\frac{2\ell+1}{\ell+1})^{\ell+1} (\frac{\ell}{\ell+1}\ \frac{\varepsilon}{H_b})^{\ell}\ \frac{(V_a + V)^{\ell+1}}{d^{2\ell+1}} \tag{5.111}$$

This equation is similar in form to that derived by Hwang and Kao[78] for metallic Ohmic contacts, except that V_a has been replaced with $V_a + V$, which takes into account the equilibrium potential difference created due to the presence of the electrolytic electrode.

For the case of high injection, we can assume that $x_{ob} >> d$, and then simplification of Eqn. (5.108) yields

$$\frac{1}{J} = \frac{1}{J_o} - \frac{d}{q\mu\, p_f(0)\, [V_a + V]} \qquad (5.112)$$

where $p_f(0)$ is calculated in Section 5.1.2 and is given by

$$p_f(0) = \left(\frac{\ell \varepsilon V_T}{K_b q d^2}\right)^{\ell} \left[\cos^{-1} \exp\left(-V/\ell V_T\right)\right]^{2\ell} \exp\left(2V/V_T\right) \qquad (5.113)$$

Equation (5.112) is similar in form to Eqn. (5.90) for the case without traps and to Eqn. (5.101) for the case with traps confined in a single discrete energy level, except that the expressions for $p_f(0)$ are different for these three cases.

5.4.3 With traps distributed non-uniformly in space

(i) The traps confined in a single discrete energy level

For this case $h(E,x)$ can be written as

$$h(E,x) = H_a \delta\,(E - E_t)\, S(x) \qquad (5.114)$$

Again, we shall assume that E_t is a shallow trap level located below E_F. Then, we can write

$$p_f^* + p_t = \Phi_a p_f^* \tag{5.115}$$

where

$$\Phi_a = 1 + \frac{H_a}{gN_v} \exp (E_t/kT)\, S(x)$$

$$= K_a \{ 1 + \eta [S(x) - 1] \} \tag{5.116}$$

$$\eta = \frac{H_a}{K_a g N_v} \exp (E_t/kT) \tag{5.117}$$

Substituting Eqn. (5.115) into Eqn. (5.79), and then solving Eqn. (5.78) and (5.79) with the aid of Eqns. (5.82) and (5.83), we obtain

$$F = F_a(0) \left[1 + \frac{\gamma_a(x)}{x_{oa}}\right]^{\frac{1}{2}} \tag{5.118}$$

and

$$Va + V = - F_a(0) \int_0^d \left[1 + \gamma_a(x)/x_{oa}\right]^{\frac{1}{2}} dx \tag{5.119}$$

in which

$F_a(0)$ and x_{oa} are given by Eqns. (5.98) and (5.99), and

$$\gamma_a(x) = \int_0^x \{ 1 + \eta S(t) - 1 \}\, dt \tag{5.120}$$

For the case of low injection in which $x_{oa} << d$, equation

(5.119) reduces to

$$J = \frac{9}{8} \frac{\varepsilon\mu}{K_a} \frac{(Va + V)^2}{d_{eff}^3} \qquad (5.121)$$

where

$$d_{eff} = \{\frac{3}{2} \int_0^d \left(\int_0^x [1 + \eta (S(t) - 1)]dt \right)^{\frac{1}{2}} dx\}^{2/3} \qquad (5.122)$$

Equation (5.121) is similar in form to Eqn. (5.100) except that d has been replaced with d_{eff} which can be considered as "effective thickness" to take into account the effect of the inhomogeneous spatial distribution of free and trapped carriers.

For the case of high injection in which $x_{oa} >> d$, Eqn. (5.101) is applicable except that for this case $p_f(0)$ is given by

$$p_f(0) = A_1 \, \mathrm{Sec}^2 B_1 \qquad (5.123)$$

where A_1 and B_1 are constants, the values of which are given in Section 5.1.3

(ii) <u>The traps distributed exponentially within the forbidden energy gap</u>

For this case, h(E,x) can be written as

$$h(E,x) = \frac{H_b}{kT_c} \exp(-E/kT_c) S(x) \tag{5.124}$$

By introducing the following parameter

$$\Phi_b = K_b S(x) \tag{5.125}$$

equation (5.79) becomes

$$\frac{dF}{dx} = \frac{q}{\varepsilon} \Phi_b {p_f}^{*1/\ell} \tag{5.126}$$

Solution of Eqns. (5.78) and (5.126) with the aid of Eqns. (5.82) and (5.83) yields

$$F = F_b(0) \left[1 + \frac{\gamma_b(x)}{x_{ob}} \right]^{\ell/(\ell+1)} \tag{5.127}$$

and

$$V_a + V = -F_b(0) \int_0^d \left[1 + \gamma_b(x)/x_{ob} \right]^{\ell/(\ell+1)} dx \tag{5.128}$$

in which $F_b(0)$ and x_{ob} are given in Eqns. (5.109) and (5.110), and

$$\gamma_b(x) = \int_0^x S(t)dt \tag{5.129}$$

For the case of low injection in which $x_{ob} << d$, Eqn. (5.128) reduces to

$$J = q^{1-\ell}\mu N_v \left(\frac{2\ell+1}{\ell+1}\right)^{\ell+1} \left(\frac{\ell}{\ell+1}\ \frac{\varepsilon}{H_b}\right)^{\ell} \frac{(V_a + V)^{\ell+1}}{d_{eff}^{2\ell+1}} \qquad (5.130)$$

where

$$d_{eff} = \left\{\frac{2\ell+1}{\ell+1} \int_0^d \left[\int_0^x S(t)dt\right]^{\ell/(\ell+1)} dx\right\}^{(\ell+1)/(2\ell+1)} \qquad (5.131)$$

Equation (5.130) is similar in form to Eqn. (5.111) except that d has been replaced with d_{eff}. Again, the difference between d_{eff} and d is caused by the inhomogeneous spatial distribution of free and trapped carriers.

For the case of high injection, in which $x_{ob} >> d$, Eqn. (5.112) is applicable except that for this case $p_f(0)$ is given by

$$p_f(0) = \left[\frac{C_1 \varepsilon}{K_{b1} q}\ \mathrm{Sec}^2\ D_1\right]^{\ell} \qquad (5.132)$$

where C_1, D_1 and K_{b1} are constants, the value of which are given in Section 5.1.3.

5.5 RESULTS AND DISCUSSION

In thin films the traps are generally exponentially distributed in energy [78,69]. We shall consider the following different forms of spatial trap distribution.

(A) Uniform spatial distribution

For this case the distribution function may be written as

$$S(x) = 1 \tag{5.133}$$

(B) Linear spatial distribution with the maximum density at the injecting electrode (at x = 0).

For this case the distribution function may be written as

$$S(x) = 1 + A - x/x_o \tag{5.134}$$

where A and x_o are constants.

(C) Exponential spatial distribution with maximum density at the injecting electrode (at x = 0).

For this case the distribution function may be written as

$$S(x) = 1 + B \exp(-x/x_o) \tag{5.135}$$

where B is a constant.

(D) Exponential spatial distribution with the maximum densities at both electrodes (at x = o and x = d).

For this case the distribution function may be written as

$$S(x) = 1 + C \exp(-x/x_o) + D \exp\{-[(d - x)/x_o]\} \quad (5.136)$$

where C and D are constants.

In order to show the effect of traps on the steady-state current-voltage characteristics, we choose anthracene films as an example. Using the following physical parameters for anthracens film at 300^0 K [126, 60]

$N_v = 2.4 \times 10^{25}\ m^{-3}$

$\varepsilon = 3.2 \times 10^{-11}\ Fm^{-1}$

$\mu = 8 \times 10^{-5}\ m^2 v^{-1}\ sec^{-1}$

$H_b = 10^{25}\ m^{-3}$

$T_c = 600^0$ K

$V = 0.147$ V

$J_o = 2 \times 10^{-2}$ Amp m^{-2}

We have computed the current as a function of d at a fixed applied field of 0.6 MV m^{-1} for the electrolytic electrode, 0.1 m $Ce(SO_4)_2$ in 0.5 m $H_2\ SO_4$. We choose this particular average field and this particular electrode because we shall use these computed results to correlate some experimental results of Mehl [126]. In all figures, the subscript A denotes the case of absence of traps, the subscript U denotes the case with traps exponentially distributed in energy and

uniformly distributed in space and the subscript NU denotes the cases with traps exponentially distributed in energy and non-uniformly distributed in space. Figure 5.6 shows the ratio of J_U/J_A at a constant applied average field of 0.6 MV m^{-1} as a function of specimen thickness d. It can be seen that the presence of traps affects greatly the value of J. Figure 5.7 shows J_{NU}/J_U as a function of specimen thickness for four different types of non-uniform spatial distribution of traps. These results indicate that the thinner the specimen the more significant is the effect of non-uniformity of spatial distribution, and that for very thick specimens this effect may be negligible. The critical value of d for this effect to become negligible depends on the distribution function S(x). However, for thin specimens this effect should not be ignored.

By plotting the ratio J/J_U as a function of d with the values of J extracted from the experimental results obtained by Mehl [126] and comparing the ratio J_{NU}/J_U as a function of d, in Fig. 5.8 we have found that the most probable spatial distribution function of the specimens used by Mehl may be exponential with the maximum trap densities at x = 0 and x = d. Based on this comparison, we have estimated that for S(x) independent of d, the value of x_o is about 50 $\pm$ 5 μm, C about 0.9 and D about 0.3. For a more rigorous treatment, the

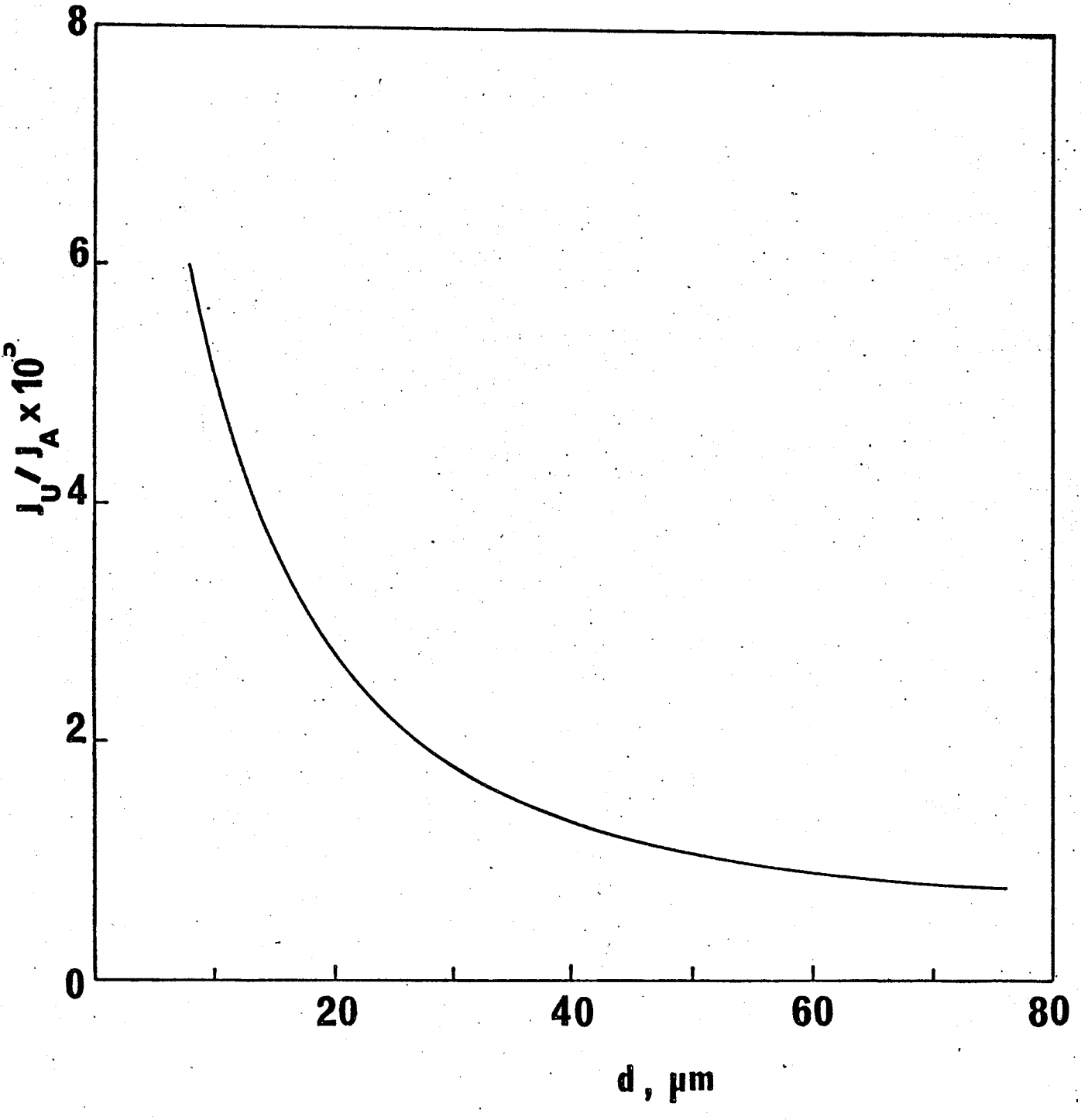

Fig. 5.6 J_U/J_A as a function of d for a fixed value of V/d = 0.6 MV m^{-1}

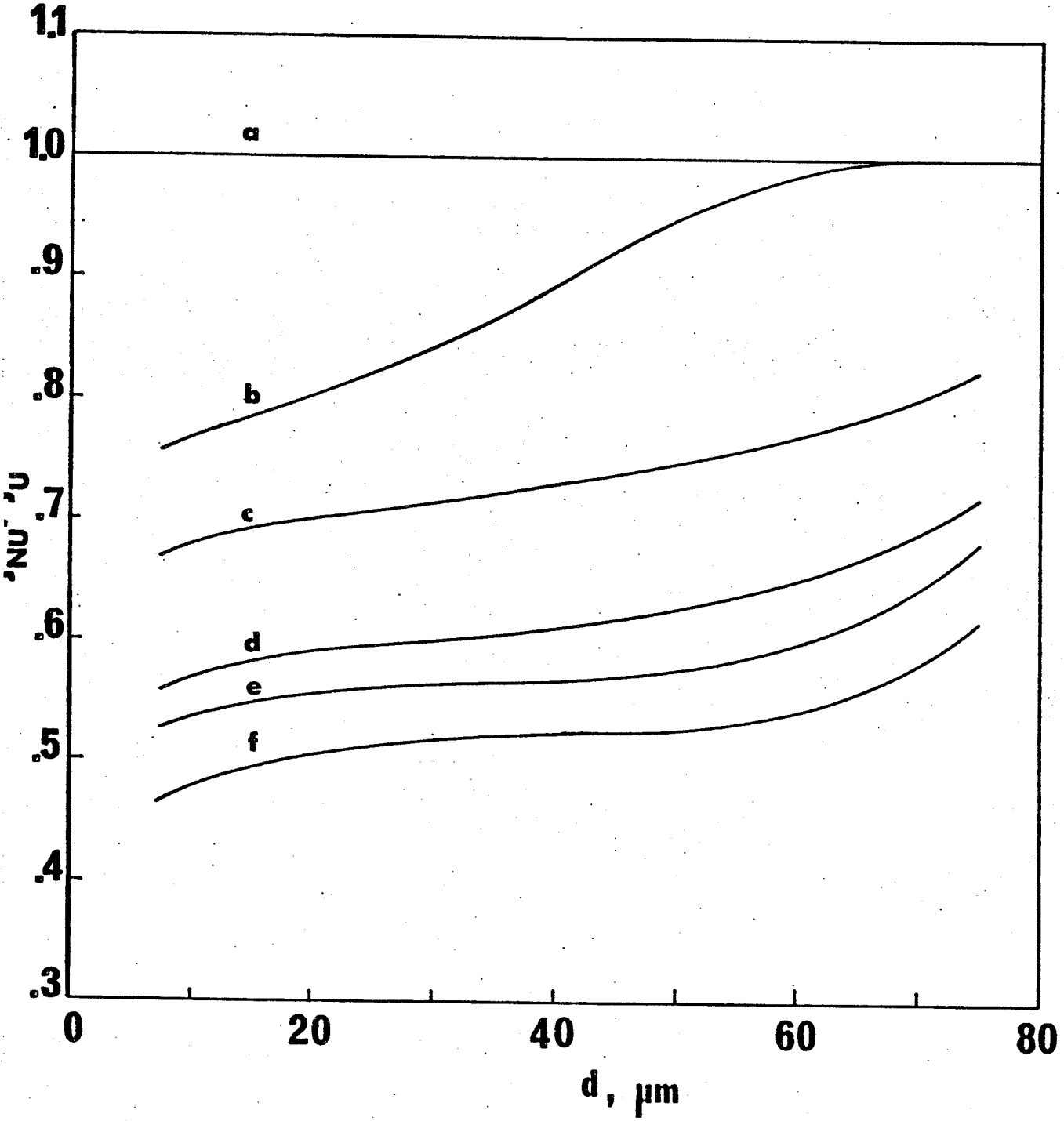

ig. 5.7 J_{NU}/J_U as a function of d for a fixed value of V/d = 0.6 MV m^{-1} for different forms of spatial distribution of traps. (a) S(x) = 1; (b) S(x) = 1 + 0.9 - x/x_o = 70 μm; (c) S(x) = 1 + 0.6 exp($-x/x_o$), x_o = 60 μm; (d) S(x) = 1 + exp ($-x/x_o$) + 0.6 exp[$-(d-x)/x_o$], x_o = 60 μm; (e) S(x) = 1 + exp ($-x/x_o$) + exp[$-(d-x)/x_o$], x_o = 60 μm; and (f) S(x) = 1 + 2 exp($-x/x_o$) = 1.5 exp[$-(d-x)/x_o$], x_o = 60 μm.

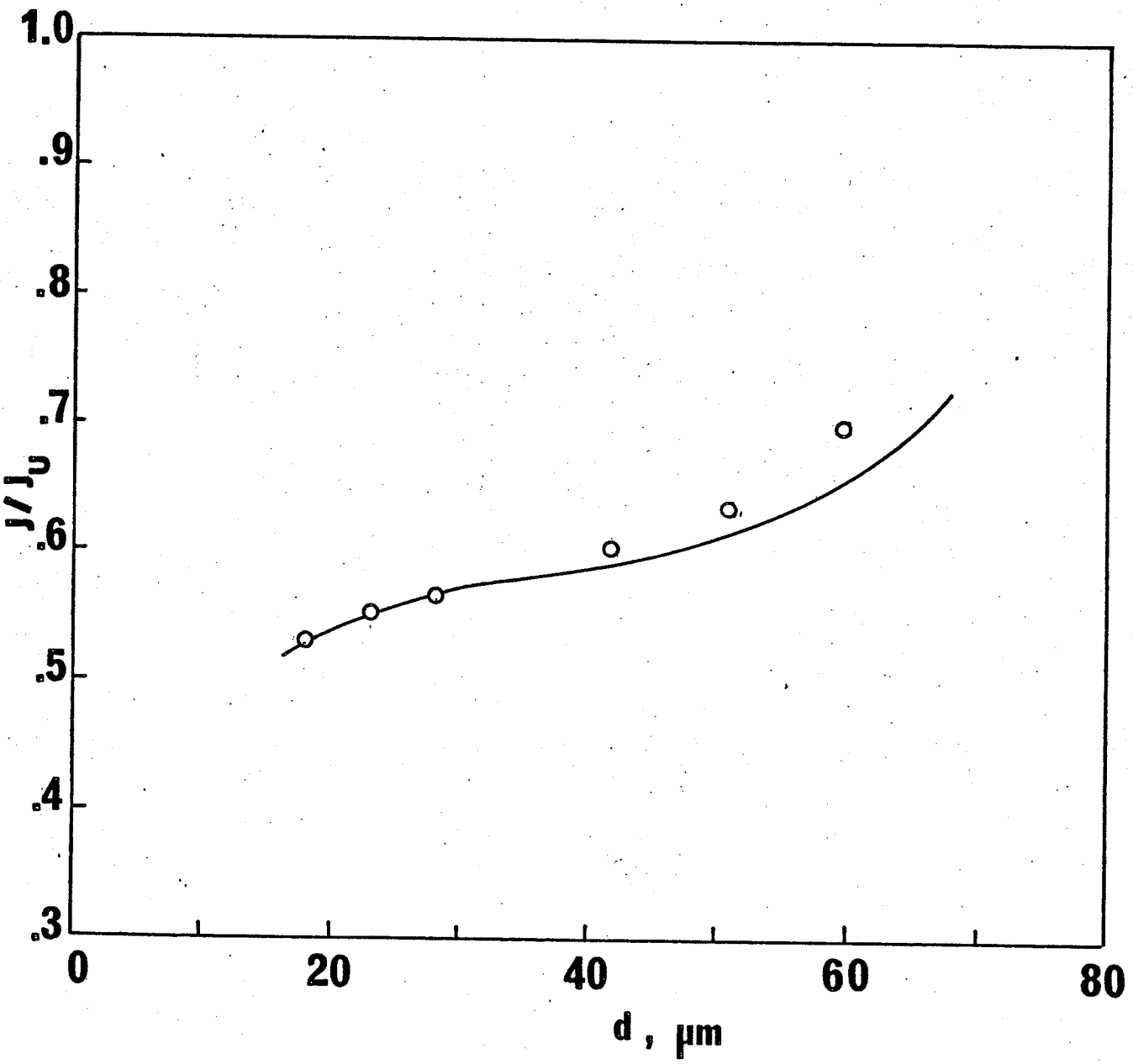

Fig. 5.8 Comparison of J_{NU}/J_U with J/J_U. J denotes the experimental results extracted from the results of Mehl [126]. Solid line: Theoretical, O: Experimental

curve fitting techniques of the experimental data to find the values of the unknown parameters C, D and x_o of the spatial trap distribution function can be used.

5.6 CONCLUDING REMARKS

The general expressions for the steady-state current-voltage characteristics of an insulator-electrolyte system with traps uniformly and non-uniformly distributed in energy and space have been derived using a unified mathematical approach. The analysis techniques illustrated with anthracene thin films as an example may, in principle, be used to analyse any types of trap distribution in space, since any tvpe of distribution can always be resolved into components to fit these four general distribution functions.

CHAPTER VI

DOUBLE INJECTION OF CHARGE CARRIERS INTO THIN FILMS

It is well known that the presence of charge carrier traps is unavoidable in thin organic films. Several authors [79,104] have attempted an analytical solution of the problem of double injection into thin films containing traps uniformly and non-uniformly in energy, but uniformly distributed in space. As has been pointed out in Chapter V, the assumption for the traps uniformly distributed in space in thin organic films is not realistic. In this chapter a unified approach to the theory of double injection in solids with traps uniformly and non-uniformly distributed in energy and space, is presented, based on a discrete regional approximation.

A. THEORY OF PLANAR DOUBLE INJECTION

In the theoretical analysis we make the following assumptions:

(i) The energy band model can be used to treat the behaviour of injected carriers.

(ii) Both the anode for injecting holes and the cathode for injecting electrons form perfect contacts

at z = 0 and z = d, respectively, the specimen thickness being d.

(iii) The electric field is so large that the current components due to diffusion and due to carriers thermally generated in the specimen can be neglected.

(iv) The free hole and electron densities follow the Maxwell-Boltzmann statistics, while the trapped hole and electron densities follow the Fermi-Dirac statistics.

(v) The mobilities of the free holes and electrons are independent of field and are not affected by the presence of traps.

(vi) The fields at both injecting contacts are negligibly small.

(vii) The indirect recombination through traps is predominant so that the direct band to band recombination can be ignored.

The behaviour of double injection in a solid is governed by the current flow equations

$$J_n = q\mu_n n_f F \tag{6.1}$$

$$J_p = q\mu_p p_f F \tag{6.2}$$

$$J = J_n + J_p \tag{6.3}$$

the continuity equations

$$\frac{dJ_n}{dz} = qnp < v\sigma_R > \tag{6.4}$$

$$\frac{dJ_p}{dz} = -qnp \langle v\sigma_R \rangle \tag{6.5}$$

and the Poisson's equation

$$\frac{dF}{dz} = \frac{q}{\varepsilon}(p-n) \tag{6.6}$$

where

$$p = p_f + p_t \tag{6.7}$$

and

$$n = n_f + n_t \tag{6.8}$$

On the basis of the assumptions given above, we have

$$n_f = N_c \exp\left[-(E_c - E_{Fn})/kT\right] \tag{6.9}$$

$$p_f = N_v \exp\left[-(E_{Fp} - E_v)/kT\right] \tag{6.10}$$

$$n_t = \int_{E_{\ell n}}^{E_{un}} h_n(E,z)\, f_n(E)\, dE \tag{6.11}$$

and

$$P_t = \int_{E_{\ell p}}^{E_{up}} h_p(E,z)\, f_p(E)\, dE \tag{6.12}$$

where

$$f_n(E) = \{1 + g_n^{-1} \exp\left[(E - E_{Fn})/kT\right]\}^{-1} \tag{6.13}$$

and

$$f_p(E) = \{1+g_p \exp [(E_{Fp} - E)/kT]\}^{-1} \quad (6.14)$$

6.1 TRAP-FREE CASE

In this case

$$n_t = h_n(E,z) = 0 \quad (6.15)$$

and

$$p_t = h_p(E,z) = 0 \quad (6.16)$$

We introduce the following parameters to simplify the mathematical treatment

$$\alpha_1 = \langle v\sigma_R \rangle \quad (6.17)$$

$$\alpha_2 = 2q/\varepsilon \quad (6.18)$$

$$\mu_o = \varepsilon \langle v\sigma_R \rangle /2q \quad (6.19)$$

$$S_o = q\mu_p n_f F/J \quad (6.20)$$

$$T_o = q\mu_p p_f F/J \quad (6.21)$$

$$U_o = qF^2/J \quad (6.22)$$

Using these parameters, Eqns. (6.3) - (6.6) can be written as

$$S_o + T_o = 1 \tag{6.23}$$

$$\frac{d}{dz} S_o = \alpha_1 S_o T_o / \mu_n \mu_p U_o \tag{6.24}$$

$$\frac{d}{dz} T_o = -\alpha_1 S_o T_o / \mu_n \mu_p U_o \tag{6.25}$$

and

$$\frac{d}{dz} U_o = \alpha_2 [T_o/\mu_p - S_o/\mu_n] \tag{6.26}$$

The solution of the above simultaneous equation is given by

$$U_o = C_o S_o^{\mu_n/\mu_o} (1 - S_o)^{\mu_p/\mu_o} \tag{6.27}$$

where C_o is the constant of integration.

Since the current is carried mainly by the electrons at the cathode and by the holes at the anode, then we have $S_o = 0$ at $z = 0$ and $S_o = 1$ at $z = d$. Hence, using Eqn. (6.27) into Eqn. (6.24) and integrating we obtain

$$C_o = \alpha_1 d/\mu_n \mu_p \int_0^1 S_o^{\mu_n/\mu_o - 1} (1 - S_o)^{\mu_p/\mu_o - 1} dS_0 \tag{6.28}$$

The voltage across the specimen is given by

$$V = -\int_0^d F dz \tag{6.29}$$

Substituting Eqns. (6.27) and (6.22) into Eqn. (6.29), we obtain

$$V = d^{3/2} J^{1/2} \left(\frac{\langle v\sigma_R \rangle}{q\mu_n\mu_p}\right)^{1/2} \frac{\int_0^1 S_o^{3\mu_n/2\mu_o-1} (1-S_o)^{3\mu_p/2\mu_o-1} dS_o}{\int_0^1 S_o^{\mu_n/\mu_o-1} (1-S_o)^{\mu_p/\mu_o-1} dS_o} \tag{6.30}$$

or

$$J = \frac{q\mu_n\mu_p}{\langle v\sigma_R \rangle} \left\{ \frac{\int_0^1 S_o^{3\mu_n/2\mu_o-1} (1-S_o)^{3\mu_p/2\mu_o-1} dS_o}{\left[\int_0^1 S_o^{\mu_n/\mu_o-1} (1-S_o)^{\mu_p/\mu_o-1} dS_o\right]^{3/2}} \right\}^{-2} \frac{V^2}{d^3} \tag{6.31}$$

Equation (6.31) is the current-voltage relation for double injection into a trap free solid. Comparing Eqn. (6.31) with Child's law for single injection into trap free solids given by

$$J = \frac{9}{8} \varepsilon\mu \frac{V^2}{d^3} \tag{6.32}$$

Then Eqn. (6.31) can be written as

$$J = \frac{9}{8} \varepsilon\mu_{eff} \frac{V^2}{d^3} \tag{6.33}$$

where

$$\mu_{eff} = \frac{8}{9} \frac{\mu_n\mu_p}{2\mu_o} \frac{\left[B\left(\frac{\mu_n}{\mu_o}, \frac{\mu_p}{\mu_o}\right)\right]^3}{\left[B\left(\frac{3\mu_n}{2\mu_o}, \frac{3\mu_p}{2\mu_o}\right)\right]^2} \tag{6.34}$$

6.2 THE TRAPS UNIFORMLY DISTRIBUTED IN SPACE BUT NON-UNIFORMLY DISTRIBUTED IN ENERGY

We consider two different cases:

6.2.1 The traps confined in a single discrete energy level

For simplicity, we assume that the traps are shallow, that is, $E_{tn} > E_{Fn}$ and $E_{tp} < E_{Fp}$. For this case, the electron and hole trap distribution functions are respectively given by

$$h_n(E,z) = H_{an}\,\delta(E - E_{tn}) \tag{6.35}$$

and

$$h_p(E,z) = H_{ap}\,\delta(E - E_{tp}) \tag{6.36}$$

Substitution of Eqns. (6.35) and (6.36) into Eqns. (6.11) and (6.12) gives

$$n_t = n_{at} = H_{an}\, g_n \exp\left[(E_{Fn} - E_{tn})/kT\right] \tag{6.37}$$

and

$$p_t = p_{at} = H_{ap}\, g_p^{-1} \exp\left[(E_{tp} - E_{Fp})/kT\right] \tag{6.38}$$

To simplify the mathematical treatment, we introduce the following parameters:

$$K_{an} = 1 + g_n H_{an} N_c^{-1} \exp [(E_c - E_{tn})/kT] \quad (6.39)$$

$$K_{ap} = 1 + g_p^{-1} H_{ap} N_v^{-1} \exp [(E_{tp} - E_v)/kT] \quad (6.40)$$

$$\nu_{an} = \mu_n/K_{an} \quad (6.41)$$

$$\nu_{ap} = \mu_p/K_{ap} \quad (6.42)$$

$$S_a = q\mu_n n_f F/J \quad (6.43)$$

$$T_a = q\mu_p p_f F/J \quad (6.44)$$

$$U_a = qF^2/J \quad (6.45)$$

Using these parameters together with those defined by Eqns. (6.17) - (6.19), then Eqns. (6.3) - (6.6) can be written as

$$S_a + T_a = 1 \quad (6.46)$$

$$\frac{d}{dz} S_a = \alpha_1 S_a T_a/\nu_{an}\nu_{ap} U_a \quad (6.47)$$

$$\frac{d}{dz} T_a = -\alpha_1 S_a T_a/\nu_{an}\nu_{ap} U_a \quad (6.48)$$

and

$$\frac{d}{dz} U_a = \alpha_2 [T_a/\nu_{ap} - S_a/\nu_{an}] \quad (6.49)$$

The solution of the above simultaneous equations is given by:

$$U_a = C_a S_a^{\nu_{an}/\mu_o} (1-S_a)^{\nu_{ap}/\mu_o} \tag{6.50}$$

where C_a is the constant of integration. Using the same boundary condition discussed in Section 6.2, then C_a is given by

$$C_a = \alpha_1 d/\nu_{an}\nu_{ap} \int_0^1 S_a^{\nu_{an}/\mu_o - 1} (1-S_a)^{\nu_{ap}/\mu_o - 1} dS_a \tag{6.51}$$

Using the boundary condition given in Eqn. (6.29) and Eqns. (6.45) and (6.50), the current-voltage relation is given by

$$J = \frac{q\mu_n\mu_p}{\langle v\sigma_R \rangle} \{(K_{an}K_{ap})^{\frac{1}{2}} \frac{\int_0^1 S_a^{3\nu_{an}/2\mu_o - 1} (1-S_a)^{3\nu_{ap}/2\mu_o - 1} dS_a}{\left[\int_0^1 S_a^{\nu_{an}/\mu_o - 1} (1-S_a)^{\nu_{ap}/\mu_o - 1} dS_a\right]^{3/2}}\}^{-2} \frac{V^2}{d^3} \tag{6.52}$$

or

$$J = \frac{9}{8} \varepsilon\mu_{eff} \frac{V^2}{d^3} \tag{6.53}$$

where

$$\mu_{eff} = \frac{8}{9} \frac{q\mu_n\mu_p}{\varepsilon \langle v\sigma_R \rangle} \{(K_{an}K_{ap})^{\frac{1}{2}} \frac{\int_0^1 S_a^{3\nu_{an}/2\mu_o - 1} (1-S_a)^{3\nu_{ap}/2\mu_o - 1} dS_a}{\left[\int_0^1 S_a^{\nu_{an}/\mu_o - 1} (1-S_a)^{\nu_{ap}/\mu_o - 1} dS_a\right]^{3/2}}\}^{-2}$$

$$= \frac{8}{9} \frac{\mu_n \mu_p}{2\mu_o} \frac{1}{K_{an} K_{ap}} \frac{\left[B\left(\frac{\nu_{an}}{\mu_o}, \frac{\nu_{ap}}{\mu_o}\right)\right]^3}{\left[B\left(\frac{3\nu_{an}}{2\mu_o}, \frac{3\nu_{ap}}{2\mu_o}\right)\right]^2} \qquad (6.54)$$

6.2.2 The traps distributed exponenetially within the forbidden energy gap

In this case, the electron and hole trap distribution functions are, respectively, given by

$$h_n(E,z) = \frac{H_{bn}}{kT_c} \exp\left[(E - E_c)/kT_c\right] \qquad (6.55)$$

and

$$h_p(E,z) = \frac{H_{bp}}{kT_c} \exp\left[(E_v - E)/kT_c\right] \qquad (6.56)$$

If $T_c > T$, we can assume $f_n(E) = 1$ for $E < E_{Fn}$ and $f_n(E) = 0$ for $E > E_{Fn}$; and $f_p(E) = 1$ for $E > E_{Fp}$ and $f_p(E) = 0$ for $E < E_{Fp}$, as if we take $T = 0$. This is a good approximation particularly when T_c is much larger than T [121]. Substitution of Eqns. (6.55) and (6.56) into Eqns. (6.11) and (6.12) gives

$$n_t = n_{bt} = H_{bn} N_c^{-1/\ell} n_f^{1/\ell} \qquad (6.57)$$

$$p_t = p_{bt} = H_{bp} N_v^{-1/\ell} p_f^{1/\ell} \qquad (6.58)$$

In this type of trap distribution, particularly in thin films, we can assume [156] that $n_t >> n_f$ and $p_t >> p_f$ (this implies that the direct band to band recombination is ignored).

Thus,

$$n = n_f + n_t \simeq H_{bn} N_c^{-1/\ell} n_f^{1/\ell} \tag{6.59}$$

and

$$p = p_f + p_t \simeq H_{bp} N_v^{-1/\ell} p_f^{1/\ell} \tag{6.60}$$

To simplify matters, we introduce the following parameters:

$$\alpha_1 = q < v\sigma_R > /J \tag{6.61}$$

$$\alpha_2 = q^2/\varepsilon J \tag{6.62}$$

$$\mu_b = \varepsilon < v\sigma_R > /q \tag{6.63}$$

$$K_{bn} = H_{bn} N_c^{-1/\ell} \tag{6.64}$$

$$K_{bp} = H_{bp} N_v^{-1/\ell} \tag{6.65}$$

$$\nu_{bn} = \mu_n^{1/\ell}/K_{bn} \tag{6.66}$$

$$\nu_{bp} = \mu_p^{1/\ell}/K_{bp} \tag{6.67}$$

$$S_b = q \mu_n n_f F/J \tag{6.68}$$

$$T_b = q \mu_p p_f F/J \tag{6.69}$$

$$U_b = q F/J \tag{6.70}$$

Using these parameters, Eqns. (6.3) - (6.6) can be written as

$$S_b + T_b = 1 \tag{6.71}$$

$$\frac{d}{dz} S_b = \alpha_1 S_b^{1/\ell} T_b^{1/\ell}/\nu_{bn}\nu_{bp}U_b^{2/\ell} \tag{6.72}$$

$$\frac{d}{dz} T_b = -\alpha_1 S_b^{1/\ell} T_b^{1/\ell} /\nu_{bn}\nu_{bp} U_b^{2/\ell} \tag{6.73}$$

and

$$\frac{d}{dz} U_b = \alpha_2 [T_b^{1/\ell}/\nu_{bp} - S_b^{1/\ell}/\nu_{bn}]/U_b^{1/\ell} \tag{6.74}$$

The solution to the above simultaneous equations is

$$U_b = [\frac{\nu_{bn}}{\mu_b} S_b^{(\ell-1)/\ell} + \frac{\nu_{bp}}{\mu_b} (1-S_b)^{(\ell-1)/\ell} + C_b]^{\ell/(\ell-1)} \tag{6.75}$$

where C_b is the integration constant which can be determined by the solution of

$$\int_0^1 [\frac{\nu_{bn}}{\mu_b} S_b^{(\ell-1)/\ell} + \frac{\nu_{bp}}{\mu_b} (1-S_b)^{(\ell-1)/\ell} + C_b]^{2\ell/(\ell-1)} [S_b(1-S_b)]^{-1/\ell} dS_b$$

$$= \alpha_1 d/\nu_{bn}\nu_{bp} \tag{6.76}$$

Using the boundary condition given in Eqn. (6.29) and Eqns. (6.70) and (6.75), we obtain the current-voltage relation;

$$J = q [\frac{(N_c N_y \mu_n \mu_p)^{1/\ell}}{H_{bn} H_{bp} \langle v\sigma_R \rangle}]^{\ell/(2-\ell)} \cdot \frac{V^{2/(2-\ell)}}{d^{(\ell+2)/(2-\ell)}}$$

$$\times \left\{ \frac{\int_0^1 \left[\frac{\nu_{bn}}{C_b \mu_b} S_b^{(\ell-1)/\ell} + \frac{\nu_{bp}}{C_b \mu_b} (1-S_b)^{(\ell-1)/\ell} + 1 \right]^{(\ell+2)/(\ell-1)} \left[S_b (1-S_b) \right]^{-1/\ell} dS_b}{\left[\int_0^1 \left[\frac{\nu_{bn}}{C_b \mu_b} S_b^{(\ell-1)/\ell} + \frac{\nu_{bp}}{C_b \mu_b} (1-S_b)^{(\ell-1)/\ell} + 1 \right]^{2/(\ell-1)} \left[S_b (1-S_b) \right]^{-1/\ell} dS_b \right]^{(\ell+2)/2}} \right\}^{-2/(2-\ell)}$$

(6.77)

where C_b is given by Eqn. (6.76). Equation (6.77) is the current-voltage relation for the traps exponentially distributed within the forbidden energy band gap. It can be seen that Eqn. (6.77) is not valid for ℓ equal to or very close to 2, since there is a singularity point at $\ell = 2$ and also not valid for $\ell > 2$, since physical reality does not permit a negative exponent of the voltage because this would lead to an unrealistic situation. It should be noted that the assumptions used to simplify the mathematical treatment in this case ($n_t >> n_f$ and $p_t >> p_f$) require that the value of ℓ should not be too large. As has been pointed out by Lampert and Mark [104] that for $\ell < 1$ the solution would reduce to the case of traps confined in a single discrete shallow energy level and for large values of ℓ, to the case of uniformly distributed traps within the forbidden energy band gap. It is reasonable to assume that, in most cases, the mathematical assumption mentioned above may not be good enough to approach a general

analytical solution for all values of ℓ. However, a numerical solution for the cases when $\ell > 2$ could always be worked out with or without the assumptions, using the numerical values of the physical parameters for a particular material. It should be noted that in most practical cases the values of ℓ are always less than 2 and hence, Eqn. (6.77) which is valid only for $1 < \ell < 2$, applies.

For $\ell = 2$ the analytical solution could be easily obtained and it is given by

$$V = \frac{\varepsilon}{q^3} \frac{\nu_{bn}\nu_{bp}}{\mu_b} J^2 \int_0^1 \left[\frac{\nu_{bn}}{\mu_b} S_b^{\frac{1}{2}} + \frac{\nu_{bp}}{\mu_b} (1-S_b)^{\frac{1}{2}} + C_b\right]^4 [S_b(1-S_b)]^{-\frac{1}{2}} dS_b \tag{6.78}$$

where C_b is given by

$$\int_0^1 \left[\frac{\nu_{bn}}{\mu_b} S_b^{\frac{1}{2}} + \frac{\nu_{bp}}{\mu_b} (1-S_b)^{\frac{1}{2}} + C_b\right]^2 [S_b(1-S_b)]^{-\frac{1}{2}} dS_b = \frac{q < v\sigma_R >}{\nu_{bn}\nu_{bp}} \frac{d}{J} \tag{6.79}$$

6.3 THE TRAPS NON-UNIFORMLY DISTRIBUTED IN BOTH ENERGY AND SPACE

We consider two different cases of energy distribution

6.3.1 The traps confined in a single discrete energy level

For simplicity, we assume that the traps are shallow. For this case, the electron and hole distribution functions are, respectively, given by

$$h_n(E,z) = H_{an}\,\delta(E - E_{tn})\,S_n(z) \tag{6.80}$$

and

$$h_p(E,z) = H_{ap}\,\delta(E - E_{tp})\,S_p(z) \tag{6.81}$$

Substitution of Eqns. (6.80) and (6.81) into Eqns. (6.11) and (6.12) gives

$$n_t = n_{at} = H_{an}\,g_n \exp\left[(E_{Fn}-E_{tn})/kT\right] S_n(z) \tag{6.82}$$

and

$$p_t = p_{at} = H_{ap}\,g_p^{-1} \exp\left[(E_{tp}-E_{Fp})/kT\right] S_p(z) \tag{6.83}$$

Following the same principle, we introduce the following parameters:

$$K_{anz} = 1 + g_n H_{an} N_c^{-1} \exp\left[(E_c - E_{tn})/kT\right] S_n(z) \tag{6.84}$$

$$K_{apz} = 1 + g_p^{-1} H_{ap} N_v^{-1} \exp\left[(E_{tp} - E_v)/kT\right] S_p(z) \tag{6.85}$$

$$\nu_{anz} = \mu_n / K_{anz} \tag{6.86}$$

$$\nu_{apz} = \mu_p / K_{apz} \tag{6.87}$$

$$S_a = q\, \mu_n\, n_f\, F/J \tag{6.88}$$

$$T_a = q\, \mu_p\, p_f\, F/J \tag{6.89}$$

$$U_a = q\, F^2/J \tag{6.90}$$

Using these parameters, together with those defined by Eqns. (6.17)-(6.19), Eqns. (6.3)-(6.6) can be written as

$$S_a + T_a = 1 \tag{6.91}$$

$$\frac{d}{dz} S_a = \alpha_1 S_a T_a / \nu_{anz} \nu_{apz} U_a \tag{6.92}$$

$$\frac{d}{dz} T_a = -\alpha_1 S_a T_a / \nu_{anz} \nu_{apz} U_a \tag{6.93}$$

$$\frac{d}{dz} U_a = \alpha_2 [T_a/\nu_{apz} - S_a/\nu_{anz}] \tag{6.94}$$

Since ν_{anz} and ν_{apz} are functions of the independent parameter z through the non-uniform spatial distribution functions of traps $S_n(z)$ and $S_p(z)$, the solution of the above simultaneous equations is complicated. However, if S_n and S_p are continuous and non-singular functions in the region between z = 0 and z = d, we can employ a regional approximation technique to solve the problem as described in Chapter V.

Consider the general spatial distribution function shown in Fig. 6.1. We can devide the region $0 \leq z \leq d$ into M equal intervals, within each of which the values of S_n and S_p can be approximated by constant values b_{ni} and b_{pi}, respectively, which are expressed as,

$$b_{ni} = \frac{1}{z_{i+1} - z_i} \int_{z_i}^{z_{i+1}} S_n(z)dz = \frac{M}{d} \int_{z_i}^{z_{i+1}} S_n(z)dz \tag{6.95}$$

and

$$b_{pi} = \frac{1}{z_{i+1} - z_i} \int_{z_i}^{z_{i+1}} S_p(z)dz = \frac{M}{d} \int_{z_i}^{z_{i+1}} S_p(z)dz \tag{6.96}$$

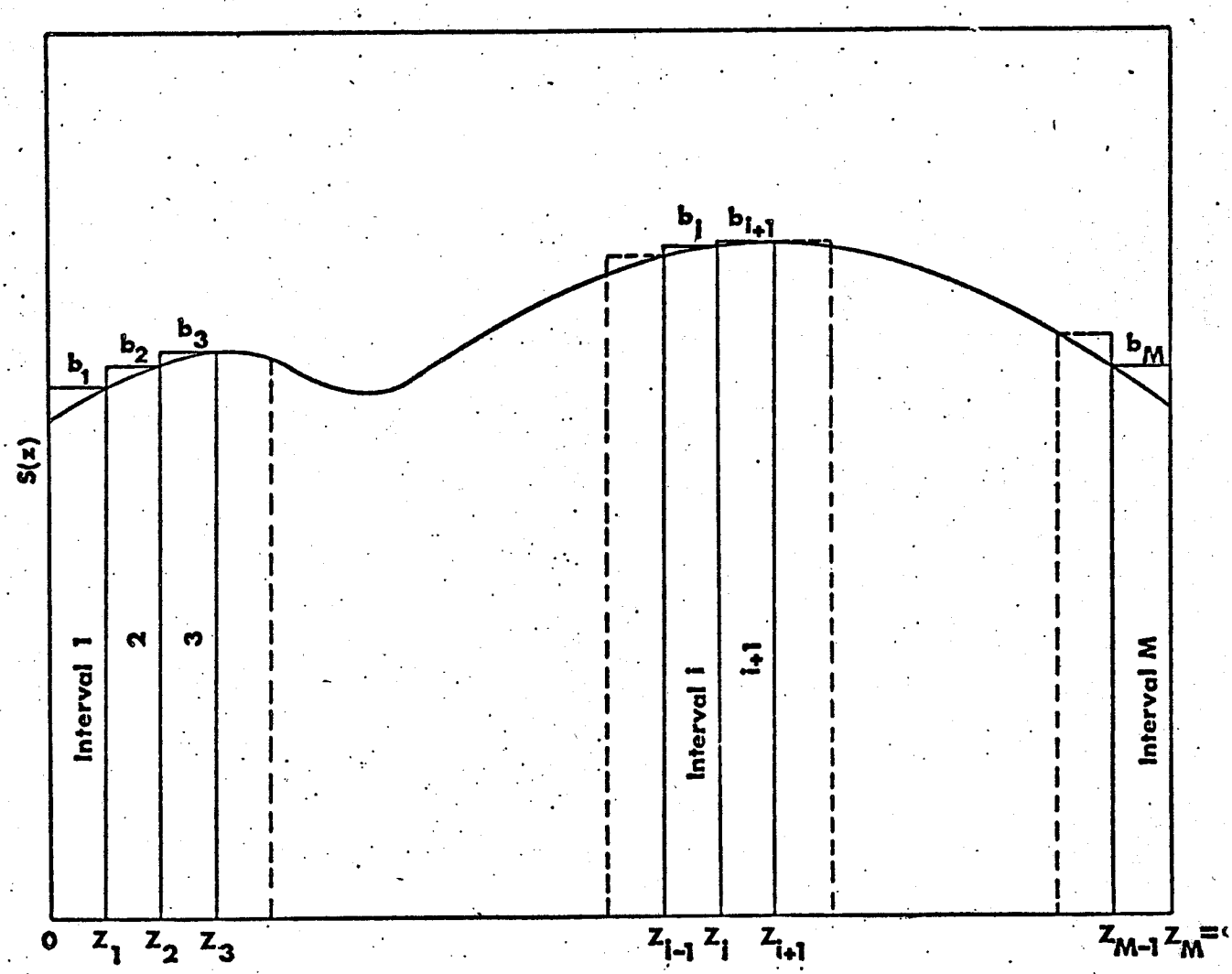

Fig. 6.1 Illustrating the discrete regional approximation for an arbitrary spatial distribution function of traps

where $z_i = \frac{d}{M} i$ (6.97)

The voltage across the ith interval located between $z_i \leq z \leq z_{i+1}$ is given by

$$V_i = -\int_{z_i}^{z_{i+1}} F_i dz \tag{6.98}$$

where F_i is the electric field distribution within the ith interval. The total voltage across the whole specimen is the applied voltage, which is

$$V = \sum_{i=o}^{M-1} V_i \tag{6.99}$$

Now the problem reduces to the solution of Eqns. (6.91) - (6.94) in the intervals $z_i \leq z \leq z_{i+1}$, within each of which ν_{ani} and ν_{api} are replacing ν_{anz} and ν_{apz}, and are constants. Thus, in the ith interval the solution is given by

$$U_{ai} = C_{ai} S_a^{\nu_{ani}/\mu_o} (1-S_a)^{\nu_{api}/\mu_o} \tag{6.100}$$

where C_{ai} is the integration constant. Since the electric field is continuous at each boundary between intervals, it can be easily shown that for

$$(F_i)_{z=z_{i+1}} = (F_{i+1})_{z=z_{i+1}} \tag{6.101}$$

we get the recurrence formula for C_{ai} given by

$$C_{ai+1} = C_{ai} \left[S_{ai+1}^{(\nu_{ani}-\nu_{ani+1})} (1-S_{ai+1})^{(\nu_{api}-\nu_{api+1})} \right]^{1/\mu_o} \tag{6.102}$$

and for each interval, substituting Eqn. (6.100) into (6.92), we obtain

$$C_{ai} = \alpha_1 d/\nu_{ani}\nu_{api} \, M \int_{S_{ai}}^{S_{ai+1}} S_a^{\nu_{ani}/\mu_o - 1} (1-S_a)^{\nu_{api}/\mu_o - 1} \, dS_a \tag{6.103}$$

We have M unknown C_{ai}'s and M + 1 unknown S_{ai}'s. However, as has been pointed out before that the entire current at the anode is carried by holes and the entire current at the cathode is carried by electrons, therefore $S_{ao} = 0$ and $S_{aM} = 1$. Hence, the number of unknowns reduces to 2M - 1. From Eqns. (6.102) and (6.103) we can have 2M -1 simultaneous equations, so that these unknowns can be solved by an iterative technique.

Substituting Eqns. (6.90), (6.99) and (6.100) into Eqn. (6.98), we obtain the current-voltage relation

$$J = \frac{q\mu_n\mu_p}{\langle v\sigma_R \rangle} \cdot \left\{ \frac{1}{M^{3/2}} \sum_{i=o}^{M-1} (K_{ani}K_{api})^{1/2} \frac{\int_{S_{ai}}^{S_{ai+1}} S_a^{3\nu_{ani}/2\mu_o - 1} (1-S_a)^{3\nu_{api}/2\mu_o - 1} \, dS_a}{\left[\int_{S_{ai}}^{S_{ai+1}} S_a^{\nu_{ani}/\mu_o - 1} (1-S_a)^{\nu_{api}/\mu_o - 1} \, dS_a \right]^{3/2}} \right\}^{-2} \frac{v^2}{d^3} \tag{6.104}$$

Eqn. (6.104) can be also written as

$$J = \frac{9}{8} \varepsilon \mu_{eff} \frac{v^2}{d^3_{eff}} \tag{6.105}$$

where

$$d_{eff} = d\left[\frac{9}{8} \frac{\varepsilon \prec v\sigma_R \succ}{q} \frac{\mu_{eff}}{\mu_n \mu_p}\right]^{1/3} \left\{\frac{1}{M^{3/2}} \sum_{i=o}^{M-1} (K_{ani} K_{api})^{\frac{1}{2}} \right.$$

$$\left. \frac{\left[\int_{S_{ai}}^{S_{ai+1}} S_a^{3\nu_{ani}/2\mu_o - 1} (1-S_a)^{3\nu_{api}/2\mu_o - 1} dS_a\right]^{2/3}}{\int_{S_{ai}}^{S_{ai+1}} S_a^{\nu_{ani}/\mu_o - 1} (1-S_a)^{\nu_{api}/\mu_o - 1} dS_a} \right\} \tag{6.106}$$

where μ_{eff} is given by Eqn. (6.53). Equation (6.105) is similar in form to that obtained by Hwang and Kao [79], except that d has been replaced with d_{eff} which takes into account the inhomogeneous spatial distribution of traps. It can be easily shown that Eqn. (6.104) reduces to that for the uniform spatial distribution of traps by putting $b_{ni} = b_{pi} = 1$ and those for trap free solids by putting $b_{ni} = b_{pi} = 0$.

6.3.2. The traps distributed exponenetially within the forbidden energy gap

In this case, the trap distribution functions are, respectively, given by

$$h_n(E,z) = \frac{H_{bn}}{kT_c} \exp\left[(E - E_c)/kT_c\right] S_n(z) \qquad (6.107)$$

and

$$h_p(E,z) = \frac{H_{bp}}{kT_c} \exp\left[(E_v - E)/kT_c\right] S_p(z) \qquad (6.108)$$

Similar to the approximation described in Section 6.2.2, we can write

$$n_t = n_{bt} = H_{bn} N_c^{-1/\ell} n_f^{1/\ell} S_n(z) \qquad (6.109)$$

$$p_t = p_{bt} = H_{bp} N_v^{-1/\ell} p_f^{1/\ell} S_p(z) \qquad (6.110)$$

By assuming $n_t >> n_f$ and $p_t >> p_f$, then

$$n = n_f + n_t \simeq K_{bnz} n_f^{1/\ell} \qquad (6.111)$$

and

$$p = p_f + p_t \simeq K_{bpz} p_f^{1/\ell} \qquad (6.112)$$

where

$$K_{bnz} = H_{bnz} N_c^{-1/\ell} S_n(z) \tag{6.113}$$

and

$$K_{bpz} = H_{bpz} N_v^{-1/\ell} S_p(z) \tag{6.114}$$

To simplify matters, we introduce the following parameters:

$$\nu_{bnz} = \mu_n^{1/\ell}/K_{bnz} \tag{6.115}$$

$$\nu_{bpz} = \mu_p^{1/\ell}/K_{bpz} \tag{6.116}$$

$$S_b = q \mu_n n_f F/J \tag{6.117}$$

$$T_b = q \mu_p p_f F/J \tag{6.118}$$

$$U_b = q F/J \tag{6.119}$$

Using these parameters together with those defined by Eqns. (6.61) - (6.63), Eqns. (6.3) - (6.6) can be written as

$$S_b + T_b = 1 \tag{6.120}$$

$$\frac{d}{dz} S_b = \alpha_1 S_b^{1/\ell} T_b^{1/\ell}/\nu_{bnz}\nu_{bpz}U_b^{2/\ell} \tag{6.121}$$

$$\frac{d}{dz} T_b = -\alpha_1 S_b^{1/\ell} T_b^{1/\ell}/\nu_{bnz}\nu_{bpz}U_b^{2/\ell} \tag{6.122}$$

$$\frac{d}{dz} U_b = \alpha_2 [T_b^{1/\ell}/\nu_{bpz} - S_b^{1/\ell}/\nu_{bnz}]/U_b^{1/\ell} \qquad (6.123)$$

Using the regional approximation technique described in Eqns. (6.95) - (6.99), the solution of Eqn. (6.123) with the aid of Eqns. (6.120) - (6.122) in the ith interval gives

$$U_{bi} = \left[\frac{\nu_{bni}}{\mu_b} S_b^{(\ell-1)/\ell} + \frac{\nu_{bpi}}{\mu_b} (1-S_b)^{(\ell-1)/\ell} + C_{bi} \right]^{\ell/(\ell-1)} \qquad (6.124)$$

where C_{bi} is the integration constant. On the basis of the continuity of the field at the boundaries between the intervals, the recurrence formula for C_{bi} is given by

$$C_{bi+1} = C_{bi} + \frac{1}{\mu_b} \left[(\nu_{bni} - \nu_{bni+1}) S_{bi+1}^{(\ell-1)/\ell} + (\nu_{bpi} - \nu_{bpi+1}) (1-S_{bi+1})^{(\ell-1)/\ell} \right] \qquad (6.125)$$

and for each interval. Substituting Eqn. (6.124) into Eqn. (6.121) we obtain

$$\int_{S_{bi}}^{S_{bi+1}} \left[\frac{\nu_{bni}}{\mu_b} S_b^{(\ell-1)/\ell} + \frac{\nu_{bpi}}{\mu_b} (1-S_b)^{(\ell-1)/\ell} + C_{bi} \right]^{2\ell/(\ell-1)} [S_b(1-S_b)]^{-1/\ell} dS_b$$

$$= \alpha_1 d/M \nu_{bni} \nu_{bpi} \qquad (6.126)$$

Following the same method described in Section 6.3.1, it can be easily shown that the current-voltage relation is given by

$$J = q\left[\frac{(N_c N_v \mu_n \mu_p)^{1/\ell}}{H_n H_p \langle v\sigma_R \rangle}\right]^{\ell/(2-\ell)} \frac{v^{2/(2-\ell)}}{d^{(\ell+2)/(2-\ell)}} \left\{\frac{1}{M^{(\ell+2)/2}} \sum_{i=o}^{M-1} (b_{ni} b_{pi})^{\ell/2} \right.$$

$$\left. \frac{\int_{S_{bi}}^{S_{bi+1}} \left[\frac{\nu_{bni}}{C_{bi}\mu_b} S_b^{(\ell-1)/\ell} + \frac{\nu_{bpi}}{C_{bi}\mu_b} (1-S_b)^{(\ell-1)/\ell} + 1\right]^{(\ell+2)/(\ell-1)} [S_b(1-S_b)]^{-1/\ell} dS_b}{\left[\int_{S_{bi}}^{S_{bi+1}} \left[\frac{\nu_{bni}}{C_{bi}\mu_b} S_b^{(\ell-1)/\ell} + \frac{\nu_{bpi}}{C_{bi}\mu_b} (1-S_b)^{(\ell-1)/\ell} + 1\right]^{2/(\ell-1)} [S_b(1-S_b)]^{-1/\ell} dS_b\right]^{(\ell+2)/2}} \right\}^{-2/(\ell}$$

(6.127)

Equation (6.127) can be written in the form of Eqn.(6. 77) by replacing d by d_{eff} where

$$d_{eff} = d \left\{\frac{1}{M^{(\ell+2)/2}} \sum_{i=0}^{M-1} (b_{ni} b_{pi})^{\ell/2} \frac{\int_{S_{bi}}^{S_{bi+1}} [\quad]^{2/(\ell} ds_b}{\left[\int_{S_{bi}}^{S_{bi+1}} [\quad] ds_b\right]^{(\ell+2)/2}}\right\}$$

$$\left\{\frac{\int_0^1 [\quad]^{2/(\ell+} ds_b}{\left[\int_0^1 [\quad] ds_b\right]^{(\ell+2)/2}}\right\} \quad (6.128)$$

Again, the validity of this equation is for $1 < \ell < 2$ and the reason has been given in Section 6.2.2. d_{eff} takes into account the inhomogeneous spatial distribution of traps. It can be easily shown that Eqns (6.104) and (6.128) reduce to those for the uniform spatial distribution of traps by putting $b_{ni} = b_{pi} = 1$.

B. THEORY OF FILAMENTARY DOUBLE INJECTION

Since the interface between the insulator and the electrode is unlikely to be homogeneous and uniform microscopically [12,81], therefore, we would expect that there may be one or more microregions on the electrode surfaces at which the potential barrier has a more favorable profile to carrier injection than at other regions of the interface. Furthermore, due to film imperfections and energy considerations, the current passing through a film specimen is likely to be filamentary at least from a microscopic point of view. Experimental observations have confirmed the existence of such filaments [12]. The filament develops first at some device inhomogeneity, is stationary, and grows in size about the nucleation region as the current is increased. Consequently, the current density will not be radially uniform due to the filament formation.

We now present a theoretical model for the filamentary double injection by using cylindrical co-ordinates and consider only one filament formed along the z direction which coincides with the central line joining the two circular plane electrodes, the effective radius of the filament being r_d. In addition to the assumptions given in Part A, we make, also, the following assumptions for the theoretical analysis.

(i) For mathematical simplicity we use cylindrical co-ordinates and the whole system is symmetrical about the z axis.

(ii) In the filament the longitudinal component of the diffusion current can be ignored because of the large longitudinal component of the electric field, and the radial component of the drift current can be ignored because of the small radial component of the electric field.

(iii) The recombination rate R consists of a longitudinal componenet R_z and a radial component R_r.

The behaviour of double injection in a solid is governed by the current flow equations

$$J_n = J_{nz} + J_{nr}$$
$$= q \mu_n n_f F \hat{i}_z + q D_n \frac{\partial n_f}{\partial r} \hat{i}_r \qquad (6.129)$$

$$J_p = J_{pz} + J_{pr}$$
$$= q \mu_p p_f F \hat{i}_z - q D_p \frac{\partial p_f}{\partial r} \hat{i}_r \qquad (6.130)$$

the continuity equations

$$\mu_n \frac{\partial}{\partial z} (n_f F) = -\mu_p \frac{\partial}{\partial z} (p_f F) = np \langle v\sigma_R \rangle_z \qquad (6.131)$$

$$D_n \frac{1}{r} \frac{\partial}{\partial r} (r \frac{\partial n_f}{\partial r}) = D_p \frac{1}{r} \frac{\partial}{\partial r} (r \frac{\partial p_f}{\partial r}) = np \langle v\sigma_R \rangle_r \qquad (6.132)$$

and the Poisson's equation

$$\nabla \cdot F = \frac{q}{\varepsilon} (p-n) \qquad (6.133)$$

We shall consider the following cases:

6.4 TRAP-FREE CASE

We define the following parameters to simplify the mathematical treatment

$$C_o = q^{-1} \left[\frac{\mu_n D_p + \mu_p D_n}{D_n D_p}\right] \frac{\langle v\sigma_R \rangle_r}{\mu_n \mu_p} \tag{6.134}$$

$$A_o = C_o \frac{\mu_n/\mu_p}{[1+\mu_n/\mu_p]^2} \tag{6.135}$$

$$S_{oz} = q\, \mu_n\, n_f\, F_z/J_{zo} \tag{6.136}$$

$$T_{oz} = q\, \mu_p\, p_f\, F_z/J_{zo} \tag{6.137}$$

$$U_{oz} = \varepsilon\, \mu_n \mu_p\, F_z^2/2J_{zo} \tag{6.138}$$

$$W_{oz} = J_z/J_{zo} \tag{6.139}$$

Using these parameters, the total current in the z-direction

can be written as

$$W_{oz} = S_{oz} + T_{oz} \tag{6.140}$$

and equation (6.132) becomes

$$\frac{1}{r}\frac{\partial}{\partial r}\left(r\frac{\partial W_{oz}}{\partial r}\right) = C_o \frac{J_{zo}}{F_z} S_{oz} T_{oz} \tag{6.141}$$

By assuming that the radial variation of F_z is negligible, it has been shown that [81]

$$T_{oz} = (\mu_p/\mu_n)\, S_{oz} \tag{6.142}$$

Hence,

$$S_{oz} = [1 + \mu_p/\mu_n]^{-1} W_{oz} \tag{6.143}$$

and

$$T_{oz} = (\mu_p/\mu_n)\, [1 + \mu_p/\mu_n]^{-1} W_{oz} \tag{6.144}$$

Hence, equation (6.139) becomes

$$\frac{1}{r}\frac{\partial}{\partial r}\left(r\frac{\partial}{\partial r} W_{oz}\right) = \lambda_o J_{zo} W_{oz}^2 \tag{6.145}$$

where

$$\lambda_o = A_o/F_z \tag{6.146}$$

To obtain an equation for an average profile, we average the parameters over the specimen thickness. Thus, Eqn. (6.145) becomes

$$\frac{d^2}{dr^2}\,\bar{W}_{oz} + \frac{1}{r}\,\frac{d}{dr}\,\bar{W}_{oz} = \langle \lambda_o \rangle\, J_{zo}\, \bar{W}_{oz}^2 \qquad (6.147)$$

where $\langle \lambda_o \rangle$ is the average value of λ_o over the specimen thickness, given by

$$\langle \lambda_o \rangle = \frac{1}{d}\int_0^d \lambda_o\, dz$$

$$= \frac{\langle v\sigma_R \rangle}{dq}\, r\, \left[\frac{\mu_n D_p + \mu_p D_n}{D_n D_p}\right] (\mu_n+\mu_p)^{-2} \int_0^d F_z^{-1}\, dz \qquad (6.148)$$

The term $\frac{1}{r}\frac{d}{dr}\bar{W}_{oz}$ in Eqn. (6.147) can be neglected, since physical reality requires a finite solution for all values of r including r = 0 [81]. Hence, Eqn. (6.147) becomes

$$\frac{d^2}{dr^2}\,\bar{W}_{oz} = \langle \lambda_o \rangle\, J_{zo}\, \bar{W}_{oz}^2 \qquad (6.149)$$

The solution of this differential equation is subjected to the boundary conditions $r \to 0$, $\bar{W}_{oz} \to 1$ and $r \to \infty$, $\bar{W}_{oz} \to 0$. Hence, the solution is given by

$$\bar{W}_{oz}(r) = \left[1 + \left(\frac{1}{6}\langle \lambda_o \rangle J_{zo}\right)^{\frac{1}{2}} r\right]^{-2} \qquad (6.150)$$

or

$$\bar{J}_z(r) = J_{zo}\left[1 + \left(\frac{1}{6} < \lambda_o > J_{zo}\right)^{\frac{1}{2}} r\right]^{-2} \qquad (6.151)$$

and the total current in the filament is given by

$$I = \int_0^{2\pi}\int_0^{r_d} \bar{J}_z\,(r)\; r\; dr\; d\theta$$

$$= \frac{12\pi}{<\lambda_o>}\left\{\ln\left[1+\left(\frac{1}{6} < \lambda_o > J_{zo}\right)^{\frac{1}{2}} r_d\right]+\left[1+\left(\frac{1}{6}< \lambda_o > J_{zo}\right)^{\frac{1}{2}} r_d\right]-1\right\} \qquad (6.152)$$

J_{zo} is given by the solution of planar double injection given by Eqn. (6.31). It is likely that multiple filaments may simultaneously exist between the electrodes. The total current can be represented by the summation of all individual filamentary currents. For multiple filaments, the total current can be written as

$$I_t = NI \qquad (6.153)$$

where N is the number of filaments and I is given by Eqn. (6.152). It should be noted that N may be field-dependent, since the number of current filaments is field dependent.

6.5. THE TRAPS UNIFORMLY DISTRIBUTED IN SPACE BUT NON-UNIFORMLY DISTRIBUTED IN ENERGY

We consider the two different cases

6.5.1 The traps confined in a single discrete energy level

For simplicity, we assume that the traps are shallow.

We also introduce the following parameters:

$$C_a = q^{-1} \left[\frac{\mu_n D_p + \mu_p D_n}{D_n D_p}\right] \frac{\langle v\sigma_R \rangle r}{\mu_n \mu_p} K_{an} K_{ap} \tag{6.154}$$

$$A_a = C_a \frac{\mu_n K_{an}/\mu_p K_{ap}}{[1+\mu_n K_{an}/\mu_p K_{ap}]^2} \tag{6.155}$$

$$S_{az} = q\, \mu_n\, n_f\, F_z/J_{zo} \tag{6.156}$$

$$T_{az} = q\, \mu_p\, p_f\, F_z/J_{zo} \tag{6.157}$$

$$U_{az} = \varepsilon\, \mu_n \mu_p\, F_z^2/2J_{zo} \tag{6.158}$$

$$W_{az} = J_z/J_{zo} \tag{6.159}$$

Similarly, the solution for this case is given by

$$I = \frac{12\Pi}{\langle \lambda_a \rangle} \left\{ \ell n\left[1+\left(\frac{1}{6}\langle \lambda_a \rangle J_{zo}\right)^{\frac{1}{2}} r_d\right] + \left[1+\left(\frac{1}{6} \langle \lambda_a \rangle J_{zo}\right)^{\frac{1}{2}} r_d\right] - 1 \right\} \tag{6.160}$$

where

$$\langle \lambda_a \rangle = \frac{\langle v\, \sigma_R \rangle r}{dq} \left[\frac{\mu_n D_p + \mu_p D_n}{D_n D_p}\right] (\mu_n K_{an} + \mu_p K_{ap})^{-2} \int_0^d F_z^{-1} dz \tag{6.161}$$

K_{an} and K_{ap} are given by Eqns. (6.39) and (6.40), respectively;

and J_{zo} is given by Eqn. (6.52). The total current is obtained by substitution of Eqn. (6.160) into Eqn. (6.153).

6.5.2 The traps distributed exponenetially within the forbidden energy gap

Using the same principle described in the above section, the filamentary current in this case is given by

$$I = 2\Pi \int_0^{r_d} \bar{J}_z(r)\, r\, dr \tag{6.163}$$

where

$$\bar{J}_z(r) = J_{zo}\left[1 + \left(\frac{2-\ell}{2\ell}\right)\left(\frac{2\ell}{\ell+2} < \lambda_b >\right)^{\frac{1}{2}} J_{zo}^{(2-\ell)/2\ell} r\right]^{2\ell/(\ell-2)} \tag{6.164}$$

and

$$< \lambda_b > = q^{\frac{\ell-2}{\ell}} \frac{< v q_R > r}{d} \left[\frac{\mu_n D_p + \mu_p D_n}{D_n D_p}\right] \frac{(\mu_n \mu_p)^{1/\ell} / (K_{bn} K_{bp})^2}{[\mu_n / K_{bp}^{\ell} + \mu_p / K_{bn}^{\ell}]^{1/\ell}}$$

$$x \int_0^{d} F_z^{(\ell-2)/\ell}\, dz \tag{6.165}$$

K_{bn} and K_{bp} are given by Eqns. (6.66) and (6.67), respectively; and J_{zo} is given by Eqn. (6.77). The filamentary current is obtained by substitution of Eqn. (6.163) in Eqn. (6.153).

6.6 THE TRAPS NON-UNIFORMLY DISTRIBUTED IN BOTH ENERGY AND SPACE

We consider two different cases of energy distribution

6.6.1 The traps confined in a single discrete energy level

This case is similar to that of the uniformly distributed traps in space described in Section 5.1. Hence, Eqn. (6.160) still holds in this case except that we need to replace J_{zo} given by Eqn. (6.52) with J_{zo} given by Eqn. (6.104) and to replace $<\lambda_a>$ given by Eqn. (6.161) with the following equation

$$<\lambda_a> \quad \frac{<v\sigma_R>_r}{dq}\left[\frac{\mu_n D_p+\mu_p D_n}{D_n D_p}\right]\left\{\sum_{i=o}^{M-1}\int_{z_i}^{z_{i+1}} F_{zi}^{-1}(\mu_n K_{ani}+\mu_p K_{api})^{-2}\,dz\right\} \quad (6.166)$$

which is obtained by means of the regional approximation technique described in Section 6.3.

6.6.2 The traps distributed exponentially within the forbidden energy gap

Using the same approach, Eqn. (6.163) gives the filamentary current in this case, except that we need to replace J_{zo} given by Eqn. (6.77) with J_{zo} given by Eqn. (6.127)

and to replace $< \lambda_b >$ given by Eqn. (6.165) with the following equation

$$< \lambda_b > = q^{\frac{\ell-2}{\ell}} \frac{< v\sigma_R > r}{d} \left[\frac{\mu_n D_p + \mu_p D_n}{D_n D_p}\right] \left\{ \sum_{i=o}^{M-1} \left[\frac{(\mu_n/\mu_p)^{1/\ell} (K_{bni} K_{bpi})^2}{(\mu_n / K_{bpi}^{\ell} + \mu_p / K_{bni}^{\ell})^{1/\ell}}\right] \right.$$

$$\left. \times \int_{z_i}^{z_{i+1}} F_{zi}^{(\ell-2)/\ell} \, dz \right\} \qquad (6.167)$$

which is obtained by means of the regional approximation technique described in Section 6.3.

6.7 RESULTS AND DISCUSSION

As has been pointed out in Chapter 5, the traps in thin films are generally exponentially distributed in energy. Moreover, the spatial distribution function of traps is likely to be exponential with the maximum density at both the injecting electrodes (z = 0 and z = d). Hence, we shall carry out all the calculations using the following form for the electron and hole trap distribution functions in space, respectively

$$S_n(z) = 1 + A_n \exp(-z/z_{on}) + B_n \exp[-(d-z)/z_{on}] \quad (6.168)$$

$$S_p(z) = 1 + A_p \exp(-z/z_{op}) + B_p \exp[-(d-z)/z_{op}] \quad (6.169)$$

where A_n, A_p, B_n, B_p, z_{on} and z_{op} are constants. Substitution of Eqns. (6.168) and (6.169) into Eqn. (6.95) gives

$$b_{ni} = 1 - \frac{Mz_{on}}{d} \{ A_n \exp(-di/Mz_{on}) [\exp(-d/Mz_{on})-1] - B_n \exp[\frac{-d(M-i)}{Mz_{on}}] [\exp(d/Mz_{on})-1]\} \quad (6.170)$$

and

$$b_{pi} = 1 - \frac{Mz_{op}}{d} \{ A_p \exp(-di/Mz_{op}) [\exp(-d/Mz_{op}-1] - B_p \exp[\frac{-d(M-i)}{Mz_{op}}][\exp(d/Mz_{op})-1]\} \quad (6.171)$$

We shall consider only the case of filamentary double injection for the reasons discussed in Section B. In order to show the effect of non-uniformity of the charge carrier trap distribution, we chose anthracene thin films as an example. We have computed the electric field, net space charge, current distribution and the filamentary current I as functions of d using 20 intervals (M = 20) for the discrete regional

approximation and the following physical parameters for anthracene films at 300^0K [81, 60]

$$\varepsilon = 3.2 \times 10^{-11} \text{ F m}^{-1}$$

$$N_c = 1.96 \times 10^{26} \text{ m}^{-3}$$

$$N_v = 2.4 \times 10^{25} \text{ m}^{-3}$$

$$\mu_n = 4.0 \times 10^{-5} \text{ m}^2 \text{ v}^{-1} \text{ sec}^{-1}$$

$$\mu_p = 8.0 \times 10^{-5} \text{ m}^2 \text{ v}^{-1} \text{ sec}^{-1}$$

$$H_{bn} = 2.0 \times 10^{25} \text{ m}^{-3}$$

$$H_{bp} = 10^{25} \text{ m}^{-3}$$

$$T_c = 400^0\text{K}$$

Figure 6.2 shows the electric field and net space charge distribution along the filament; γ denotes the ratio of A_p/A_n, B_p/B_n and z_{op}/z_{on}. It can be seen from Fig. 6.2 that the electric field displays a maximum value at the point where the net charge density (electrons and holes) is equal to zero. This particular point corresponds to a value

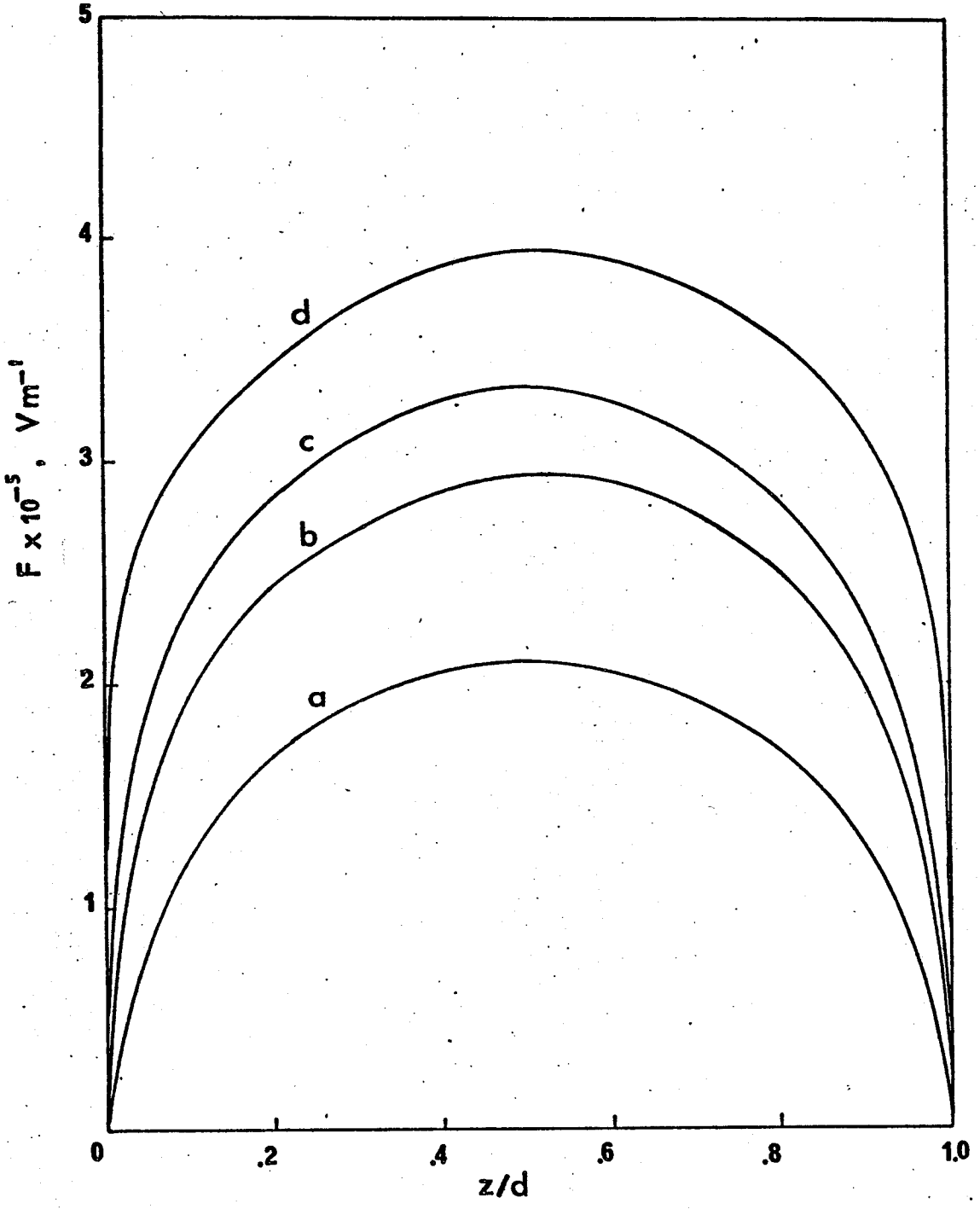

Fig. 6.2 (a) F as a function of z/d, for different forms of spatial distribution of traps

a: $\gamma = 1$, b: $\gamma = 2$, c: $\gamma = 3$, d: $\gamma = 4$

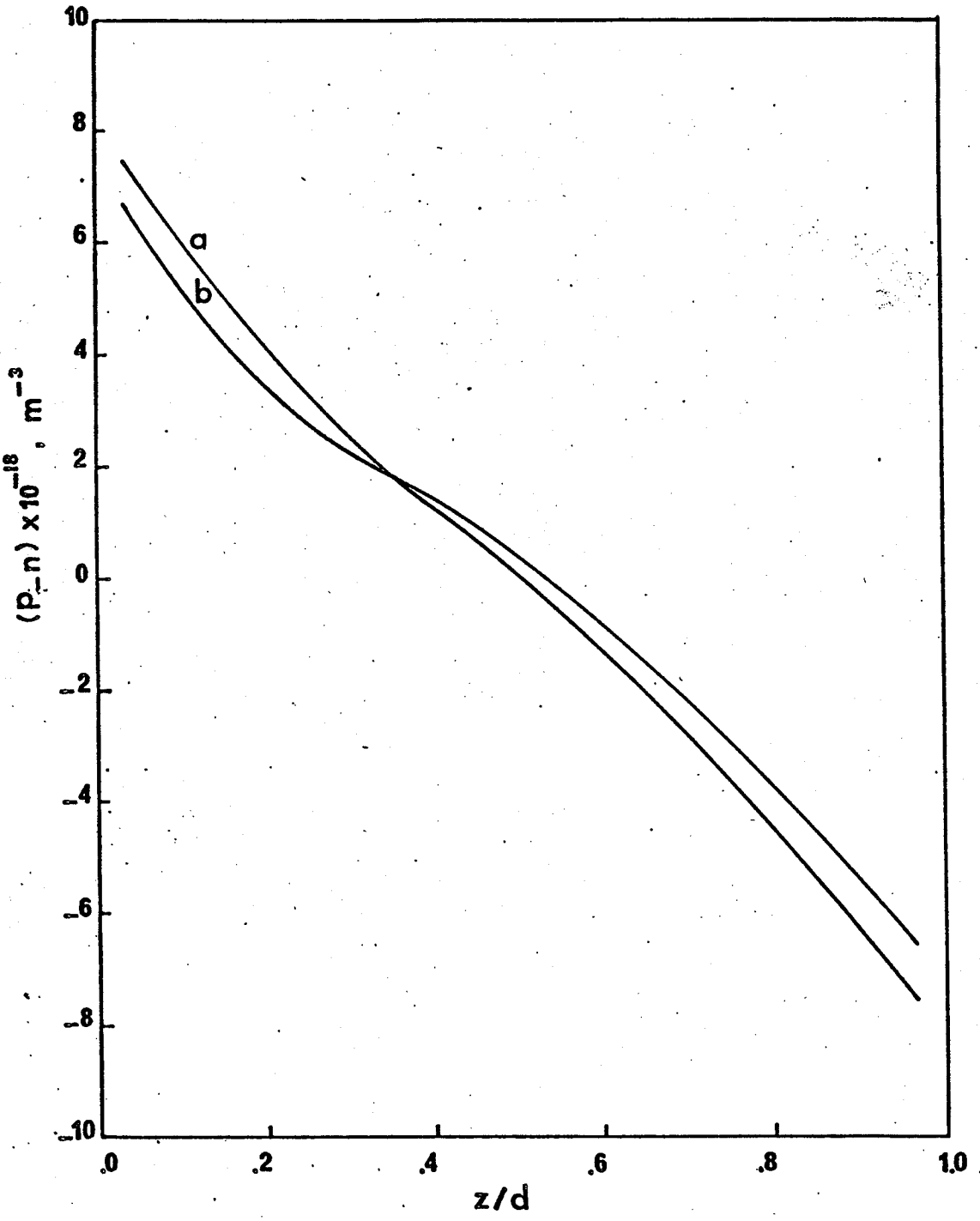

Fig. 6.2 (b) (P - n) as a function of z/d, for different forms of spatial distribution of traps

a: $\gamma = 2$, b: $\gamma = 4$

of S_b given by

$$S_{bmax} = [1 + (K_{bpi}/K_{bni})^{\ell}]^{-1} \qquad (6.172)$$

The value of S_{bmax} depends on the ratio of electron to hole trap densities. As one type of trap increases in the concentration, the location of the maximum electric field will tend to shift towards the electrode which injects that particular type of charge carriers. Figure 6.3 shows the current density distribution across the filament. It can be seen that the variation rate, and hence, the total filamentary current is greatly affected by the form of the non-uniformity trap distribution functions.

Figure 6.4 shows I_{NU}/I_U as a function of the specimen thickness d, where U denotes the case of uniformity and NU the case of non-uniformity traps distributed in space. These results indicate that the thinner the specimen the more significant is the effect of non-uniformity of spatial distribution and that for very thick specimens this effect may be negligible. The critical value of d for this effect to become negligible depends on the distribution functions $S_n(z)$ and $S_p(z)$. However, for thin films this effect should not be ignored.

The above results indicate that the analysis described in this chapter may, in principle, be used to analyse any

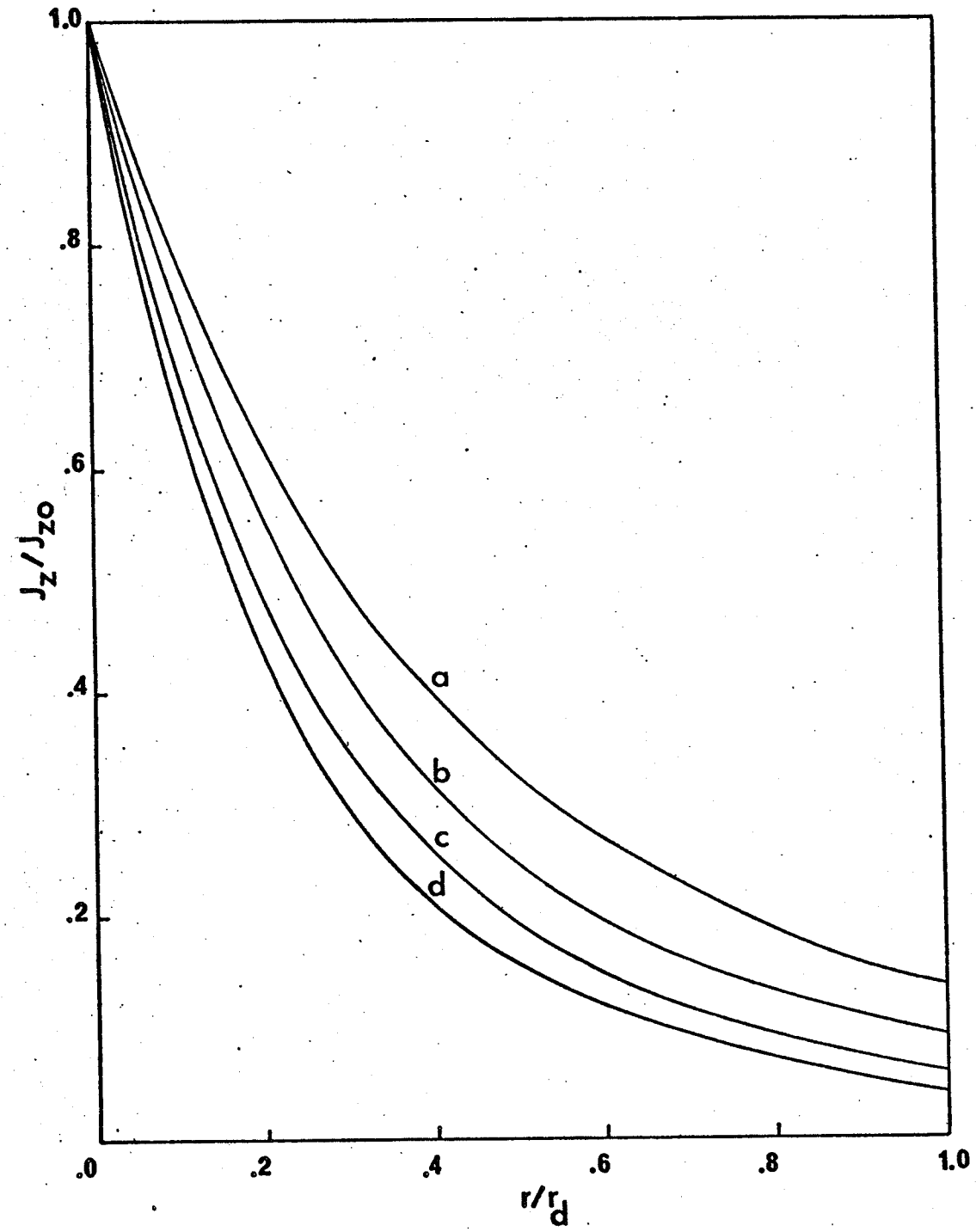

Fig. 6.3 J_z/J_{zo} as a function of r/r_d, for different forms of spatial distribution of traps

a: $\gamma = 1$, b: $\gamma = 2$, c: $\gamma = 3$, d: $\gamma = 4$

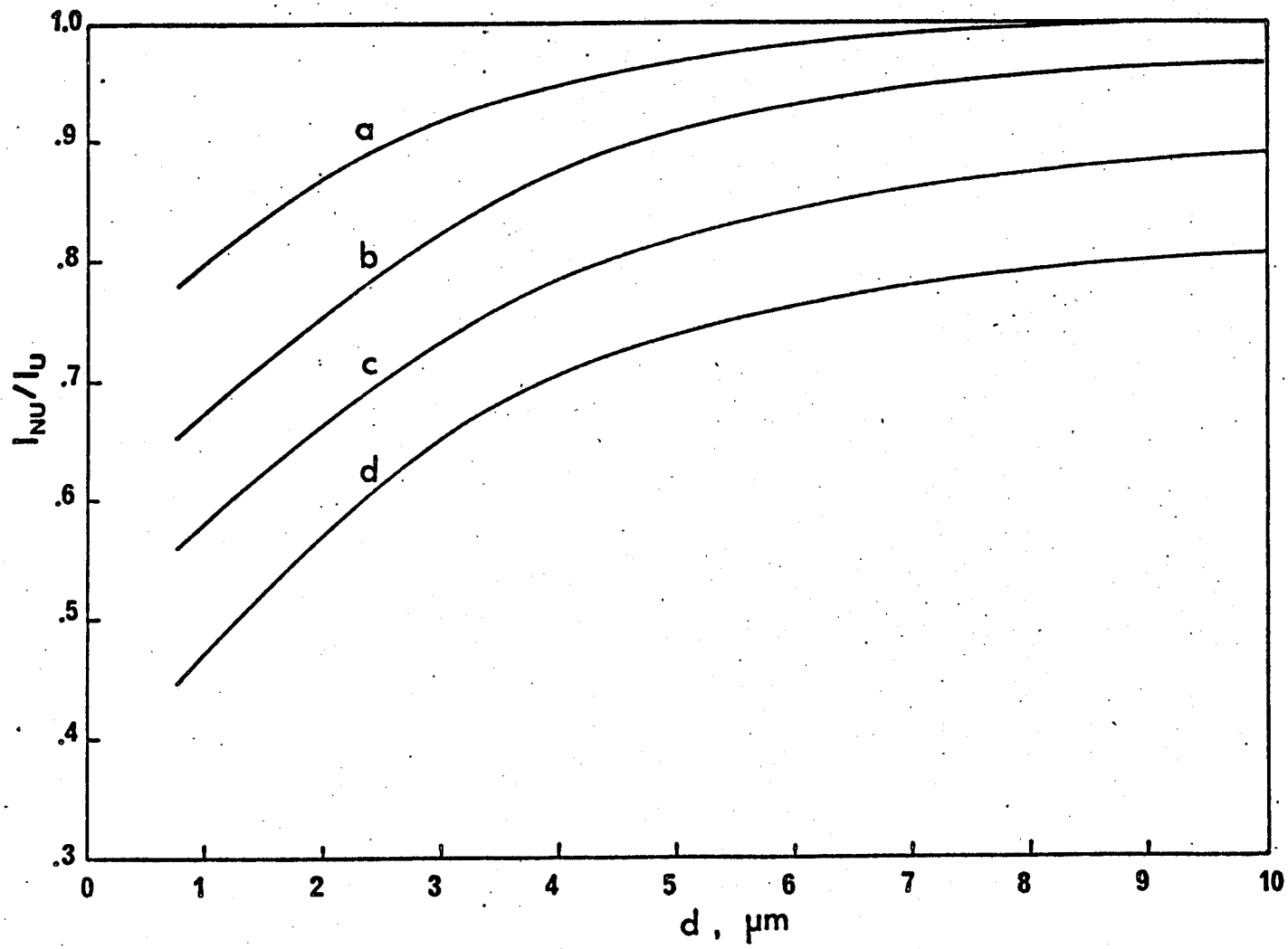

Fig. 6.4 I_{NU}/I_U as a function of d, for different forms of spatial distribution of traps
a: $\gamma = 1$, b: $\gamma = 2$, c: $\gamma = 3$, d: $\gamma = 4$

spatial distribution of traps. This can be done by comparing the experimental values of d_{eff} obtained from the measurements of thickness dependence of the current, with the calculated values given in Fig. 6.4. Hence, an estimate of the parameters of the trap spatial distribution function can be obtained. A more rigorous approach may be done by curve fitting the experimental data using the theory discussed in this chapter.

6.8 CONCLUDING REMARKS

The general expression for the planar and filamentary double injection current-voltage characteristics in a thin film with traps uniformly and non-uniformly distributed in energy and space have been derived using a unified mathematical approach. The computed results for filamentary double injection with exponential trap distribution in energy and space show that the effect of non-uniformity of spatial distribution of traps can be very serious if the specimen is very thin, and suggests that for thin films this effect should not be ignored.

CHAPTER VII

CONCLUSIONS

On the basis of the present investigations, we can now draw the following conclusions:

(1) The techniques of ellipsometry have been used to measure the refractive indicies and thickness of anthracene thin films. The refractive index is the highest along the z-axis and the lowest along the x-axis indicating the anisotropy of this material. The refractive indicies in all directions decrease with increasing ratio of film thickness to wavelength and reaches a practically constant value for the ratios higher than 10. This thickness dependence phenomena is attributed to the effect of surface states on the contribution of excitons to the optical constants.

(2) The switching and memory phenomena observed in anthracene thin films are similar to those reported in inorganic amorphous semiconductors. But, in organic materials, these occur only in films of thickness less than 5 μm. The general trend is that the specimen exhibiting switching and memory phenomena do not exhibit electroluminescence and vice-versa. The threshold voltage for the onset of switching, decreases with increasing temperature. In the

"ON" state the conductance decreases with increasing temperature, reaches a minimum at 37°C and then increases with increasing temperature. All these phenomena are attributed to double injection couples with the effects of traps on excitons and charge carriers, carrier exciton interactions and the formation of charge transfer complexes.

(3) The general expressions for the electric field, free and trapped charge carrier densities created by single injection in a solid with traps uniformly and non-uniformly distributed in energy and space have been derived using a unified mathematical approach. The computed results based on these expressions, using anthracene films as an example, show that the effect of the non-uniformity of spatial distribution of traps can be very serious if the specimen is very thin, and suggests that for thin films this effect should not be ignored.

(4) The general expressions for the steady-state current-voltage characteristics of an insulator-electrolyte system with traps uniformly and non-uniformly distributed in energy and space have been derived using a unified mathematical approach. Comparison of the computed results with presently available experimental results indicates that the thin films, in general, have exponential trap distribution in both energy and space. The analysis

techniques illustrated with anthracene thin films as an example may, in principle, be used to analyse any types of trap distribution in space, since any type of distribution can always be resolved into components to fit the four general distribution functions, namely uniform, linear with the maximum density at the injecting electrode, exponential with the maximum density at the injecting electrode and exponential with the maximum densities at both electrodes, which have been studied.

(5) The general expressions for the current-voltage characteristics due to planar and filamentary double injection into thin insulating films with traps non-uniformly distributed in energy and space have been derived. The computed results for filamentary double injection with exponential trap distribution in energy and in space show that the effect of the non-uniformity of spatial distribution of traps is significant and should not be ignored for thin films.

BIBLIOGRAPHY

1. Akamutu, H. and Inokuchi, H., "On the electrical conductivity of violanthrone, iso-violanthrone and pyranthrone", J. Chem. Phys., 18, 810-811, 1950.

2. Akamutu, H. and Inokuchi, H., "Photoconductivity of Violanthrone", J. Chem. Phys. 20, 1481-1484, 1952.

3. Akamutu, H., Inokuchi, H. and Matsunaga Y., "Electrical conductivity of the perylene-bromine complex", Nature, 173, 168-169, 1954.

4. Akamutu, H., Inokuchin, H. and Matsunaga Y., "Organic semiconductors with high conductivity. I complexes between polycyclic aromatic hydrocarbons and halogens", Bull. Chem. Soc. Jap., 29, 213, 1956.

5. Allen, T. H., "Ellipsometry measurements on thin organic films", 1972 Ann. Meeting Opt. Soc. America, Abs. #TUG14, J. Opt. Soc. Am., 62, p. 1375.

6. Allen, T. H., "The study of molecular contamination kenetics using ellipsometry", 7th Space Simulation Conference, November 12-14, 1973.

7. Archer, R. J., "Determination of the properties of films on silicon by the method of ellipsometry", J. Opt. Soc. Amer. 52, 970-977, 1962.

8. Avakian, P. and Merrifield, R. E., "Triplet excitons in anthracene crystals - a review", Mol. Cryst., 5, 37-77, 1968.

9. Azzam, R. M. H. and Bashara, N. M., "Generalized Ellipsometry for surfaces with directional preference: Application to diffraction gratings", J. Opt. Soc. Amer., 62, #12, 1521-1523, 1972.

10. Baessler, H., Hermann, G., Riehl, N. and Vanbel, G., "Space charge limited currents in tetracene single crystals", J. Phys. Chem. Sol., 30, 1579-1585, 1969.

11. Ballard, W. P. and Christy, R. W., "Switching effects in electron-beam-deposited polymer films", J. Non-Cryst. Sol., 17, 81-88, 1975.

12. Barnett, A. M. and Milnes, A. G., "Filamentary injection in semiinsulating silicon", J. Appl. Phys., 37, 4215-4223, 1966.

13. Beckmann, K. H. and Memming, R., "Photoexcitation and luminescence in redox processes on gallium phosphide electrodes", J. Electrochem. Soc., 116, 368-373, 1969.

14. Berdersku, V. A. and Lawrushko, A. G., "Reabsorption of light and photoconductivity of anthracene crystals", Sov. Phys. Sol. St. 13, 1072-1076, 1971.

15. Berman, M., Kerchner, H. R. and Ergun, S., "Determination of the optical properties of absorbing uniaxial crystals from reflectance at oblique incidence", J. Opt. Soc. Am., 60, 646-648, 1970.

16. Blodgett, K. B. and Langmuir, I., "Built-up films of barium stearate and their optical properties", Phys. Rev. 51, 964-982, 1937.

17. Bradley, A. and Hammes, J. P., "Photoconductivity in thin organic films", J. Electrochem. Soc., 110, 543-548, 1963.

18. Bree, A. and Lyons, L. E., "Effect of the gaseous atmosphere on the photoconduction and semiconduction of aromatic hydrocarbon crystals", J. Chem. Phys. 25, 384A, 1956.

19. Bree, A., Carswell D. J. and Lyons, L. E., "Photo and semiconductance of organic crystals. I. Photo-effects in tetracene and anthracene", J. Chem. Soc., 1728-1733, 1955.

20. Bree, A. and Lyons, L. E., "Effect of heat upon anthracene photoconductance in air", J. Chem. Phys. 25, 1284-1285, 1956.

21. Bree, A. and Lyons, L. E., "The intensity of ultraviolet light absorption by monocrystals, Part I: Measurement of thickness of thin crystals by interferometry", J. Chem. Soc., 2658-2662, 1956.

22. Bree, A. and Lyons, L. E., "The intensity of ultraviolet light absorption by monocrystals, Part II: Absorption and reflection by anthracene of plane-polarized light", J. Chem. Soc., 2662-2670, 1956.

23. Brodin, M. S. and Pekar, S. I., "On an experimental demonstration of the existence of additional anamalous light waves in a crystal in the exciton absorption region", Sov. Phys. JETP, 1, 55-60, 1960.

24. Brodin, M. S. and Pekar, S. I., "Additional anamalous light waves in anthracene in the exciton absorption region", J. Exptl. Theoret. Phys. (USSR) 38, 1910-1912, 1960.

25. Brodin, M. S. and Prikhotko, A. F., "Influence of the thickness of anthracene crystals on their absorption curves at 20°K", Opt. and Spect., 12, 82-83, 1959.

26. Buke, R. H., "Trap density determination by space-charge-limited currents", J. Appl. Phys. 33, 1733-1737, 1962.

27. Carethano, H., Lacoste, R. and Segui, Y., "Bistable electrical switching in polymer thin films", Appl. Phys. Letts., 19, #10, 414-415, 1971.

28. Cardew, M. H. and Eley, D. D., "The semiconductivity of organic substances, Part 3: Hemoglobin and some amino acids", Disc. Faraday Soc. 27, 115-128, 1959.

29. Carswell, D. J., "Correlation between photoconductance and ultraviolet spectrum of anthracene crystals", J. Chem. Phys., 21, 1890, 1953.

30. Carswell, D. J. and Lyons, L. E., "Photo and semi-conductance of organic crystals with spectral dependence, quantum efficiency and relation between semi- and photo-effects in anthracene", J. Chem. Soc., 1734-1740, 1955.

31. Caywood, J. M., "Photoemission from metal contacts into anthracene crystals: a critical review", Mol. Cryst. Liq. Cryst. 12, 1-26, 1970.

32. Chopra, K. L., Thin film phenomena , McGraw-Hill Book Company, Ch. 2, 1969.

33. Chowdhury, M. and Basu, S., "Some notes on molecular complexes between iodine and polynuclear aromatic hydrocarbons", J. Chem. Phys. 32, 1450-1452, 1960.

34. Chynoweth, A. G., "The effect of oxygen on the photoconductivity of anthracene, II", J. Chem. Phys., 1029-1032, 1954.

35. Chynoweth, A. G. and Schneider, W. G., "The photoconductivity of anthracene, I", J. Chem. Phys., 22, 1021-1028, 1954.

36. Compton, D. M. J., Schneider, W. G. and Waddington, T. C., "Photoconductivity of anthracene, III", J. Chem. Phys., 27, 160-172, 1957.

37. Cook, B. E. and Le Comber, P. G., "The optical properties of anthracene in vacuum ultraviolet", J. Phys. Chem. Sol., 32, 1321-1329, 1971.

38. Davydov, A.S., "Excitons in thin crystals", Sov. Phys. JETP, 18, 496-499, 1963.

39. Davydov, A. S., Theory of molecular excitons , Plenum Press, 1971.

40. den Engelsen, D., "Ellipsometry of anisotropic films", J. Opt. Soc. Am., 61, #9, 1460-1466, 1971.

41. De Smet, D. J., "Ellipsometry of anisotropic thin films", J. Opt. Soc. Am., 64, #5, 631-638, 1974.

42. Dignam, M. J. and Moskovits, M., "A zimuthal misalignment and surface anisotropy as sources of error in ellipsometry", Appl. Opt., 9, 1868-1873, 1970.

43. Dresner, J., "Double injection electroluminescence in anthracene", RCA Rev., 30, 322-334, 1969.

44. Dresner, J. and Goodman, A. M., "Anthracene electroluminescent cells with tunnel injection cathodes", Proc. IEEE (Letters), 8, #11, 1868-1869, 1970.

45. Dresner, J. and Shallcross, F. V., "Rectification and space-charge-limited currents in CAS films", Sol. St. Electron., 5, 205-210, 1962.

46. Eley, D. D. and Parfitt, J. D., "The semiconductivity of organic substances", Trans. Faraday Soc., 51, 1529-1533, 1955.

47. Eley, D. D., Parfitt, S. D., Perry, M. J. and Taysum, D. H., "The semiconductivity of organic substances, Part 1." Trans. Faraday Soc. 49, 79-86, 1953.

48. Eley, D. D. and Spivey, D. I., "The semiconductivity of organic substances, Part 6: a range of proteins", Trans. Faraday Soc. 56, 1432-1442, 1960.

49. Fox, D., Labes, M. M. and Weissberger, A., eds. Physics and chemistry of the organic solid state , Interscience Pub., New York, 1967.

50. Frankevitch, E. L. and Baiabanow, E. F., "A study of carrier mobility in organic materials", Sov. Phys. Sol. St., 7, 570-575, 1965.

51. Garrett, S. G. E., Pethig, R. and Soni, V., "Switching and other high field effects in organic films", J. Chem. Soc. Farad. Trans. II, 70, 1732-1740, 1974.

52. Gazso, J., "Electrical behaviour of thin layer Au-poly-ethylene-Al sandwiches", Hung. Acad. Sci. (Budapest) rept. KFKI-7354, 1973.

53. Geacintoo, N. and Pope, M., "Photogeneration of charge carriers in anthracene", J. Chem. Phys. 45, 3884-3885, 1966.

54. Gheorghita-Oançea, C., "Electrical dark-and photoconductivity of thin anthracene layers in vacuum", Bait. J. Appl. Phys., 12, 579-580, 1961.

55. Gheorghita-Oançea, C., "On the structure and semiconductor properties of thin anthracene layers, Part 1", Rev. Phys. Acad. Rep. Populaire Romaine, 8, 361-375, 1964.

56. Gheorghita-Oançea, C., "On the structure and semiconductor properties of thin anthracene layers", Rev. Roumaine Phy., 9, 23-53, 1964.

57. Greenaway, D. L. and Harbeke, G., "Anisotropy of the optical constants and the band structure of graphite", Phys. Rev. 178, 1340-1348, 1969.

58. Gregor, L. V., "Polymer dielectric films", IBM J. Res. Dev., 12, 140-162, 1968.

59. Gunther, K., "Interfacial and condensation processes occuring with multicomponent vapors" in "The use of thin films in physical investigation", J. C. Anderson, ed., Acad. Press, New York, 1966.

60. Gutmann, F. and Lyons, L. E., Organic semiconductors , John Wiley and Sons, Inc., New York, 1967.

61. Guyton, A. C., Textbook of medical physiology , W. B. Saunders, Comp., 15, 1971.

62. Hale, J. M. and Mehl, W., "Approximate solution to the one carrier problem of a semiconductor-electrolyte system", Surf. Sci., 4, 221-233, 1966.

63. Hamann, C., "On the trap distribution in thin film of copper phthalocyanine", Phys. Stat. Sol. 26, 311-318, 1968.

64. Hanai, T., Haydon, D. A. and Taylor, J., "Polar group orientation and the electrical properties of lecithin bimolecular leaflets", J. Theor. Biol., 9, 278-296, 1965.

65. Hanai, T., Haydon, D. A. and Taylor, J., "The influence of lipid composition of some adsorbed proteins on the capacitance of black hydrocarbon membranes", J. Theor. Biol., 9, 422-432, 1965.

66. Hannay, N. B., Semiconductors , Reinhold Pub. Co., New York, 1959.

67. Heavens, O. S., Optical properties of thin solid films , Dover Pub., Inc., New York, 1965.

68. Heilmeir, G. H. and Warfield, B. G., "Investigation of bulk currents in metal-free phthalocyanine crystals", J. Chem. Phys. 38, 163-168, 1963.

69. Helfrich, W. and Lipsett, F. R., "Fluorescence and defect fluorescence of anthracene at 4.2°K", J. Chem. Phys., 43, 4368-4376, 1965.

70. Helfrich, W. and Schneider, W. G., "Recombination radiation in anthracene crystals", Phys. Rev. Lett., 14, 229-231, 1965.

71. Helfrich, W. and Schneider, W. G., "Transients of volume controlled current and of recombination radiation in anthracene", J. Chem. Phys. 44, 2902-2909, 1966.

72. Hickmott, T. W., "Electron emission, electroluminescence and voltage-controlled negative resistance in Al-Al_2O_3-Au diodes", J. Appl. Phys., 36, 1885-1896, 1965.

73. Hickmott, T. W., "Electroluminescence and Photoresponse of Ta_2O_5 and TiO_2 diodes", J. Electrochem. Soc., 113, 1223-1225, 1966.

74. Hodgkin, A., Conduction of the nervous impulse, Thomas, 1964.

75. Hoesterey, D. C., and Letson, G. M., "The trapping of photocarriers in anthracene by anthraquinone, anthrone and naphthracene", J. Phys. Chem. Sol., 24, 1609-1615, 1963.

76. Holmes-Walker, W. A. and Ubbelohdl, A. R., "Electron transfer in alkli metal-hydrocarbon complexes", J. Chem. Soc., 720-728, 1954.

77. Houde, A. L., Vacuum microbalance techniques, Plenum Press, 1963.

78. Hwang, W. and Kao, K. C., "A unified approach to the theory of current injection in solids with traps uniformly and non-uniformaly distributed in space and energy, and side effects in anthracene films", Sol. St. Electron., 15, 523-529, 1972.

79. Hwang, W. and Kao, K. C., "A unified approach to the theory of double injection in solids with traps uniformly and non-uniformly distributed in the energy band gap", Sol. St. Electron., 16, 407-415, 1973.

80. Hwang, W. and Kao, K. C., "Electroluminescence in anthracene crystals caused by field-induced minority carriers at moderate temperatures", J. Chem. Phys., 58, 3521-3522, 1973.

81. Hwang, W. and Kao, K. C., "On the theory of filamentary double injection and electroluminescence in molecular crystals", J. Chem. Phys., 60, 3845-3855, 1974.

82. Ince, A. N and Oatley, C. W., "The electrical properties of electroluminescent phosphors", Phil. Mag. VII-46, 1081-1103, 1955.

83. Inokuchi, H., "Semi- and photoconductivity of molecular single crystals, anthracene and pyrene", Bull. Chem. Soc. Japan, 29, 131-133, 1956.

84. Inokuchi, H., Harada, Y. and Marugama, Y., "Electrical properties of the single crystal and thin film of α,α' - diphenyl-β picrylhydrazul", Bull. Chem. Soc. Japan, 35, 1559-1561, 1962.

85. Inokuchi, H., Kuroda, H. and Akamato, H., "On the electrical conductivity of the organic thin films: perylene, coronene, and violanthrene", Bull. Chem. Soc. Japan, 34, 749-753, 1961.

86. Ioffe, A. F., Physics of semiconductors , Eng. Transl. Info. Search, Ltd., London, 126, 194, 1960.

87. Kallmann, H. and Pope, H., "Surface controlled bulk conductivity in organic crystals", Nature (London), 185, 753, 1960.

88. Kallmann, H. P. and Pope, M., "Theory of hole injection and conductivity in organic materials", J. Chem. Phys. 36, 2482-2485, 1961.

89. Katul, J. and Zahlan, A. B., "Evidence for the existence of surface states in tetracene microcrystals", Phys. Rev. Lett., 6, 101-102, 1961.

90. Kawabe, M., Masuda, K., and Namba, S., "Electroluminescence of green light region in doped anthracene", Jap. J. Appl. Phys., 10, 527-528, 1971.

91. Kepler, R. G., "Charge carrier production and mobility in anthracene crystals", Phys. Rev., 119, 1226-1229, 1960.

92. Kepler, R. G. and Switendick, A. C., "Diffusion of triplet excitons in anthracene", Phys. Rev. Lett., 15, 56-59,1965.

93. Kevorkien, J., Labes, M. M., Larson, D. C. and Wu, D. C., "Bistable switching in organic thin films", Disc. Faraday Soc., #51, 139-143, 1971.

94. Kingston, R. H. and Neustadter, S. F., "Calculation of the space charge, electric field and free carrier concentration at the surface of a simeconductor", J. Appl. Phys., 26, 718-720, 1955.

95. Klug, H. P. and Alexander, L. E., X-ray diffraction procedures , John Wiley and Sons, Inc., New York, 1954.

96. Kommandeur, J., Korinek, G. J. and Schneider, W. G., "The activation energies of photoconduction for some aromatic hydrocarbons", Can. J. Chem. 35, 998-1001, 1957.

97. Kommandeur, J., Korinek, G. J. and Schneider, W. G., "The change of photoconduction and semiconduction in aromatic hydrocarbons on melting" Can. J. Chem. 36, 513-517, 1958.

98. Kommendeur, J. and Schneider, W. G., "Photoconductivity of anthracene, IV: Bulk photoconduction in single crystals", J. Chem. Phys., 28, 582-589, 1958.

99. Kommandeur, J. and Schneider, W. G., "Photoconductivity of anthracene, V: Effect of imperfections on the bulk photocurrent", J. Chem. Phys., Vol. 28, #4, 590-595, 1958.

100. Labes, M. M., Sehr, R. and Bose, M., "Organic semiconductors, II: The electrical resistivity or organic molecular complexes", J. Chem. Phys., 33, 868-872, 1960.

101. Labes, M. M., Sehr, R. and Bose, M., "Organic semiconductors, I. Some characteristics of the p-phenylenediaminechloranil complex", J. Chem. Phys. 32, 1570-1572, 1960.

102. Lamb, D. R., Electrical conduction mechanisms in thin insulating films , Methuen and Co., London, 1967.

103. Lampert, M. A., "Injection currents in insulators", Proc. IRE, 50, 1781-1796, 1962.

104. Lampert, M. A., Current injection in solids , Acad. Press, New York, 1970.

105. Lampert, M. A., "Volume-controlled current injection in insulators", Rept. Progr. Phys., 27, 329-367, 1964.

106. LeBlanc, Jr., O. H., "Hole and electron drift mobilities in anthracene", J. Chem. Phys., 33, 626, 1960.

107. Liang, C. Y. and Scala, E. G., "Photoconductivity of sodium deoxyribonuclic acid in the dry state", Nature (London), 198, 86-87, 1963.

108. Lindmayer, J., Reynolds, J. and Wrigley, C., "One charge space-charge-limited currents in solids", J. Appl. Phys., 34, 809-812. 1963.

109. Lindmayer, J. and Slobodsky, A., "Two-carrier space-charge-limited current in solids and the dielectric capacitor", Sol. St. Electron., 6, 495-503, 1963.

110. Lipsett, F. R., "On the production of single crystals of naphthalene and anthracene", Can. J. Phys., 35, 284-298, 1957.

111. Lipsett, F. R., Compton, D. M. J. and Waddington, T. C., "Effect of surface condition on the fluorescence and surface photoconductivity of anthracene", J. Chem. Phys. 26, 1444-1445, 1957.

112. Loescher, D. H., Defry, R. J. and Clauser, M. J., "Least square analysis of the film-substrate problem in ellipsometry", J. Opt. Soc. Am., 61, #9, 1230-35, 1971.

113. Lohamann, F. and Mehl, W., "Dark injection and radiative recombination of electrons and holes in naphthalene crystals", J. Chem. Phys., 50, 500-506, 1969.

114. Lumb, M. D. and Stephan, J. A., "On the interpretation of thermal activation energies for conduction in organic semiconductors", Chem. Phys. Lett., 22, 81-86, 1973.

115. Lunin, A. F., Paushkin, Ya. M., Mkrtchan, V. A. and Surovtsev, N. A., "Semiconducting polymers with conjugated bonds", TsNIITEneftekhim., Moscow, 108, 1966.

116. Lyons, L. E., "Photo- and semi-conductance in organic crystals, Part V. Ionized states in molecular crystals", J. Chem. Soc., 10, 5001-5007, 1957.

117. Lyons, L. E. and Morris, G. C., "Photo- and semi-conduction of aromatic hydrocarbon crystals", Proc. Phys. Soc., 69, 1162-1164, 1956.

118. Lyons, L. E. and Morris, G. E., "Photo- and semi-conductance in organic crystals, Part III. Photoeffects in dry air with eleven organic compounds", J. Chem. Soc. 8, 3648-3660, 1957.

119. Lyons, L. E. and Morris, G. C., "Photo- and semi-conductance in organic crystals, Part IV. Spectral dependence of photocurrents in aromatic hydrocarbon crystals in dry air with polarized light", J. Chem. Soc., 8, 3661-3668, 1957.

120. Maricic, S., Pifat, G. and Prandic, V., "Proton conductivity in the solid hydrated haemoglobin", Biochem. Biophys. Acta, 79, 293-300, 1964.

121. Mark, P. and Helfrich, W., "Space charge limited currents in organic crystals", J. Appl. Phys., 33, 205-215, 1962.

122. Maruyama, Y. and Iwasaki, N., "Electrical conduction in amorphous organic films", J. Non-cryst. Sol., 16, 399-406, 1974.

123. Mason, R., "The crystallography of anthracene at 95^{0}K and 290^{0}K", Acta. Cryst., 17, 547-555, 1964.

124. Matsui, A. and Ishii, Y., "Optical properties of anthracene single crystals", J. Phys. Soc. Japan, 23, #3, 581-590, 1967.

125. Mehl, W., Reactions of molecules at electrodes, (N. S. Hush, ed.), Wiley, New York, 1971.

126. Mehl, W., "Redoxreaktionen an anthracenelectroden", Ber. Buns. Phys. Chem., 69, 583-589, 1965.

127. Mehl, W. and Funk, B., "Dark injection of electrons and holes and radiative recombination in anthracene with metalic contacts", Phys. Rev. Lett. 25A, 364-365, 1967.

128. Mehl, W. and Hale, J. M., "Advances in electrochemistry and electrochemical engineering", (P. Delahay, ed.), Interscence, 6, 399-458, 1967.

129. Mett, H. and Pick, H., "Elektronenleit fahigkeit von anthracen-einkristallen", Z. Phys., 134, 566-575, 1953.

130. Mey, W. and Hermann, M. A., "Drift mobilities of holes and electrons in naphthalene single crystals", Phys. Rev., B7, 1652-1656, 1973.

131. Meyer, F., de Klinzenaar, E. E. and den Engelsen, D., "Ellipsometric determination of the optical anisotropy of gallium selenide", J. Opt. Soc. Am., 63, #5, 529-532, 1973.

132. Morantz, D. J. and James, H., "Structural effects on photoconduction in amorphous films of organic solids", J. Vacuum Sci. Tech. (U.S.A.), 6, 637-640, 1969.

133. Mott, N. F. and Gurney, R. W., Electronic processes in ionic crystals, Oxford University Press, 1948.

134. Muller, R. S., "A unified approach to the theory of space-charge-limited currents in an insulator with traps", Sol. St. Electron., 6, 25-32, 1963.

135. Munn, R. W. and Siebrand, W., Theory of charge carrier transport in aromatic hydrocarbon crystals", J. Chem. Phys., 52, 6391-6406, 1970.

136. McClure, D. S., "Electronic spectra of molecules and ions in crystals. Part I. Molecular crystals", Sol. St. Phys., 8, 1-47, 1959.

137. Nakada, J., "The optical properties of anthracene single crystals", J. Phys. Soc. Jap., 17, #1, 113-118, 1962.

138. Nelson, R. C., "Photoelectric phenomena in hemoglobin and dyed gelatin", J. Chem. Phys., 39, #1, 112-115, 1963.

139. Nicolet, M. A., "Unipolar space-charge-limited current in solids with non-uniform spatial distribution of shallow traps", J. Appl. Phys., 36, 4224-4235, 1966.

140. Okamoto, Y. and Brenner, W., Organic semiconductors , Reinhold Pub. Co., New York, 1964.

141. Parmenter, R. H. and Ruppel, W., "Two-carrier space-charge-limited current in a trap free insulator", J. Appl. Phys., 30, 1548-1558, 1959.

142. Pekar, S. I., "The theory of electromagnetic waves in crystal in which excitons are produced", Sov. Phy. JETP, 6, 785-796, 1958.

143. Pekar, S. I., "Dispersion of light in the exciton absorption region of crystals", Sov. Phy. JETP, 7, 813-822, 1958.

144. Pekar, S. I., "On the theory of absorption and dispersion of light in crystals", Sov. Phys., JETP, 36, #2, 314-323, 1959.

145. Perry, D. L., "Low-loss multilayer dielectric mirror", Appl. Optics, 4, #8, 987-991, 1965.

146. Petrova, M. L. and Rozenshtein, L. D., "Field effect in the organic semiconductor chloranil", Sov. Phys. Sol. St., 12, 756-757, 1970.

147. Petrova, M. L. and Rozenshtein, L. D., "Field effect and slow states in thin films of organic semiconductors", Sov. Phys. Sol. St., 13, 1948-1952, 1972.

148. Pick, H. and Wissman, W., "Electronenleitung ven naphthalin - einkristallen", Z. Phys., 138, 436-440, 1954.

149. Pohl, H. A. and Makenzie, J. D., ed., "Modern aspects of the vitreous state", Butlerworth, London, Ch. 2, 105, 1962.

150. Pohl, H. A., and Opp, D. A., "The nature of semiconduction in some acenequinone radical polymers", J. Phys. Chem., 66, 2121-2126, 1962.

151. Pope, M. and Kallmann, H., "A-C and D-C photoconductivity in anthracene single crystals", Symp. Elect. Cond. Org. Sol., Duke Univ. N.D. April 20-22, 83-103, 1960.

152. Pope, M., Burgos, J. and Wotherspoon, N., "Singlet exciton-trapped carrier interaction in anthracene", Chem. Phys. Lett., 12, 140-143 (1971).

153. Pope, M., Kallmann, H., Chen, A. and Gordon, P., "Charge injection into organic crystals: Influence of electrodes on dark and photoconductivity", J. Chem. Phys., 36, 2486 2492, 1961.

154. Pott, G. T. and Williams, D. F., "Low temperature electron injection and space-charge-limited transients in anthracene crystals", J. Chem. Phys., 51, 1901-1906, 1969.

155. Reucroft, P. J. and Mullins, F. D., "Physical basis for exponential carrier trap distributions in molecular solids", J. Chem. Phys., 58, 2918-2921, 1973.

156. Rose, A., "Space-charge-limited currents in solids", Phys. Rev., 97, 1538-1544, 1955.

157. Ruiz-Urbieta, M., Sparrow, E. M. and Eckert, E. R. G., "Film thickness and refractive indicies of dielectric films on dielectric substrate", J. Opt. Soc. Am., 61, #9, 1392-1396, 1971.

158. Schadt, M. and Williams, D. F., "Low temperature hole injections and hole trap distribution in anthracene", J. Chem. Phys., 50, 4364-4368, 1969.

159. Schmidt, P. F., "On the mechanisms of electrolytic rectification", J. Electrochem. Soc., 115, 167-176, 1968.

160. Schmidt, K. and Wedel, K., "Negative photoeffect by double injection", Phys. Stat. Sol., 34, 167-168, 1969.

161. Schneider, W. G. and Waddington, T. C., "Effect of gases on the photoconductivity of anthracene", J. Chem. Phys., 25, 358, 1956.

162. Schopper, H., "Zur optic dünner deppelrechner und dichroitischer schichten", Z. Phy., 132, 146-170, 1952.

163. Schwob, H. P. and Zschokke-Gränacher, I., "Doppelinjektion und elektrolumineszenz in dotiertern anthracenkrisatallen", Mol. Cryst. Liq. Cryst., 13, 115-136, 1971.

164. Seiwatz, R. and Green, M., "Space charge calculation for semiconductors", J. Appl. Phys., 29, 1034-1040, 1958.

165. Selivaneko, A. S., "The exciton state of an imperfect molecular crystal", Sov. Phys., JETP, 5, #1, 79-83, 1957.

166. Skinner, S. M., "Diffusion, static charges and the conduction of electricity in non-metallic solids by a single charge carrier. Part I. Electric charges in plastics and insulating materials", J. Appl. Phys., 26, 498-508, 1955.

167. Simpson, O., "Electronic properties of aromatic hydrocarbons", Proc. Roy. Soc. (London), A238, 402, 1956.

168. Stafeev, V. et al., "Negative resistance of very thin organic films between metal electrodes", Sov. Phys. semiconduct., 2, 642-643, 1968.

169. Steinberger, I. T., "Further experimental evidences on majority carrier injection in Cds single crystals", J. Phys. Chem. Sol., 15, 354-355, 1960.

170. Sussman, A., "Space-charge-limited current in copper phthalocyanine thin films", J. Appl. Phys., 38, 2738-2748, 1967.

171. Suna, A., "Kinematics of exciton-exciton annihilation in molecular crystals", Phys. Rev. B1., 1716-1739, 1970.

172. Sworakowski, J., "Space-charge-limited currents in solids with non-uniform spatial trap distribution", J. Appl. Phys., 41, 292-295, 1970.

173. Sworakowski, J. and Mager, J., "Space-charge-limited currents in single crystals of anthracene doped with perylene", Acta. Phys. Polon., 36, 483-486, 1969.

174. Sworakowski, J. and Pigon, K., "Trap distribution and space-charge-limited currents in organic crystals", J. Phys. Chem. Sol., 30, 491-496, 1969.

175. Szent-Györyi, A., "The study of energy levels in biochemistry", Nature (London), 148, 157-159, 1941.

176. Szymanski, A., "Space-charge-limited currents in polycrystalline p-quaterphenyl layers", Mol. Cryst., 3, 339-355, 1968.

177. Szymanski, A. and Labes, M. M., "Charge carrier mobility in tetracene", J. Chem. Phys., 50, 1898-1899, 1966.

178. Szymanski, A., Larson, D. C. and Labes, M. M., "A temperature-independent conducting state in tetracene thin film", Appl. Phys. Lett., 14, 88-90, 1969.

179. Thomas, J. M., Williams, J. O. and Turton, L. M., "Lattice imperfection in organic solids, IV: A study - using space-charge-limited currents of trapping centers in crystalline anthracene", Trans. Faraday Soc., 64, 2505-2013, 1968.

180. Tolansky, S., Surface microtopography , Wiley and Sons, New York, 1960.

181. Tomaino, M. F., "Report on semiconductive plastics", Electron., 33, 68-71, 1960.

182. Tomar, M. S. and Srivastava, V. K., "Anisotropic effects in the ellipsometry of built-up films and determination of their optical constants", Thin Sol. Films, 15, 207-215, 1973.

183. Touraine, A., Vautier, C. and Charles, D., "Characteristiques courant-tension en regimed de charge d'espace en presence d'une distribution uniform de pieges - II: Application aux results experimenteaux des couches mine de selenium amorphe", Thin Sol. Films, 9, 229-239, 1972.

184. Vidadi, Y. A. and Rozenshtein, L. D., "Photocapcitance and photocurrent 'memory' of thin organic dye films", Sov. Phys. Semiconduct., 2, 231-232, 1968.

185. Vijh, A. K., Electrochemistry of metals and semiconductors, Marcel Dekker, Inc., New York, 1973.

186. Wakayama, N. and Williams, D.F., "Singlet exciton-charge carrier interaction in anthracene", Chem. Phys. Lett., 9, 45-47, 1971.

187. Wakayama, N. and Williams, D.F., "Carrier-exciton interactions in crystalline anthracene", J. Chem. Phys., 57, 1770-1779, 1972.

188. Weigh, J. W., "Spectroscopic properties of organic photoconductors, I. Absorbtion spectra of cationic dye films", J. Chem. Phys., 24, 364-370, 1956.

189. Williams, D. F. and Schadt, M., "DC and pulsed electroluminescence in anthracene and doped anthracene crystals", J. Chem. Phys., 53, 3480-3487, 1970.

190. Williams, D. F. and Schadt, M., "A simple organic electroluminescent diode", Proc. IEEE (letters), 58, #3, 476, 1970.

191. Williams, W. G., Spong, P. L. and Gibbons, D. J., "Double injection electroluminescence in anthracene and carrier injection properties of carbon fibers", J. Phys. Chem. Sol., 33, 1879-1884, 1972.

192. Winchell, A. N., The optical properties of organic compounds, Acad. Press, New York, 81, 1954.

193. Wolf, H. C., "Electronic spectra of aromatic molecular crystals", Sol. St. Phys., 9, 1-81, 1959.

194. Wright, G. T., "Mechanisms of space-charge-limited currents in solids", Sol. St. Electron., 2, 165-189, 1961.

195. Zschokke-Gränacher, I., Schwob, H. P. and Baldinger, E., "Recombination radiation in anthracene doped with tetracene", Sol. St. Commun., 5, 825-828, 1967.